Hybrid Solid-State Hydrogen Storage Materials

A Thesis

submitted in partial fulfilment

of the requirements for the Degree

of

Master of Science

at the

University of Waikato

by

Kathryn Ruth Benge

THE UNIVERSITY OF
WAIKATO
Te Whare Wānanga o Waikato

University of Waikato

2008

Abstract

This thesis investigates the chemistry of ammonia borane (NH_3BH_3) relevant to the development of hydrogen storage systems for vehicular applications.

Because of its high hydrogen content and low molecular weight ammonia borane has the potential to meet stringent gravimetric hydrogen storage targets of >9 wt%. Two of the three moles of H_2 in ammonia borane can be released under relatively mild conditions, with the highest gravimetric yield obtained in the solid-state. However, ammonia borane does not deliver sufficient H_2 at practical temperatures and the products formed upon H_2 loss are not amenable to regeneration back to the parent compound.

The literature synthesis of ammonia borane was modified to facilitate large scale synthesis, and the deuterated analogues ND_3BH_3 and NH_3BD_3 were prepared for the purpose of mechanistic studies.

The effect of lithium amide on the kinetics of dehydrogenation of ammonia borane was assessed by means of solid-state reaction in a series of specific molar ratios. Upon mixing lithium amide and ammonia borane, an exothermic reaction ensued resulting in the formation of a weakly bound adduct with an $H_2N\cdots BH_3$-NH_3 environment. Thermal decomposition at or above temperatures of 50°C of this phase was shown to liberate >9 wt% H_2. The mechanism of hydrogen evolution was investigated by means of reacting lithium amide and deuterated ammonia borane isotopologues, followed by analysis of the isotopic composition of evolved gaseous products by mass spectrometry. From these results, an intermolecular multi-step reaction mechanism was proposed, with the rates of the first stage strongly dependent on the concentration of lithium amide present. Compounds exhibiting a BN_3 environment (identified by means of solid-state ^{11}B NMR spectroscopy) were formed during the first stage, and subsequently cross link to form a non-volatile solid. Further heating of this non-volatile solid phase ultimately resulted in the formation of crystalline Li_3BN_2 - identified by means of powder X-ray diffractometry. This compound has been identified as a potential hydrogen storage material

due to its lightweight and theoretically high hydrogen content. It may also be amenable to hydrogen re-absorption.

The $LiNH_2/CH_3NH_2BH_3$ system was also investigated. Thermal decomposition occurred through the same mechanism described for the $LiNH_2/NH_3BH_3$ system to theoretically evolve >8 wt% hydrogen. The gases evolved on thermal decomposition were predominantly H_2 with traces of methane detected by mass spectrometry.

Acknowledgements

First and foremost I would like to thank everybody who supported me throughout the course of my studies.

To my fiancé Jeremy. Thank you for keeping me grounded throughout this process, you are my backbone, and none of this would have been possible without your constant love, support and expert computer skills.

Thank you to my supervisors Dr Brian Nicholson for your constant guidance and assistance during the writing process, and Dr Tim Kemmitt for assistance and supervision of laboratory work conducted for the purpose of this research.

I would like to especially thank Dr Mark Bowden. Your willingness to drop everything at a moments notice to help me and going beyond what was expected of you has been greatly appreciated.

I would also like to thank Dr Herbert Wong and Professor Ken MacKenzie for assistance with NMR spectroscopy, and Caleb Higham for laboratory assistance.

Thank you to the Foundation for Research, Science and Technology for funding this research (IIOF contract C08X0501), and The University of Waikato for providing me with financial support in the form of a Masters Research Scholarship.

Finally, I would like to thank Industrial Research for giving me this opportunity to study a subject relatively foreign to me, and for providing me with the facilities to undertake this research.

Contents

List of Figures

List of Tables

Chapter 1

Introduction

New energy concepts are essential for the future of industrial society due to the current increase in pollution and exploitation of fossil energy resources. Renewable energy sources have to replace fossil fuels that produce carbon dioxide upon combustion, a greenhouse gas which is largely responsible for global warming [1]. Since the development of the proton exchange membrane (PEM) fuel cell, which is fuelled by hydrogen and oxygen (air) and produces only water [2], hydrogen has been seen to be the most promising solution. Hydrogen as an alternative to traditional energy fuels such as oil and natural gas, has been the focus of research and development efforts for more than a decade [3].

Hydrogen can be produced from a variety of sources including fossil fuels and renewable energy sources - for example there is the potential to derive this fuel from water itself should an attractive alternative to electrolysis be developed [4]. It is non-toxic as an energy carrier since water is the only exhaust product when hydrogen is converted into energy. The amount of energy produced during hydrogen combustion is higher than that released by any other fuel on a mass basis [5]. Some main cities (i.e., London) have already turned to hydrogen-powered bus fleets using internal combustion engines or PEM fuel cells to reduce the level of pollution. However, as we attempt to utilise hydro-

gen for long haul transportation it becomes obvious that vehicular hydrogen storage requires much improvement in order to be practical [6].

The current goal is to develop a system for on-board hydrogen storage and controlled release of hydrogen, which is capable of covering over 500 km on a full tank [7]. The hydrogen release should occur at temperatures below approximately 80°C so as to make use of the waste heat generated in PEM fuel cells. Another important criterion for a hydrogen storage system is reversibility of the hydrogen uptake and release. In 2004 the US Department of energy (US DOE) published a document in which technical targets for the years 2010 and 2015 were described [8]. The following criteria for a hydrogen storage technology suitable for transportation were set:

- High H_2 storage capacity (> 9.0 wt% H).
- Low H_2 generation temperature, ideally between 60-120°C.
- Favourable kinetics for H_2 absorption/desorption.
- Low cost.
- Low toxicity, hazards and environmental impact.

The US DOE hydrogen storage system targets help guide researchers by defining system requirements in order to achieve commercially viable hydrogen storage technologies. At present there are no materials that meet the above operating requirements for weight, volume, durability, efficiency and cost.

One of the biggest hurdles remaining is to find a material capable of storing enough on-board hydrogen for a vehicle to cover over 500 km on a full tank without adding significant weight or volume relative to a conventional petrol car. The weight guidelines outlined in the DOE requirements not only include the weight of the material in question, but also the vehicles physical system i.e., all components necessary to deliver hydrogen to the fuel cell (tanks,

heaters, chillers, pumps, tubes and hoses etc...). If this physical system weighs roughly one third to half the weight of the storage material, then the target material should approach a minimum of 12 wt% of hydrogen.

1.1 Methods of Storage

1.1.1 Compressed and Liquefied H_2

Hydrogen gas can be compressed and stored in tanks that hold it at the required pressure. Liquid hydrogen has long been the fuel of choice for rocket applications, however transport and storage of compressed or liquefied hydrogen are not without dangers. The level of compression required to store hydrogen at a high enough density involves very high levels of energy, which is not beneficial due to the net energy effect; also the safety of pressurised cylinders is of concern. Furthermore, the densities of compressed hydrogen (40 g L^{-1} at 700 bar) or liquefied hydrogen (70 g L^{-1} at 20K) fall far short of the DOE's volumetric targets [9]. Therefore, to meet these targets the hydrogen must be stored as a solid.

1.1.2 Metal Hydrides

Hydrogen forms solid metal-hydrogen compounds with some metals and alloys leading to solid-state storage at conditions close to room temperature and atmospheric pressure [10]. This gives them an important safety advantage over gas and liquid hydrogen storage methods. Metal hydrides have higher hydrogen storage density than hydrogen gas or liquid hydrogen, hence metal hydride storage is a safe, volume efficient storage method. Metal hydrides have the ability to absorb and desorb large amounts of hydrogen gas many times without deteriorating. Both absorption and desorption rates can be controlled by adjusting temperature or pressure. Some metal hydrides can absorb and desorb hydrogen at ambient temperature and close to atmospheric pressure.

The operating temperature and pressure for PEM fuel cell applications is in the range of 1-10 atm and 25-120°C [9]. A simple metal hydride such as $LaNi_5H_6$ that incorporates hydrogen into its crystal structure can function in this range, but its gravimetric capacity is too low (∼1.4 wt%) [11] and its cost is too high for vehicular applications.

Complex metal hydrides, such as alanate (AlH_4) materials, have the potential for higher gravimetric hydrogen capacities in the operational window than simple metal hydrides [12]. Sodium alanates ($NaAlH_4$ and $NaAlH_6$) are complex hydrides of aluminium and sodium. Sodium aluminium hydride would seem to be a possible candidate for application as a hydrogen storage material due to its theoretical capacity for storing hydrogen at 5.6 wt% [10]. Despite this high storage capacity, complex aluminium hydrides are not considered as rechargeable hydrogen carriers due to irreversibility and poor kinetics. However, it has been shown that through the use of transition or rare-earth metals as catalysts, these hydrides can be made reversible. In 1997, Bogdanović and Swickardi showed that upon activation using $TiCl_3$ the dehydriding of these hydrides could be kinetically enhanced and maintain reversibility under moderate conditions in the solid-state [13]. The reaction can be summarised as:

$$3NaAlH_4 \rightleftharpoons Na_3AlH_6 + 2Al + 3H_2 \rightleftharpoons 3NaH + 3Al + \frac{9}{2}H_2 \qquad (1.1)$$

Problems with complex metal hydrides include low hydrogen capacity, slow uptake and release kinetics, and cost.

Recently, a new complex hydride system based on lithium amide has been developed. Chen *et al.* [14] initially proposed lithium imide/nitride as a hydrogen storage material due to its high hydrogen capacity of up to 11.5 wt%. The two step decomposition reaction of ($LiNH_2$ + $2LiH$) can be shown as:

$$LiNH_2 + 2LiH \rightleftharpoons Li_2NH + H_2 + LiH \rightleftharpoons Li_3N + 2H_2 \qquad (1.2)$$

The major disadvantage of this Li_3N system is its stability. The thermal desorption profiles show hydrogen generation does not occur until 425°C. It is therefore necessary to develop ways of destabilising this structure. Chen *et al.* have reported the effect of substitution of various elements on the stability of the Li-N-H system [15], [16]. Nakamori and co-workers reported the effect of Mg substitution on the stability of the Li imide/amide systems and found that the decomposition temperature can be reduced to 77°C [17]. Several papers have been recently published [18], [19], [20] on amide/hydride systems because of its high capacity and convenient operation conditions.

A similar system with potential for development is the borohydride system, which shows the highest known hydrogen content. The compound $LiBH_4$ has a gravimetric hydrogen density of 18 wt%. $LiBH_4$ was first synthesised by Schlesinger and Brown [21]. Decomposition is given by the equation:

$$LiBH_4 \rightleftharpoons LiH + B + \frac{3}{2}H_2 \tag{1.3}$$

The decomposition takes place around 300°C [1]. However, the decomposition process is enhanced by the use of a catalyst - for example SiO_2 has been reported to reduce the decomposition temperature to 200°C [22].

Complex hydrides introduce a new field of hydrogen storage materials. While the alanates have been studied extensively during the last six years [23], there are numerous borohydrides with high gravimetric and volumetric hydrogen content being considered as storage materials [24] (Figure 1.1 shows the volumetric and gravimetric hydrogen densities of some selected hydrides). Although storage capacities of complex metal hydrides are theoretically high, there is a significant difference between the theoretical and practically attainable hydrogen capacities. The slow kinetics problem is still a major drawback to complex metal hydrides. Repeated hydrogenation cycles need to be demonstrated to ensure the reversibility of these materials [10].

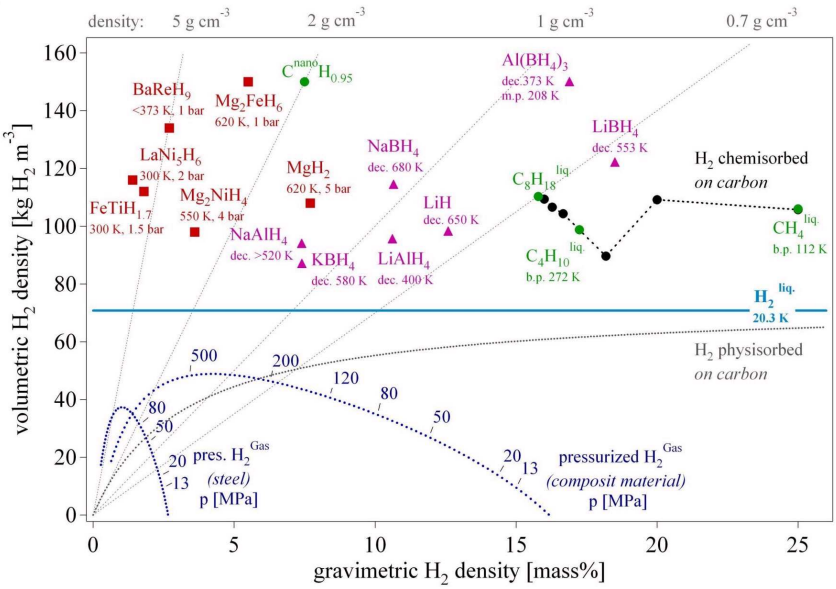

Figure 1.1: Gravimetric and volumetric hydrogen densities of selected metal hydrides [25].

1.2 Chemical Hydrogen Storage

New chemical approaches to hydrogen storage are required to help achieve the 2010 and 2015 hydrogen storage targets. Chemical hydrogen storage is defined as a process whereby the hydrogen is released by a chemical reaction which is induced by hydrolysis or thermolysis. Many materials with high volumetric and/or gravimetric hydrogen densities have been studied over the last few years. A suitable hydrogen storage material needs to form a complex with hydrogen in a solid or liquid state. The optimum material would have hydrogen binding energies greater than a few kcal/mol so the hydrogen would be stable near room temperature, and less than a few dozen kcal/mol to minimise the amount of energy needed to release it [9].

The current focus has been on materials composed of the lighter elements; the driving force for focus on light elements arises from gravimetric and density targets set by the US DOE outlined in section **1**. The major challenges in chemical hydrogen storage are controlling the thermodynamics and kinetics of chemical transformations related to the release and uptake of hydrogen from

materials that meet gravimetric, volumetric, and economic targets.

Much attention has been focused on materials in which hydrogen is stored as E-H bonds - where E is a light main group element such as C, B, N, or O [24]. An example of such a system is the hydrolysis of sodium borohydride. $NaBH_4$ is the most widely commercially produced borohydride and is used in the paper and textile industries, and as a reducing agent in organic synthesis [21]. It is also a commonly used starting material for synthesis of other metal borohydrides. An alternative way of using sodium borohydride is to make use of its reaction with water in an alkaline solution in the presence of a catalyst:

$$NaBH_4 + 2H_2O \rightarrow 4H_2 + NaBO_2 + 300\ kJ \tag{1.4}$$

Hydrolysis of sodium borohydride was controlled using a heterogeneous ruthenium catalyst in Millenium Cell's Hydrogen on Demand^{TM} technology which was demonstrated in the Natrium^{TM} car [26], [27]. If the solution starts at the maximum concentration, the gravimetric yield of hydrogen is about 7.5% [1]. In practice, the product sodium metaborate solution ($NaBO_2$) would be drained away from the catalyst at a refuelling station and replaced with fresh sodium borohydride. However, the high cost of sodium borohydride makes this process unfeasible, and therefore a method of regeneration is needed. This requirement for regeneration hinders commercialisation of borohydride hydrolysis as there are currently no energy efficient routes to convert the stable borate product back to borohydride. Therefore, the main research in this area is in the development of alternative processes for regenerating $NaBH_4$ from the $NaBO_2$ [28].

Following this idea of storing hydrogen in E-H bonds, ammonia has been considered as a potential chemical storage medium. The thermodynamics of hydrogen release from ammonia are less exothermic (more favourable) than hydrocarbons and there is no CO_2 emission. Ammonia presents a cheap and convenient way of storing hydrogen and is particularly stable for transporta-

tion. Pure ammonia is easily liquefied at room temperature and can also be dissolved in water up to very high levels [29], offering further advantages for delivery. Ammonia has been compared with other liquid fuels such as methanol and gasoline [30]. However, ammonia is toxic both to people and to PEM fuel cells [31], and is therefore not suitable for use.

Ammonia borane (NH_3BH_3) also utilised the storage potential of ammonia, furthermore the borane is a good hydrogen source. It is isoelectronic with ethane yet solid at room temperature, and therefore provides comparable gravimetric densities with the corresponding hydrocarbon. However, because it is a solid at standard conditions, it has a far superior volumetric density to that of ethane [9].

1.3 Ammonia Borane

Because of their protic amine-hydrogens and hydridic borane-hydrogens, amineboranes such as ammonia borane (NH_3BH_3) and ammonia triborane ($NH_3B_3H_7$) are unique when compared with other chemical hydrides in their potential ability to store and deliver large amounts of molecular hydrogen through dehydrogenation and hydrolysis (chemical structures of boron compounds discussed in this thesis are shown in figure A.1 in appendix A). With both protic NH and hydridic BH bonds, three H atoms per main group element, and a low molecular weight, ammonia borane has the potential to meet the stringent gravimetric and volumetric hydrogen storage capacity targets needed for transportation applications. Ammonia borane has gravimetric and volumetric hydrogen contents of 19.6 wt% [32] and 0.145 kg L^{-1} respectively giving the compound more hydrogen per unit mass and unit volume than liquid hydrogen (this is illustrated in Figure 1.2, in which ammonia borane occupies half the volume of an equivalent quantity of liquid hydrogen). Ammonia borane is also thermally stable at ambient temperature and is therefore suitable to transport

and store. The US DOE has a target to develop an on-board hydrogen storage system with at least 9 wt% hydrogen by the year 2015 (discussed in section **1**). It appears that an amine-borane-based system has reasonable potential to meet this goal. Ammonia borane was first synthesised and characterised

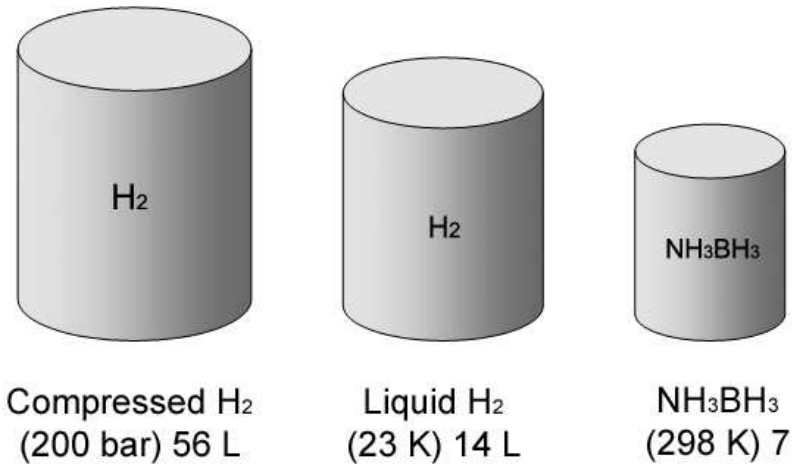

Figure 1.2: Volumes of 1 kg of hydrogen in various forms.

by Shore in the 1950s [33]. Ammonia borane and ammonium borohydride (NH_4BH_4) were first studied in the 1950s for their possible use in rocket fuel [34], an idea that was later abandoned until the late 1990s in which Wolf *et al.* suggested its potential as a good medium for storing hydrogen in a vehicle [35].

1.4 Synthesis

The two most important methods for laboratory-scale preparation of ammonia borane are salt metathesis and direct reaction. Direct reaction of ammonia with diborane occurs via an asymmetrical cleavage to give an ionic solid [36],

which is called the diammoniate of diborane ($[(NH_3)_2BH_2]^+[BH_4]^-$) (equation 1.5). Preparation of the diammoniate of diborane involves passing diborane into liquid ammonia at low temperatures [37], [38]. If diborane is first symmetrically cleaved to give a reactive borane-base adduct, then the direct reaction with ammonia is reported to give a mixture of ammonia borane plus the diammoniate of diborane (equation 1.6) [38].

$$2NH_3 + B_2H_6 \rightarrow [(NH_3)_2BH_2]^+[BH_4]^- \tag{1.5}$$

$$3THF - BH_3 + 3NH_3 \rightarrow [(NH_3)_2BH_2]^+[BH_4]^- + NH_3BH_3 + 3THF \tag{1.6}$$

When ammonia borane is prepared from borane/tetrahydrofuran (borane-THF) or borane/dimethyl sulfide (borane-SMe_2) [39], pure ammonia borane can be obtained by recrystallisation from ether due to the insolubility of the ionic diammoniate of diborane. In 1967, Beachley claimed that ammonia borane slowly rearranges at room temperature to give the thermally more stable diammoniate [40]. However, in 1971, Mayer found that ammonia borane of high purity does not undergo conversion to the diammoniate even when heated at 50°C for 13 days [41].

The reaction of lithium borohydride with ammonium salts gives ammonia borane without the need to work with diborane or a borane complex (equation 1.7 and 1.8) [33].

$$LiBH_4 + NH_4Cl \rightarrow NH_3BH_3 + LiCl + H_2 \tag{1.7}$$

$$2LiBH_4 + (NH_4)_2SO_4 \rightarrow 2NH_3BH_3 + Li_2SO_4 + 2H_2 \tag{1.8}$$

The above reactions are run in diethyl ether, any by-product diammoniate is removed during the filtration to remove the insoluble lithium salts. These reactions result in isolated yields of ammonia borane of approximately 4%. An improved and more convenient procedure has since been developed using sodium borohydride (shown in equation 1.9) [42].

$$NaBH_4 + (NH_4)_2CO_3 \overset{THF}{\rightarrow} NH_3BH_3 + Na(NH_4)CO_3 + H_2 \tag{1.9}$$

Sodium borohydride is less expensive than lithium borohydride and is much easier to handle. Also, a greater yield of pure ammonia borane was obtained (80% isolated).

1.5 Structure

A simple molecular description of NH_3BH_3 shows that it is a donor-acceptor adduct formed as a result of a dative bond between a Lewis acid (BH_3) and a Lewis base (NH_3). The lone electron pair of NH_3 delocalises over an unoccupied p_z orbital of boron in BH_3. This B-N bond is strong enough that under most conditions hydrogen loss is favoured over dissociation to ammonia and borane. NH_3BH_3 contains both hydridic BH and protic NH bonds. The compound is a solid at room temperature primarily due to dihydrogen bonding and dipole-dipole interactions.

1.5.1 Crystal Structure

The structure of ammonia borane has been investigated by several groups since its discovery in 1955 by Shore and Parry [33]. In 1956, Hughes [43] determined a body-centre tetragonal cell at room temperature, and proposed the polar space group ($I4mm$). The NH_3BH_3 molecules are located at the vertices and body-centred of the unit cell, and have all their B-N bonds orientated in the same direction parallel to *c*. This was confirmed by Lippert and Lipscomb [44] when they arrived at the same conclusion as Hughes (neither of these studies located the hydrogen atoms).

Recently Bowden *et al.* reported that a phase change from tetragonal to an orthorhombic structure (space group $Pmn2_1$) occurs below approximately 220 K [45]. Klooster *et al.* reported a structure from single crystal neutron data collected at 200 K, locating all the hydrogen atoms [46]. The orthorhombic and tetragonal structures are shown in Figure 1.3, the tetragonal structure is

depicted with hydrogen atoms in similar positions to the orthorhombic. The hydrogen atoms on the B and N are rotationally disordered and their precise positions, with respect to those in neighbouring molecules, are not known. The major difference between the orthorhombic low temperature structure and the tetragonal room temperature structure is the alignment of the B-N bond. In the orthorhombic structure it is at an angle to the c axis, but parallel to c in the tetragonal phase.

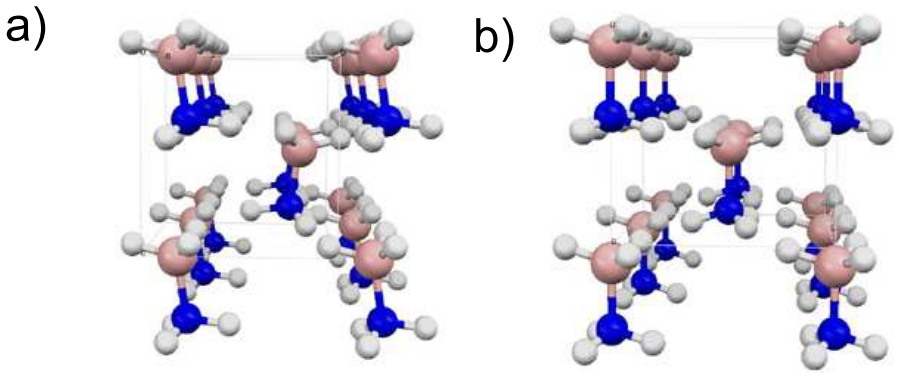

Figure 1.3: Structure of orthorhombic (a) and tetragonal (b) NH_3BH_3.

Ammonia borane exhibits an unusual bonding system that is responsible for its physical properties. The melting point of ammonia borane is much higher than that anticipated. This is due to the intramolecular polarity, the hydrogen atoms bonded to the nitrogen are protic in character while those bonded to boron are hydridic. This leads to a network of N-$H^{\delta+}\cdots^{\delta-}$H-B dihydrogen bonds. These bonds have an interaction energy of 64 kJ mol^{-1} [45]. The hydridic hydrogen atoms attached to the boron are 2.02 Å away from the protic hydrogen atoms attached to the nitrogen of an adjacent molecule [46]. As this distance is less than the Van der Waals distance of 2.4 Å [28] it was concluded that the interaction constitutes a dihydrogen bond. The stability provided by these dihydrogen bonds contributes to the existence of ammonia borane as a solid at standard conditions, giving ammonia borane more favourable hydrogen density than the isoelectronic ethane.

1.6 Hydrolysis

Ammonia borane is relatively stable to hydrolysis in aqueous solution when the pH is basic or neutral, but is rapidly hydrolysed in an acidic solution (equation 1.10) [47].

$$NH_3BH_3 + H^+ + 3H_2O \rightarrow 3H_2 + B(OH)_3 + NH_4^+ \qquad (1.10)$$

Two mechanisms have been proposed for this acid-catalysed hydrolysis [48]. Through analysis of isotope effects and reaction rates, it was concluded that the mechanism of hydrolysis occurs by H^+ interacting with the nitrogen atom which results in the formation of NH_4^+ and release of BH_3 which subsequently interacts with a boron hydride resulting in H_2 release via a five coordinate boron.

Chandra and Xu proposed the use of solid and gaseous acids in the hydrolysis of ammonia borane [47]. Heterogeneous metal-catalysed hydrolysis of ammonia borane has been reported [49], [50]. The highest catalytic activity was realised with Pt/C, followed closely by PtO_2 and $[Rh(cod)Cl]_2$. Each of these catalysts resulted in evolution of 3 molar equivalents of H_2 in less than 5 minutes. Studies of the heterogeneous catalyst materials after reaction showed that the most active catalysts contained the smallest particle sizes and were highly dispersed.

Hydrolysis of ammonia borane may not meet the long term transportation goals due to the introduction of water to the system decreasing the wt% of hydrogen. Secondly, the hydrolysis of ammonia borane generates NH_4OH which would be in a pH-dependent solution-vapour equilibrium with NH_3 [51]. Volatile ammonia in the H_2 stream would need to be removed before reaching the fuel cell. The final problem with hydrolysis is regeneration of ammonia borane from the borate products of hydrolysis, which requires overcoming a large ΔH_{rxn} [28].

1.7 Thermolysis

NH_3BH_3 can release more than 2 moles of H_2 upon heating above room temperature. The overall reaction is exothermic but requires external heating to overcome kinetic barriers. Once the compound is heated sufficiently, the decomposition reaction proceeds on its own. The reactions of hydrogen evolution can be summarised as shown in equations (1.11) through (1.14):

$$nNH_3BH_3 \xrightarrow{\Delta} (NH_2BH_2)_n + (n-1)H_2 \tag{1.11}$$

$$(NH_2BH_2)_n \xrightarrow{\Delta} (NHBH)_n + H_2 \tag{1.12}$$

$$2(NHBH)_n \xrightarrow{\Delta} (NHB - NBH)_n + H_2 \tag{1.13}$$

$$(NHBH)_n \xrightarrow{\Delta} BN + H_2 \tag{1.14}$$

The first step: reaction of ammonia borane to form polyaminoborane (PAB, $(NH_2BH_2)_n$) occurs at <120°C and is an intermolecular process (1.11). The second step: formation of polyiminoborane (PIB, $(NHBH)_n$) from polyaminoborane occurs at approximately 150°C and is also an intermolecular process (1.12). These first two steps amount to 12 wt% hydrogen. At a slightly higher temperature the cross-linking between molecules is observed to release additional hydrogen (1.13). These materials are precursors to boron nitride, which is formed at > 500°C [52], [53] (1.14).

Thermolysis of ammonia borane can occur in the gas, liquid, or solid-state. Because the last increment of hydrogen requires impracticably high temperatures to release it (for vehicular applications), efficient methods are required to dehydrogenate ammonia borane to release hydrogen at moderate temperatures and reasonable rates. As dehydrogenation of ammonia borane results in the formation of polymeric species, rehydrogenation is difficult. To date no one has successfully rehydrogenated the by-products. Devising an energy efficient chemical process to regenerate H_3NBH_3 from dehydrogenated BNH_x material is an important step toward realisation of a sustainable transportation fuel. Modifications to ammonia borane are being studied by a number

of researchers in order to influence the thermodynamics and to allow more efficient rehydriding including: solution phase thermal decomposition, transition metal catalysis, ionic liquid catalysis, ammonia borane encapsulated in silica scaffolding, metal catalysed dehydrogenation, and catalysis with metal hydrides and amides.

1.7.1 Gas Phase Thermolysis

The primary intermediate of the first dehydrogenation step in low pressure gas phase thermolysis has been studied by matrix isolation [54] and mass spectrometric studies [52], [55]. These studies confirmed that this intermediate is the aminoborane monomer NH_2BH_2. Calculations by Nguyen *et al.* [56] found that the barrier for intramolecular H_2 loss from ammonia borane in the gas phase is actually higher than its BN bond dissociation energy. They also proposed a borane catalysed dehydrogenation process, however, further experimental studies are needed to confirm the operation of this reaction pathway. Li *et al.* recently studied the mechanism of steps (1.11) and (1.12) [57]. They investigated a unimolecular transition state for step (1.11) and found that the N-H bond lengthens more than the B-H bond during the H-H bond-forming reaction. They also calculated the activation energy for this process; the activation energy was calculated to be 113.9 kJ mol^{-1}, which supports the observation that H_2 loss from NH_3BH_3 occurs at approximately 100°C. For reaction (1.12) they obtained an activation energy of approximately 290 kJ mol^{-1}.

1.7.2 Solution Phase Thermolysis

The thermal decomposition of ammonia borane in selected polar, aprotic solvents was studied by Geanangel *et al.* [58] using ^{11}B NMR at 80°C (the lowest temperature at which ammonia borane decomposes at an acceptable rate). The purpose of the work was to identify solvents and conditions best suited for preparing and carrying out reactions of NH_2BH_2 generated thermally from ammonia borane. It was hoped that NH_2BH_2, which is subject to facile asso-

ciation in the solid-state [59], would be stabilised sufficiently by solvation to be detectable in solution. If not, the quantities of its oligomers detected in the reaction mixtures would indicate the extent of its formation. Three types of reactions were observed: hydrogen-loss decomposition of NH_3BH_3 leading to cycloborazane(s) and eventually to borazine, base displacement by solvent on NH_3BH_3 giving a solvent-borane adduct, and reaction with the solvent leading to products consistent with a hydroboration pathway. In etheral solvents such as glyme, diglyme, tetrahydrofuran, and 2-methyltetrahydrofuran the reaction proceeded slowly to give mainly products suggesting hydrogen loss decomposition of NH_3BH_3. It was also noted that increasing solvent polarity appeared to lower the reaction rate.

1.7.2.1 Dehydrogenation in Ionic Liquids

Ionic liquids are salts that are liquid at temperatures below 100°C. These salts have unique properties that make them attractive substitutes for organic solvents in hydrogen storage systems [59] such as: negligible vapour pressures, stability at high temperatures, ability to dissolve a wide range of compounds and gases, stabilisation of polar transition states by weakly coordinating anions and cations that provide an inert reaction medium, and recyclability with little loss of activity.

Bluhm *et al.* recently reported dehydrogenation of ammonia borane in ionic liquids such as 1-butyl-3-methylimidazolium chloride (bmimCl) and compared it to solid-state dehydrogenation [60]. They observed that ammonia borane dehydrogenation in bmimCl showed no induction period (discussed in section **1.7.3**) with hydrogen evolution beginning immediately upon placing the sample in a heated oil bath. They measured approximately 1 equivalent H_2 per molecule of ammonia borane, a value greater than that observed in solid-state reactions. In contrast to ether solvents, primarily linear and branched acyclic $[H_2NBH_2]_n$ species were observed, as confirmed by ^{11}B NMR shift calcula-

tions. When 10 mol% $LiNH_2$ was added to solid ammonia borane and the mixture heated to 85°C, an increase in reaction rate with 1 equivalent H_2 generated in 3 hours was observed [61]. Ionic liquids are known to favour the formation of polar intermediates and transition states, and the observation that $[(NH_3)_2BH_2^+]BH_4^-$ and/or BH_4^- are produced in the bmimCl reaction (observed by ^{11}B NMR) suggests that the activating effect of the ionic liquid may be related to its ability to induce formation of such ionic species. These results are interesting as they suggest that there may be a difference in the reaction mechanism and products dependent upon the solvent environment.

Depending on the conditions, several species have been previously observed upon heating ammonia borane such as borazine, cycloborazanes, and polyamino borane. Because they could poison a fuel cell, volatile products such as borazine are undesirable in hydrogen storage applications. Bluhm *et al.* [60] observed that in the bmimCl reactions only minor traces of borazine were detected.

The major drawback of liquid phase thermolysis is the reduction of storage capacity. Solvents like water, glyme, and ionic liquids added to facilitate catalysis or movement of ammonia borane within an engineered storage system dramatically reduce the hydrogen storage capacity [28], making it difficult to meet the DOE targets.

1.7.3 Solid-State Thermolysis

The maximum gravimetric hydrogen yield is obtained from ammonia borane in the neat solid-state. The extensive network of dihydrogen bonding between amine protons and boron hydrides of adjacent ammonia borane molecules has been proposed as the key phenomenon that dictates dehydrogenation from ammonia borane in the solid-state [62].

Geanangel was one of the first researchers to report studies on the thermal dissociation of solid ammonia borane using thermomanometry, pyrolysis, DSC, DTA, and TGA in the 1980s [63], [64]. He observed a sharp endothermic peak beginning at just above 112°C, which corresponds to the melting point of pure ammonia borane ($112 - 114$°C [59]). On further heating, a sharp pressure rise near 120°C due to hydrogen evolution was observed. Upon further heating, the rate of pressure increase slowed as the hydrogen evolution from the first step reached completion. Continued temperature increase resulted in the release of a second equivalent of H_2.

In more recent studies, Wolf and co-workers have revisited the thermal analysis of ammonia borane using controlled calorimetric studies to identify the events leading to dehydrogenation and isolation of products obtained in the process. They also explored the effect of experimental conditions such as heating rate and pressure on the thermal decomposition of ammonia borane [52], [53]. They found that neither hydrogen release rate nor the enthalpic parameters during the thermal decomposition were affected by high hydrogen pressures, which is to be expected since both the transitions (AB→PAB and PAB→PIB) are exothermic. Furthermore, there was little change in the quantities of volatile products generated. However, they did observe that the rate of heating appears to have a measurable impact on the thermal events and the volatile product formation. When the heating rate was less than 1°C/ min only H_2 was observed in the gas phase and the major solid product was PAB. Higher heating rates resulted in greater quantities of volatile products such as borazine and a mixture of products was formed [52], [53]. The formation of volatile products in the absence of subsequent hydrogen purification will be problematic for PEM fuel cells that are poisoned by contaminants in the hydrogen stream.

Although the thermodynamic properties have been reported for the dehydro-

genation reaction in the solid-state, little is known about the mechanism and intermediates leading to the thermal release of hydrogen from ammonia borane. By gaining insight into the reaction mechanism, control of the rates of hydrogen release from ammonia borane might be achieved. Early work showed that hydrogen is released by heating solid-state ammonia borane resulting in a complex mixture of BN_x polymeric products and only a trace of borazine [64]. This is in contrast to decomposition in organic solvents in which cyclotriborazine $N_3B_3H_{12}$ is the predominant intermediate preceding formation of borazine as the major product [58].

Smith *et al.* [65] suggested that the mechanism of hydrogen release from the solid-state occurred through a bimolecular pathway. They analyzed the volatile gases from the thermolysis of a NH_3BH_3/ND_3BH_3 mixture and observed all three hydrogen isotopologues: H_2, D_2, and HD. They concluded that dehydrogenation occurs through a bimolecular pathway if exchange reactions do not compete with hydrogen release. These results are in agreement to those observed for decomposition of the related species dimethylamine borane [66].

Previous work using differential scanning calorimetry experiments showed the decomposition of solid-state ammonia borane followed sigmoidal kinetic behaviour, typical of a nucleation and growth pathway. However, little detail about the chemical transformations of ammonia borane during the induction, nucleation, and growth phases could be obtained by this method. Recently Stowe *et al.* [67] followed the mechanism of decomposition of ammonia borane and evolution of boron-containing non-volatile intermediates and products using *in situ* ^{11}B MAS-NMR see Figure 1.4. Ammonia borane was heated to 88°C and $^{11}B\{^1H\}$ NMR spectra were recorded at 2 minute intervals. The authors proposed a mechanism for the thermal dehydrogenation of ammonia borane showing discrete induction, nucleation, and growth steps leading to hydrogen release (Figure 1.5). Their results suggest that during the induction

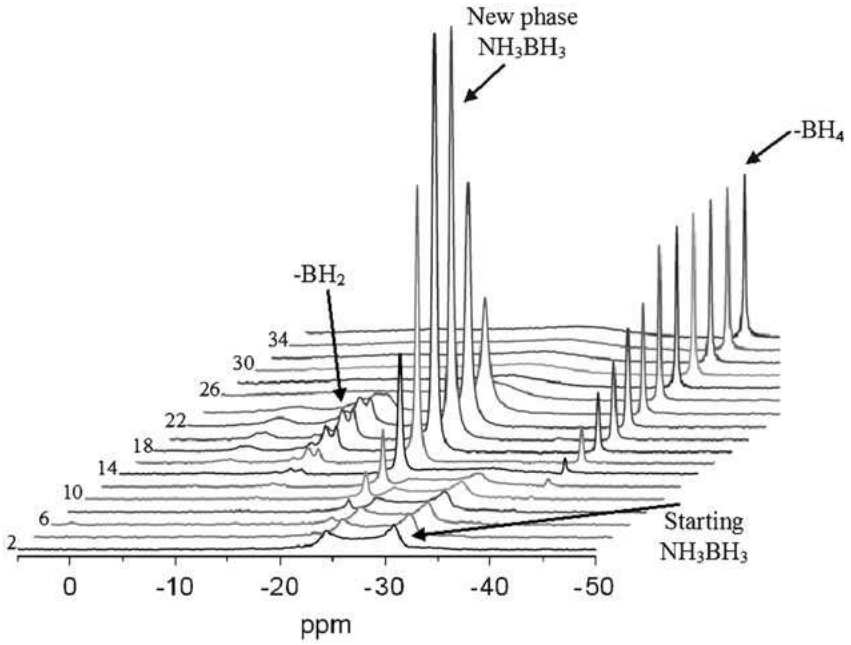

Figure 1.4: Time resolved $^{11}B\{^1H\}$NMR spectra showing the thermal decomposition of NH_3BH_3 [67].

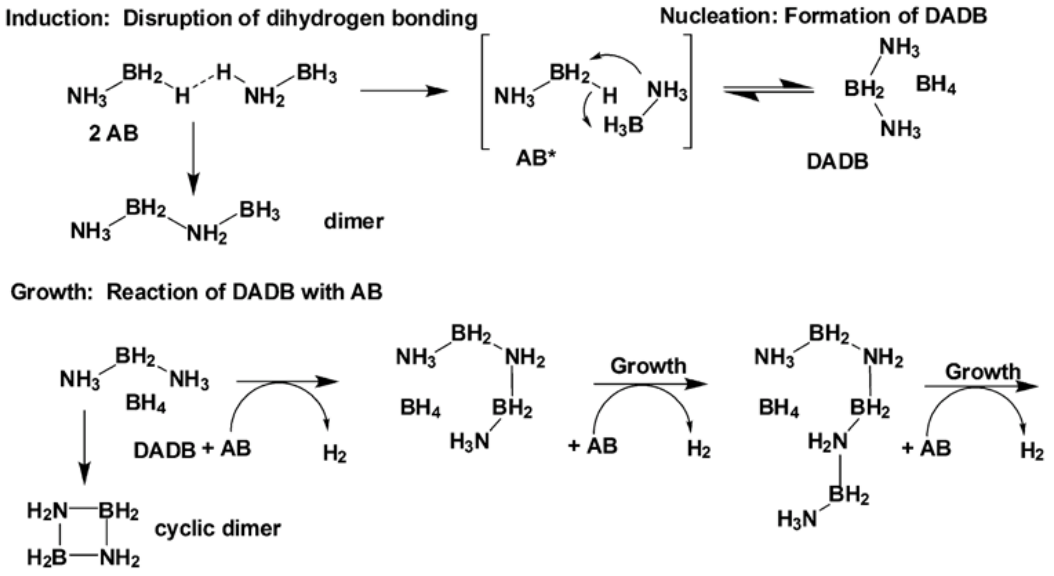

Figure 1.5: Proposed thermal dehydrogenation mechanism of ammonia borane showing discrete induction, nucleation and growth steps leading to hydrogen release [67].

period, the hydrogen bonding network is disrupted permitting greater motion of the molecules leading to the formation of a more mobile phase ammonia borane (AB*) resonating at -23 ppm. The mobile phase then converts to yield the nuclei-forming species diammoniate of diborane (DADB). Little hydrogen

is released in this stage of the reaction, however, conditions are being prepared for the nucleation - if the sample is quickly cooled back to room temperature at this stage and then reheated the decomposition reaction proceeds with little apparent induction. Once the DADB is present, growth and hydrogen release occur by bimolecular reactions between unreacted ammonia borane and the DADB leading to the formation of hydrogen and polyaminoborane precursors.

This scheme assumes that the N-H and/or B-H bonds of DADB are more reactive that the corresponding N-H or B-H bonds of ammonia borane. If the N-H bonds of DADB are more acidic than the N-H bonds of ammonia borane, there would be a lower energy barrier for the reaction of DADB + AB to yield hydrogen than between two ammonia borane molecules. If DADB is more reactive than ammonia borane, then the addition of DADB to ammonia borane would significantly reduce the induction period. The authors performed an experiment in which a small amount of DADB was added to ammonia borane, they observed a significant reduction in the induction period.

1.7.3.1 Nanophase Ammonia Borane in Mesoporous SBA-15

Gutowska *et al.* recently reported thermolysis of ammonia borane contained within mesoporous silica scaffolds SBA-15 [68] - a type of material often used as a substrate for catalysts because it provides a substantially large surface area for reactions. Ammonia borane was deposited into SBA-15 using a methanol carrier solvent, achieving a 1:1 weight ratio between the chemical hydride and the mesoporous substrate. This resulted in significantly different behaviour lowering the dehydrogenation temperature from 114°C to 85°C accompanied by a relatively low exothermicity. The two other notable effects resulting from the nanostructure of ammonia borane in the SBA-15 scaffold included the temperature threshold for H_2 release being notably lower than the temperature threshold for neat ammonia borane which is indicative of an enhanced rate of H_2 release. Also the yield of the volatile borazine side product is sig-

nificantly lower than for neat ammonia borane.

Solid-state ^{11}B NMR spectroscopy was used to analyze the non-volatile products from neat ammonia borane and ammonia borane in SBA-15 to see if the borazine became entrapped within the mesoporous scaffold. However, no ^{11}B signal for borazine was observed. As borazine is not observed as a volatile product or non-volatile product, the mesoporous scaffold appears to affect the decomposition pathways of ammonia borane that lead to hydrogen formation. While this approach has desirable effects on the kinetics of the dehydrogenation reactions, it also suffers the same problems as solution phase dehydrogenation in that the H_2 density is reduced considerably, even at 1:1 loading.

1.7.3.2 Catalysis Using Metal Hydrides and Amides

As discussed in section **1.5** NH_xBH_x materials have both hydridic and protic hydrogen. These materials can react with themselves or with other hydridic and/or protic hydrogen containing species - for example, MgH_2—H_3NBH_3—H_2NLi. In August 2005, members of the International Partnership for the Hydrogen Economy (IPHE), including researchers from Pacific Northwest National Laboratory, Los Alamos National Laboratory, University of Oxford, National University of Singapore, and Industrial Research, met at an organised American Chemical Society meeting to propose a collaborative proposal to improve the performance of ammonia borane. During this meeting the idea to alter the thermodynamic properties of ammonia borane by modifying it with amide and hydrides was proposed. It was hoped that the polarity and intermolecular interaction (dihydrogen bonding) of ammonia borane could be altered resulting in different dehydrogenation mechanisms and thermodynamics.

Ping Chen and colleagues at the National University of Singapore have been studying the reactions of LiH, NaH, and Li_2NH with ammonia borane [69].

They have found that the interaction between LiH and ammonia borane (reacted by ball milling) results in an amorphous phase in which more than 15 wt% hydrogen can desorb at temperatures below 140°C through a mild endothermic process. Solid-state ^{11}B NMR spectra of the post milled samples revealed that B in a BH_3 environment was the dominant species (chemical shift of -23 ppm), indicating that hydrogen desorption during ball milling comes from the LiH and -NH_3 in ammonia borane. As a result they proposed the following reaction:

$$LiH + NH_3BH_3 \rightarrow BH_3 - LiNH_2 + H_2 \tag{1.15}$$

The solid complex should be a complex of BH_3 and lithium amide, an analogue of ammonia borane. Replacing H by the more electropositive Li in NH_3 will lessen the charge load on the other two H atoms weakening the dihydrogen bonds between BH_3-$LiNH_2$ in the bulk material.

This group at the National University of Singapore in collaboration with Industrial Research have investigated the reaction between lithium imide (Li_2NH) and ammonia borane [70]. An amorphous product was obtained, and the following reaction was proposed:

$$Li_2NH + NH_3BH_3 \rightarrow Li_2NBH_2NH_3 + H_2 \tag{1.16}$$

This amorphous phase evolved hydrogen in two stages, the first desorption occurred at approximately 50°C, the second desorption maximum occurred at 150°C. After heating to 300°C a mixture of high and low temperature Li_3BN_2 phases and BN_2H_4 were present. The ready conversion to Li_3BN_2 is significant. This is a stable crystalline material existing in at least two temperature dependent phases. Chemically, the material exists as Li cations decorating N-B-N linear anions. The existence of this stable anion is significant as it demonstrates the persistence of the N-B-N moiety which forms on reaction of the imide (or amide) with ammonia borane with retention of ammonia.

Attempts to re-hydrogenate this phase were somewhat successful leading to 2.4 wt% hydrogen being re-absorbed at 80 bar H_2 pressure. While the wt% H_2 re-absorption is relatively low, this is the first time a boron containing material has been shown to re-absorb hydrogen under these conditions.

It is known that the base strength increases across the series:

$$NH_3 < LiNH_2 < Li_2NH < Li_3N \tag{1.17}$$

Reaction of NH_3 with ammonia borane reportedly produces an amorphous product with no gas evolution [70].

1.7.4 Regeneration of Ammonia Borane

The efficient regeneration of ammonia borane from spent fuel BNH_x is certainly one of the most challenging problems that will have to be overcome in order to utilise ammonia borane based hydrogen storage systems. Calculations indicate that direct hydrogenation reactions using H_2 or H_2-surrogates cannot regenerate ammonia borane from BNH_x materials without significant energy input. The development of a general regeneration process is further complicated by the fact that, depending on the conditions and extent of H_2-release, a variety of molecular, polymeric, and/or solid-state materials with very different chemical reactivities are formed. Figure 1.6 shows the divergent reaction pathways observed during non-aqueous dehydrogenation of ammonia borane, where each arrow represents a hydrogen loss; (a) thermolysis in ionic liquids or in the solid-state, (b) transition metal catalysed dehydrocoupling and (c) in the uncatalysed solution thermolysis. Thus, a viable process must be both capable of regenerating all of these spent fuel materials and avoid the formation of difficult to reduce intermediates (e.g., those containing boron-oxygen bonds).

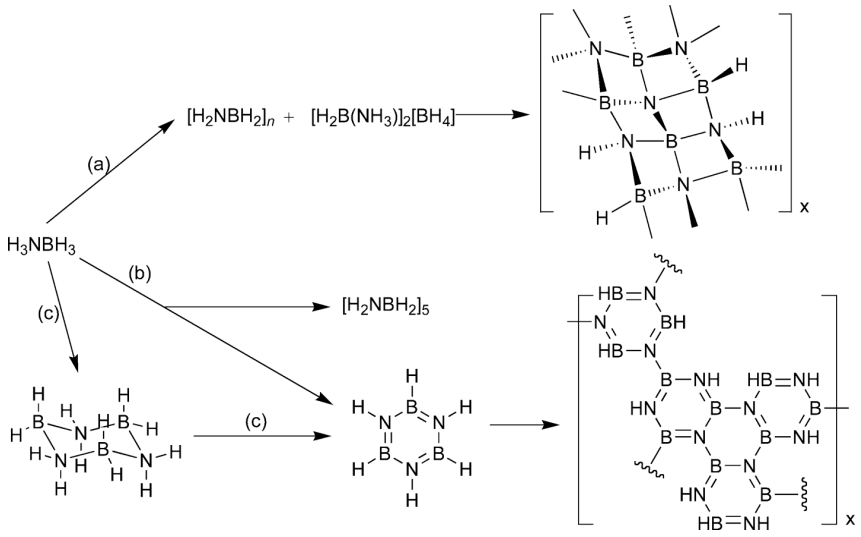

Figure 1.6: Divergent reaction pathways observed during non-aqueous dehydrogenation of ammonia [28].

1.8 Methyl Derivatives of Ammonia Borane

The properties of amine-boranes are highly dependent upon the substituent atoms or groups on boron and nitrogen. Largely through the thermodynamic studies of Brown and co-workers [71], steric effects on the substituent alkyl groups on the strength of the B-N bond have been correlated. Thus, sterically hindered alkyl ligands form significantly less stable amine boranes.

1.8.1 Methylamine Borane

Methylamine borane is the simplest methyl derivative of ammonia borane. As with ammonia borane, methylamine borane has a high hydrogen storage capacity (9 wt%). As discussed in section **1.7.4**, thermolysis of ammonia borane results in the formation of BNH_x polymeric species making regeneration of ammonia borane from the spent material difficult. The thermolysis of methylamine borane (which will be discussed in section **1.8.1.3**) results in the formation of cyclic decomposition products that are most likely soluble in a range of solvents, which increases the likelihood of chemical regeneration. It is for this reason that methyl derivatives of ammonia borane have attracted attention for use in hydrogen storage materials.

1.8.1.1 Synthesis

Mono-, di-, and tri-alkylamine-borane adducts can be prepared directly from diborane [72], or from an active borane-base complex. The second major route to alkylamine-borane adducts is the reaction of an amine hydrochloride salt with any borohydride. This route was originally reported by Schaeffer and Anderson [73] equation 1.18:

$$LiBH_4 + (CH_3)_3NHCl \rightarrow (CH_3)_3NBH_3 + LiCl + H_2 \qquad (1.18)$$

Synthesis of methylamine borane from methylamine hydrochloride and sodium borohydride in monoglyme has been reported [74].

1.8.1.2 Structure

Bowden *et al.* [75] recently determined the crystal structure of methylamine borane. The structure (Figure 1.7) was found to consist of chains of $CH_3NH_2BH_3$ molecules extending along the *b*-axis of an orthorhombic unit cell. The molecules within these chains are oriented with their B-N bonds aligned in alternate directions and are linked via N-H$^{\delta+\cdots\delta-}$H-B dihydrogen bonds shown in Figure 1.7b (similar to those in ammonia borane). It was calculated that the dihydrogen bonds are 2.21 Å in length, which is similar to the longer of the H$\cdots$H distances found by Klooster *et al.* [46] in orthorhombic ammonia borane (discussed in section **1.5.1**). Intermolecular bond distances and angles show that B, C, and N all have the expected tetrahedral coordination.

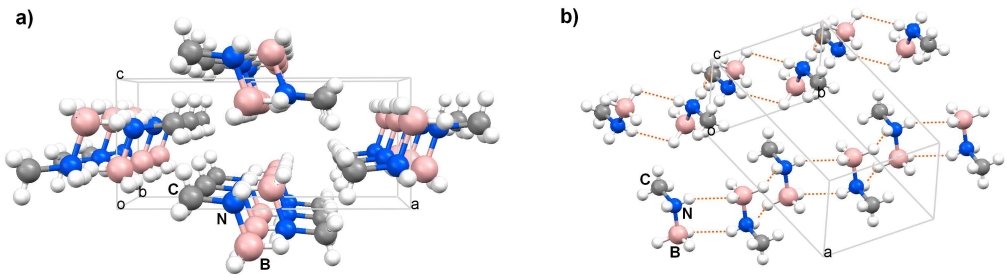

Figure 1.7: Crystal structure of $CH_3NH_2BH_3$.

1.8.1.3 Thermolysis

During thermal decomposition, methylamine borane evolves two moles of hydrogen. It has been noted that hydrogen is evolved upon heating, and the decomposition products have been identified as the *cis*- and *trans*-N-trimethylcyclotriborazane $(CH_3NHBH_2)_3$ and N-trimethylborazine $(CH_3NBH)_3$ [76], [77]. In 1967 Beachley [40] provided a detailed study of the thermal decomposition of methylamine borane, using indirect methods to propose the following reaction sequence:

$$2MeNH_2 - BH_3 \rightarrow [MeNH_2 - BH_2 - MeNH_2]^+ + BH_4^- \tag{1.19}$$

$$[MeNH_2 - BH_2 - MeNH_2]^+ + MeNH_2 - BH_3 \rightarrow [MeNH_2 - BH_2 - MeNH - BH_2 - MeNH_2]^+ + H_2 \tag{1.20}$$

$$[MeNH_2 - BH_2 - MeNH - BH_2 - MeNH_2]^+ + BH_4^- \rightarrow MeNH_2 - BH_2 - MeNH - BH_2 - MeNH - BH_3 + H_2 \tag{1.21}$$

$$MeNH_2 - BH_2 - MeNH - BH_2 - MeNH - BH_3 \rightarrow (-MeNH - BH_2 -)_3 + H_2 \tag{1.22}$$

Surprisingly, very little subsequent information has been published detailing the properties and thermolysis of methylamine borane. Bowden *et al.* [75] recently studied the decomposition using a combination of thermal analysis, mass spectrometry, and nuclear magnetic resonance spectroscopy. They found that the quantity and rate of hydrogen release is dependent on temperature and time. They observed that thermal decomposition to liberate hydrogen occurs at or above 80°C; for the first equivalent an activation energy of 115 kJ mol^{-1} and an enthalpy of -25 kJ mol^{-1} were measured. BH_4^- was identified as an early reaction intermediate, which is in agreement with Beachley's [40] prior proposal for the reaction mechanism (equations 1.19-1.22). The reaction then proceeds to form larger molecules containing N-BH_2-N sub-units until N-trimethylcyclotriborazane is formed. Cross-linking occurs to yield a

non-volatile amorphous product. Further hydrogen is liberated in a second decomposition at 90°C, but little information about this reaction was obtained.

The decomposition products *cis*- and *trans*- $(CH_3NHBH_2)_3$, and $(CH_3NBH)_3$ are most likely soluble in a range of solvents. $(CH_3NHBH_2)_3$ is reportedly soluble in chloroform, acetonitrile, monoglyme, methanol, and benzene, which increases the likelihood of chemical regeneration [74].

1.9 Research Aims

This research will be undertaken at Industrial Research Limited (IRL). IRL has joined with world leading hydrogen research teams from the US, UK, and Singapore in a sustainable long-term collaboration to develop new solutions to hydrogen storage.

The primary aim of this research is to design and synthesise new materials to safely store hydrogen in the form of new chemical hydrides (Li-NH_xBH_y) whose thermodynamics will be controlled by adjustment of the hydrogen bonding environment.

The specific aims of this project are to:

- Study the reaction between lithium amide and ammonia borane.
- Characterise any phases formed as a result of the above reaction.
- Determine the mechanism by which hydrogen is stored and released from these new phases.
- Determine the weight percent of hydrogen evolved during decomposition of these phases.
- Identify and characterise the dehydrogenated material.

- Investigate the effect of substitution of ammonia borane on the mechanism and kinetics of the above reaction.

Chapter 2

Experimental

2.1 Introduction

Outlined in this chapter are the methods used for the preparation and analysis of the chemical hydrides studied in this thesis. Also included in this chapter are details of the analytical instruments and techniques used to investigate the properties of these materials. Each subsection outlines a method or instrument employed during this research.

2.2 Sample Preparation

2.2.1 Starting Materials

All the starting materials were synthesised from commercial grade powders (used as supplied). The chemicals and their purities, as assayed by the manufacturer, are given in Table 2.1.

2.2.2 Preparation of Ammonia Borane

During the course of this research two methods of synthesising ammonia borane were used. The first method of synthesis (method 1) was originally reported by Hu *et al.* [42]. This method produced acceptable yields, however, crystal

Chemical	Purity	Manufacturer
Sodium borohydride	99%	Acros Organics
Ammonium carbonate	R.G	Sigma-Aldrich
Sodium borodeuteride	98%	Isotec
Deuterium oxide	99.9%	Cambridge Isotope Laboratories Inc.
Lithium amide	95%	Sigma-Aldrich
Ammonia borane	90%	Sigma-Aldrich
Methylamine hydrochloride	Not specified	Sigma-Aldrich
Dimethyl sulfoxide-d^6	99.9%	Cambridge Isotope Laboratories Inc.

Table 2.1: Chemicals used and their respective purities and manufacturers.

size and morphology were inconsistent and scalability was limited. Therefore, a new method of synthesis was devised to allow for large scale synthesis and high quality crystals (method 2).

Method 1:

Ammonium carbonate (0.1 mol) and sodium borohydride (0.1 mol) were stirred together in tetrahydrofuran (THF) (150 mL) in a dry 500 mL Erlenmeyer flask at 40°C - maintained by means of a water bath. The ensuing reaction resulted in the evolution of hydrogen which was monitored by means of a gas burette. Once hydrogen evolution had ceased, the reaction mixture was left to cool to room temperature and filtered through a sintered glass filter - porosity 3 (P3). The solvent was removed from the filtrate through rotary evaporation at 20°C. The resulting ammonia borane was dissolved in dry diethyl ether (dried over 5 Å molecular sieves) and filtered to remove any insoluble material. The solution was pumped under vacuum at room temperature for several hours to remove the diethyl ether resulting in large white needle-like crystals of ammonia borane (75% yield).

Purity of the product ammonia borane was assessed by means of X-ray powder

diffraction, ^{1}H NMR spectroscopy and infrared spectroscopy.

^{1}H NMR: δ 1.35 (BH_3, q), δ 4.39 (NH_3, br, s)

X-ray powder diffraction: The d spacings and intensities observed for NH_3BH_3 are summarised in Table 2.2 and the XRD trace is given in Figure 3.5

dÅ	**I (%)**
3.70	100
3.62	21
2.62	12
2.51	3
2.12	3
2.08	3
1.62	1

Table 2.2: X-ray powder diffraction peak data of ammonia borane prepared by method 1.

IR spectral bands for purified NH_3BH_3 (given in cm^{-1}): 3300 (NH stretch), 2400 (BH stretch), 1625 (NH bend), 1383 (NH rock), 1180 (BH bend), 1065, 782 (BH rock), 727 (BN stretch)

Method 2:

Ammonium carbonate (0.3 mol) and sodium borohydride (0.3 mol) were ball milled in THF (330 mL) with 10 mm zirconia balls (2.5 kg) for 8 hours. The reaction mixture was filtered though a sintered glass filter (P3). The solvent was removed from the filtrate through rotary evaporation at 20°C. The resulting ammonia borane was recrystallised via a single solvent recrystallisation from isopropyl alcohol (IPA) (16 mL g^{-1} ammonia borane) resulting in large white needle-like crystals of ammonia borane (80% yield).

Samples appeared phase-pure by analysis with X-Ray powder diffraction and proton NMR spectroscopy.

^{1}H NMR: δ 1.35 (BH_3, q), δ 4.39 (NH_3, br, s)

X-ray diffraction: The d spacings and intensities observed for NH_3BH_3 are summarised in Table 2.3, and the XRD trace is given in Figure 3.8

dÅ	**I (%)**
3.70	100
3.62	5
2.62	18
2.12	2
1.85	1
1.66	2

Table 2.3: X-ray powder diffraction peak data of ammonia borane prepared by method 2.

2.2.3 Synthesis of ND_3BH_3

ND_3BH_3 was synthesised according to the method first reported by Hu *et al.* [42] in which NH_3BH_3 (0.01 mol) was dissolved in deuterated water (0.1 mol) followed by the removal of water by vacuum on a rotary evaporator at 30°C. Once all the water was removed, the process was repeated yielding powdered white ND_3BH_3 which was used as obtained. Purity of the product ND_3BH_3 was assessed by means of ^{1}H NMR spectroscopy.

^{1}H NMR: δ 1.35 (BH_3, q)

2.2.4 Synthesis of NH_3BD_3

NH_3BD_3 was synthesised according to method 1 described in section **2.2.2** substituting sodium borodeuteride for sodium borohydride.

In a typical reaction sodium borodeuteride (0.02 mol) and ammonium carbonate (0.02 mol) were stirred together in THF (150 mL) at 40°C until hydrogen evolution ceased. The resulting mixture was cooled and filtered through a sintered glass filter (P3). The solvent was removed from the filtrate by means of rotary evaporation. The product NH_3BD_3 was dissolved in dry diethyl ether (dried over 5 Å molecular sieves) and filtered to remove any insoluble material. The solution was pumped under vacuum at room temperature for several hours to remove the diethyl ether resulting in small white needle-like crystals of NH_3BD_3 (70% yield). Purity was assessed by means of ^{1}H NMR spectroscopy.

^{1}H NMR: δ 4.39 (NH_3, s)

2.2.5 Synthesis of Methylamine Borane

Methylamine borane was synthesised via a modification of methods previously reported by Gains and Schaffer [74] and Beachley [40], by reacting sodium borohydride and methylamine hydrochloride salt, which had previously been dried at 100°C in an oven and ground using a mortar and pestle. In a typical reaction methylamine hydrochloride (0.4 mol) and sodium borohydride (0.4 mol) were stirred together magnetically in THF (150 mL). The reaction between methylamine hydrochloride and sodium borohydride occurs at ambient conditions, as a result the reaction was maintained at a temperature of 25°C using a water bath as previously described.

The reaction mixture was filtered to remove any insoluble impurities and the solvent stripped from the filtrate using a rotary evaporator. A yield of 70% $CH_3NH_2BH_3$ (based on sodium borohydride) was obtained. Purity was as-

sessed by means of ^{1}H NMR spectroscopy and X-ray diffraction.

^{1}H NMR: δ 1.35 (BH_3, q), δ 4.39 (NH_2, br, s), δ 2.36 (Me, t $J = 1.8$ Hz)

X-ray powder diffraction: The d spacings and intensities observed for $CH_3NH_2BH_3$ are summarised in Table 2.4, the XRD trace is given in Figure 3.15.

d(Å)	I	d(Å)	I
5.576	8	2.702	7
4.531	36	2.576	8
4.293	100	2.485	7
3.994	18	2.419	9
3.763	27	2.276	10
3.705	20	2.079	8
3.363	28	1.989	7
3.247	17	1.789	4
2.781	7		

Table 2.4: Methylamine borane X-ray powder diffraction data.

2.3 Synthesis of Solid-State Hydrogen Storage Materials

Unless otherwise stated, all manipulations were carried out under an argon atmosphere in dry glassware (dried in an oven at 100°C). The general reaction method is described below in section **2.3.1**. All reactions were carried out using this method unless otherwise stated.

2.3.1 Reaction between NH_3BH_3 and $LiNH_2$

In an argon atmosphere controlled glove box (section **2.3.8**) the starting materials for the experiments in a series of specific molar ratios were weighed into a clean and dry 100 mL round bottom flask.

This flask was fitted with a glass stopper (Figure 2.1) which was especially designed using polytetrafluoroethylene (PTFE)[1] taps to enable control of the atmosphere within the flask and prevent exposure of the materials to oxygen. High temperature grease was used to ensure an air-tight seal, and a metal joint clamp was used to ensure the seal remained intact when a build up of pressure within the flask occurred.

Figure 2.1: Gas flow controlling stopper.

All taps on the vessel were closed in order to retain the argon atmosphere after the vessel was removed from the glove box. This vessel was then connected to the reaction setup shown in the schematic diagram (Figure 2.2). The glass was attached to a metal inlet tube and outlet tube using Swagelok connections. The outlet was heated using heating tape to 120°C to prevent any species generated condensing in the outlet tube.

[1]PTFE is a type of polymer that can withstand heating to high temperatures (melting point 327°C).

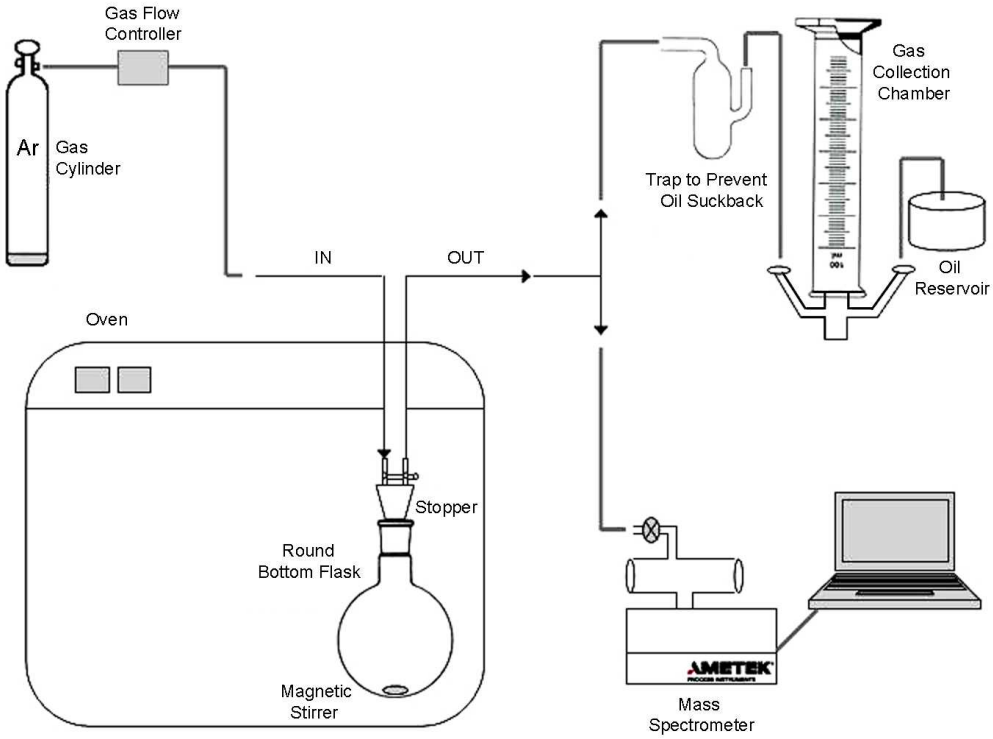

Figure 2.2: Schematic diagram of experimental setup.

The starting materials were mixed using a magnetic stirrer and stir bar. Once the starting materials were homogeneously mixed, the taps were opened to the outlet tube and the resulting material was heated from room temperature to 250°C at a rate of 1°C min^{-1} and held for 10 minutes.

During the course of heating, the outlet tube was connected to either the gas burette to measure the amount of gas generated in the reaction (this is described in more detail in section **2.3.3**) or a mass spectrometer to analyse the composition of gases generated (section **2.3.2**). The percentage of weight lost during the course of these reactions was also assessed (section **2.3.4**).

2.3.2 Mass Spectrometry

Mass spectrometry was used to analyse the composition of gases generated throughout the course of these reactions. All spectra were run on a Dymaxion

benchtop mass spectrometer (model DM100). An argon (BOC - 130) carrier gas was used at a flow of 10 mL min^{-1}, regulated using a mass flow controller. Acquisition of data, and access to data collected was via the Dycor process 200 software.

2.3.3 Gas Volume Measurements

Determination of the molar volume of gas generated in the reactions was achieved by bubbling the evolved gas through paraffin oil before collection in a gas burette (as shown in Figure 2.2) to give the total volume of gas generated.

An acid-base titration was performed for a quantitative analysis of the concentration of ammonia generated during the course of the reaction. The evolved gas was bubbled through 0.1 mol L^{-1} HCl (50 mL) before collection of gas in the burette. Once the reaction was complete (heated to 250°C), 10 mL aliquots of the HCl were titrated against 0.1 mol L^{-1} NaOH using phenolphthalein as an indicator to determine the point of neutralisation.

2.3.4 Determination of Percentage Weight Loss

The weight of the reaction vessel and sample were determined before reacting the two starting materials. Once the reaction was complete (heated to 250°C), the flask was flushed with argon to displace any residual H_2 or NH_3 gas present in the vessel. The reaction vessel and sample were then weighed to determine the percentage of weight lost during the reaction.

2.3.5 High Temperature Thermal Decomposition

2.3.5.1 Closed System

A series of post-mixed NH_3BH_3 + $LiNH_2$ samples in a series of specific molar ratios were heated in a closed system - using a stainless steel bomb which had been especially designed - to temperatures of 400°C, 500°C, and 600°C to

investigate the formation of phases during the final stage of decomposition.

2.3.5.2 Flow-Through System

A series of post-mixed NH_3BH_3 + $LiNH_2$ samples in a series of specific molar ratios were also heated to 400°C, 500°C, and 600°C in open aluminium oxide crucibles under flowing argon (BOC - 130).

All high temperature work was performed in tube furnaces, consisting of 690 mm long ceramic tubes 50 mm in diameter, heated by six surrounding silicon carbide resistance elements. The tubes are enclosed by glass fittings through which gas can be delivered to provide the desired environment for the firing. The same heating and cooling regime was used for all the samples. Samples were placed in the centre of the furnace and the temperature was ramped to the desired temperature at a rate of 1°C/min. Samples were held at the target temperature for 1 hour then cooled to room temperature.

2.3.6 Reaction Between ND_3BH_3, NH_3BD_3 and $LiNH_2$

Ammonia borane isotopologues ND_3BH_3 and NH_3BD_3 were reacted with $LiNH_2$ to study the mechanism of the reaction between ammonia borane and lithium amide.

The reaction between both ND_3BH_3 and NH_3BD_3 with $LiNH_2$ was carried out using the same method described above for the NH_3BH_3 and $LiNH_2$ reaction (section **2.3.1**). During the course of the reaction argon was flushed through the system at a flow rate of 10 mL/min. The mass spectra of the evolved gas was analysed as a function of temperature. This mass spectral data was used to study the mechanism of the reaction between ammonia borane and lithium amide.

2.3.7 Reaction Between $CH_3NH_2BH_3$ and $LiNH_2$

The reaction between $CH_3NH_2BH_3$ and $LiNH_2$ was carried out via the same method described for the NH_3BH_3 and $LiNH_2$ reaction above (section **2.3.1**).

2.3.8 Handling of Materials

Because of the air and moisture-sensitivity of the compounds, all the materials were handled using a Labmaster 100 Innovative Technology Inc. Argon Atmosphere Controlled Glove Box Version 53 basic glove box and gas purification system (O_2 content <10 ppm) (Figure 2.3).

Figure 2.3: Argon atmosphere controlled glove box.

2.4 Characterisation

2.4.1 X-ray Diffraction

Powder X-ray diffractometry was the predominant method used for the qualitative analysis of the samples prepared during the course of this research. Within the glove box the samples were loaded into a specifically designed protective gas XRD cell (Figure 2.4). Samples were analysed using a Bruker D8

Advance diffractometer with an incident beam Goebel mirror and 0.23 degree parallel plate diffracted beam collimator using Co Kα radiation (Figure 2.5).

A 2-theta scan from 4° to 80° at a rate of 0.5° per minute was used.

Figure 2.4: Protective gas X-ray diffraction cell.

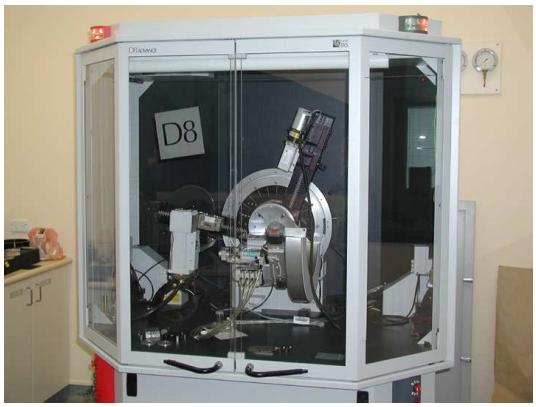

Figure 2.5: Bruker D8 Advance diffractometer.

Identification of the phases was by matching with those in the database maintained by the International Centre for Diffraction Data using the software program EVA, a module of Diffrac-Plus (Bruker AXS).

2.4.2 Infrared Spectroscopy

A Perkin Elmer Spectrum One FT-IR Spectrometer was used to obtain IR spectra. The Spectrum One FT-IR instrument (Figure 2.6) consists of a globar and mercury vapour lamp as sources, an interferometer chamber comprising KBr and Mylar beam splitters and a scan range of MIR 450-4000 cm^{-1}.

Infrared spectra of solid samples were obtained in the form of KBr discs.

2.4.3 ^{1}H NMR Spectroscopy

Proton NMR spectra were obtained in d^{6}-dimethyl sulfoxide (DMSO) using a 300 MHz Bruker AC300 spectrometer. Chemical shifts are reported in δ parts per million referenced from external tetramethylsilane (TMS).

Figure 2.6: Perkin Elmer Spectrum One FT-IR Spectrometer.

2.4.4 Solid-State ^{11}B NMR Spectroscopy

Selected powered samples were analysed by solid state ^{11}B MAS NMR spectroscopy at 11.7 T using a Varian Unity 500 spectrometer with a 4 mm Doty MAS probe spun at ∼10 kHz. The spectrometer frequency for ^{11}B was 160.36 MHz with a 1 s pulse and a 30 s delay.

Chapter 3

Synthesis of Ammonia Borane and its Derivatives

3.1 Introduction

This chapter covers the experimental work carried out on the synthesis of ammonia borane and its derivatives. Commercial grade ammonia borane is available commercially, however, because of low purity, high cost, and shipping restrictions (due to safety restrictions), ammonia borane used throughout the course of this research was synthesised. Several synthetic routes to NH_3BH_3 have been reported [33], [78], [38]. The two most important methods for laboratory-scale preparation of ammonia borane are salt metathesis and direct reaction. During the course of this research ammonia borane was synthesised via a salt metathesis method - as described in section **2.2.2**. The majority of ammonia borane used was prepared via method 2 outlined in section **2.2.2**. The main tools used for the characterisation of materials were powder X-ray diffraction and ^{1}H NMR spectroscopy.

3.2 Synthesis of Ammonia Borane

Synthesis of ammonia borane in this study initially followed the method reported by Hu *et al.* [42], in which ammonium carbonate and sodium borohy-

dride were reacted in a 1:1 molar ratio in anhydrous THF (see section **2.2.2**). The ensuing reaction resulted in the evolution of hydrogen gas (1 mol based on $NaBH_4$), which was rapid at first but gradually slowed, eventually ceasing once reaction had gone to completion. The rate of hydrogen release was monitored volumetrically by means of an attached gas collection chamber as shown in Figure 3.1.

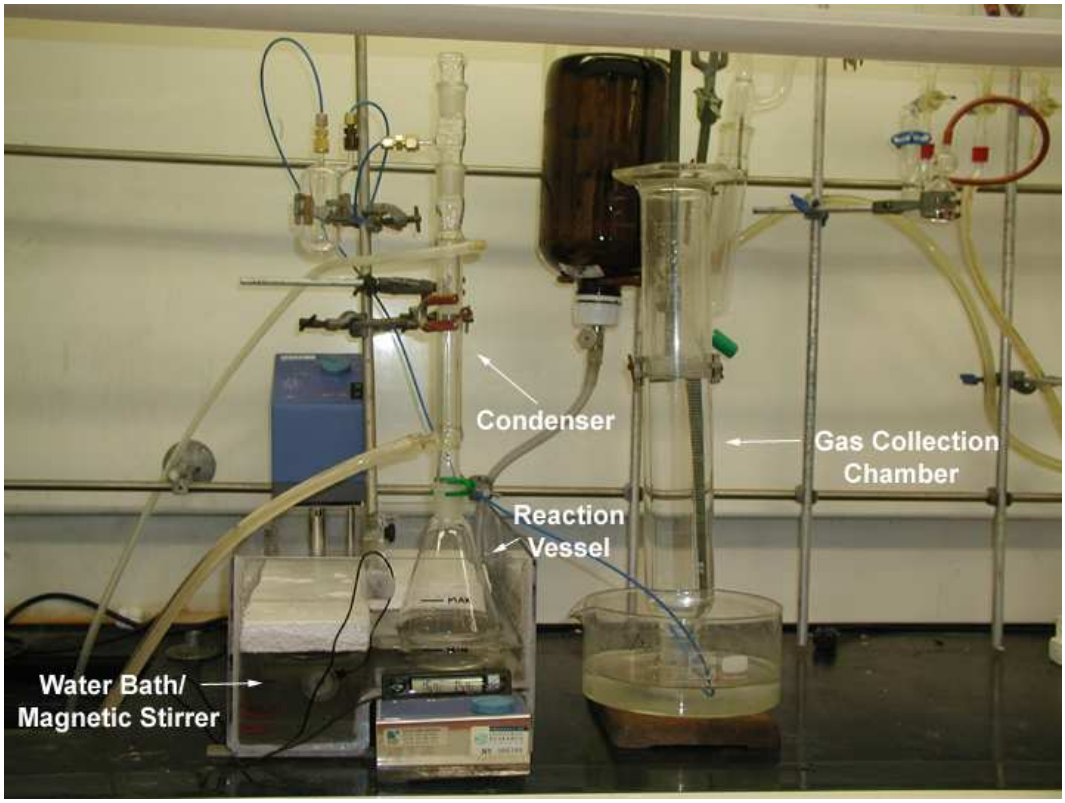

Figure 3.1: Ammonia borane synthesis apparatus.

Large needles (see Figure 3.2 and 3.3) were crystallised from diethyl ether as described in section **2.2.2**.

The above method produced ammonia borane at acceptable yields; however the method suffered from scalability limitations. The reaction was attempted on a larger scale using a 1 L flask. In order to fully dissolve the reactants in the THF solution, a large magnetic stirrer was required to complement the size of

Figure 3.2: Pure ammonia borane crystals.

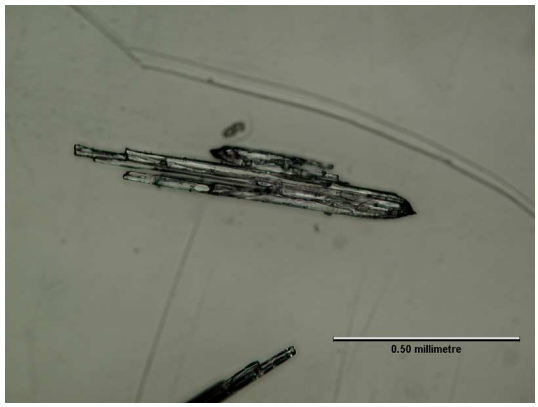

Figure 3.3: Pure ammonia borane crystals as viewed through 5x objective.

the flask. However, isolated ammonia borane yields were found to be very low ($\sim$ 3% based on sodium borohydride). It was found that in order to obtain high ammonia borane yields, the rate at which the THF-borane solution is stirred is highly critical. Ramachandran *et al.* [79] also observed that vigorous stirring was crucial for the rate of the reaction. Due to the low solubility of the reactants in THF, vigorous stirring was found to be paramount in ensuring the maximum possible dissolution attainable. It was concluded that the energy required to achieve this using a magnetic stirrer was not obtainable on such a scale. To overcome come this problem, a new method involving ball-milling[1] the reactants in THF solution was developed to allow the large scale synthesis of ammonia borane.

The second method involved ball milling ammonium carbonate and the sodium borohydride in a 1:1 molar ratio in anhydrous THF using zirconia balls. The milling vessel was fitted with a one way pressure release valve to release any hydrogen generated during the course of the reaction.

Large needles were recrystallised via single solvent recrystallisation using IPA (16 mL g^{-1} ammonia borane) as the solvent as described in section **2.2.2**.

[1] A ball mill is a type of grinder in which balls are used as the grinding medium.

3.2.1 Results and Discussion

Hu *et al.* first reported method 1 for synthesising ammonia borane. The method was successful and resulted in an average yield of 75% NH_3BH_3, however, to date no one has successfully identified the reaction mechanism. Hu *et al.* discusses the possibility of the reaction occurring through a BH_3 formate such as $Na^+H_3B.O_2CH^-$ which undergoes a base displacement reaction by ammonia forming ammonia borane. The powder X-ray diffraction pattern of insoluble solid residue, removed by filtration during ammonia borane synthesis, is shown in Figure 3.4. It shows peaks which correspond to sodium formate (ICDD pattern 0-014-0812). Other crystalline impurity peaks are present which could not be identified through the International Centre for Diffraction Data, however, they do not correspond to either the starting materials or ammonia borane. Other amorphous impurity phases may also be present.

The presence of sodium formate ($NaHCO_2$) in the X-ray diffraction pattern (Figure 3.4) supports the possibility of a BH_3 formate as discussed by Hu *et al.* Further support for the theory that the reaction occurs via a formate intermediate stems from synthesis carried out using other ammonium salts such as chloride [80] and sulphate [78]. These reactions resulted in significantly low yields of ammonia borane. This observation had led to ammonium formate and sodium borohydride being mixed together in a stoichiometric ratio as a synthesis method [28].

Method 1 described in section **2.2.2** of synthesis resulted in a typical yield of 75% NH_3BH_3 (based on sodium borohydride). Characterisation of the compound was by powder X-ray diffraction shown in Figure 3.5 (as outlined in section **2.4**), which showed peaks that matched those in the literature [43] and the International Centre for Diffraction Data pattern for ammonia borane (ICDD pattern 01-074-0894) (see Table 3.1). Table 3.1 displays the spacings d_c, and intensities I_c, calculated by Hughes [43] from the proposed room temper-

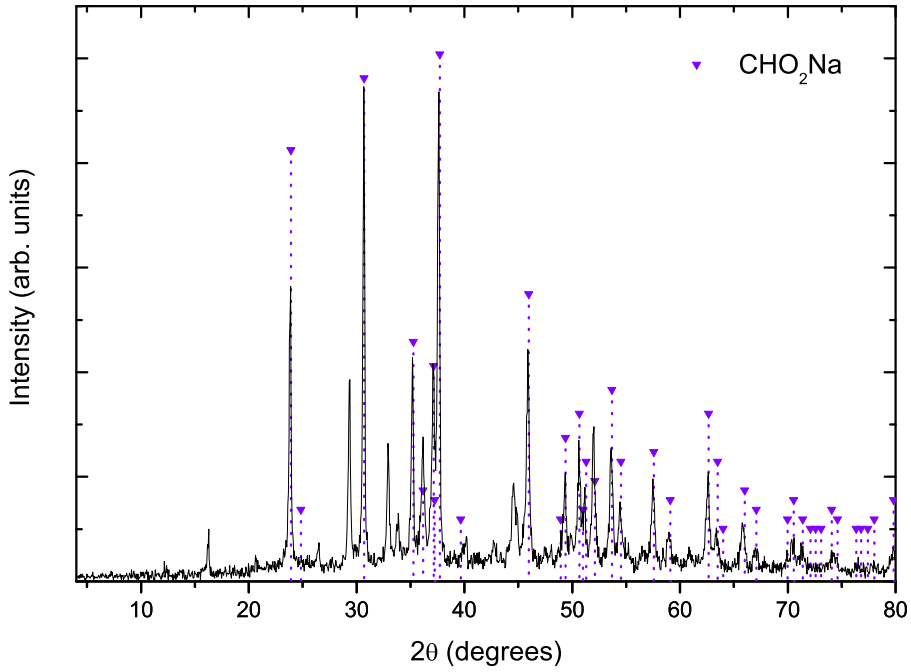

Figure 3.4: X-ray diffraction pattern of the insoluble residue from ammonia borane synthesis.

ature tetragonal crystal structure of ammonia borane as well as the observed spacings d_o, and intensities I_o.

Purity was confirmed by the lack of any unexplainable features in the X-ray diffraction trace or any peaks resulting from impurity phases pertaining to the starting materials used in the reaction. Relative intensities of the calculated peaks and those observed differ significantly. The calculations assume random distribution of orientations of the crystals, however ammonia borane crystals are needle-like and are therefore much more likely to lie in a direction parallel to the surface. This preferred orientation leads to observed intensities that differ from those calculated.

The product ammonia borane was also identified by its IR spectrum (Figure 3.6). The spectral bands seen in the obtained IR spectrum are in agreement

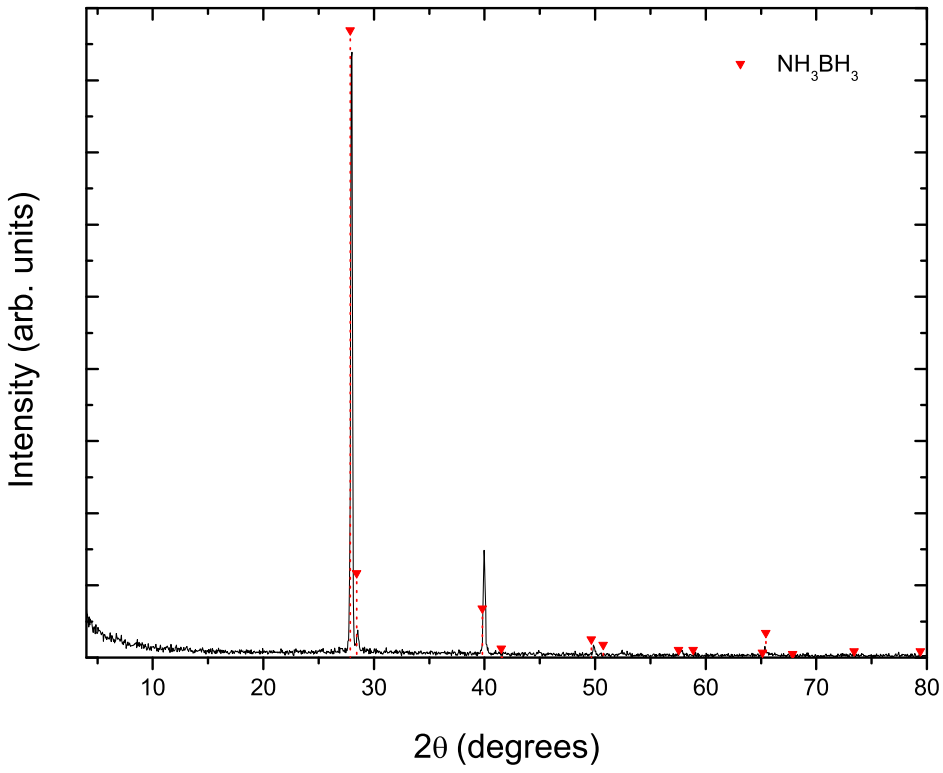

Figure 3.5: X-ray diffraction pattern of recrystallised ammonia borane.

with those published in the literature [42]. IR spectral bands for purified NH_3BH_3 are summarised in Table 3.2

Method 2 involved ball milling the reactants. Sodium borohydride (0.3 mol) and ammonium carbonate (0.3 mol) in THF (330 g) were ball milled over a range of different times in order to deduce the optimum milling time for future experiments. Figure 3.7 shows that the highest yield of ammonia borane was produced by ball-milling the sample reactants for 8 hours, which was therefore chosen as the standard.

This method of synthesis resulted in a typical yield of 80% NH_3BH_3 (based on sodium borohydride).

In method 1 ammonia borane was crystallised from diethyl ether. While this

$\mathbf{d}_c$ (Å)	$\mathbf{I}_c$(%)	$\mathbf{d}_o$ (Å)	$\mathbf{I}_o$(%)
3.72	100	3.70	100
3.64	26	3.62	5
2.63	7	2.62	18
2.52	3	-	-
2.13	3	2.12	2
2.09	3	-	-
1.86	2	1.85	1
1.82	3	-	-
1.66	2	1.66	2
1.65	6	-	-
1.60	2	-	-
1.50	2	-	-
1.40	1	-	-

Table 3.1: Calculated (c) and observed (o) powder X-ray diffraction data of ammonia borane.

Frequency (cm^{-1})	**Assignment [81]**
3300	N-H stretch
2400	B-H stretch
1625	N-H bend
1383	N-H rock
1180	B-H bend
1065	
782	B-H rock
727	B-N stretch [42]

Table 3.2: IR spectral bands and assignments for purified ammonia borane.

method produced ammonia borane, the yields were often low and the quality of the crystals was inconsistent. Isopropyl alcohol was used as the solvent for

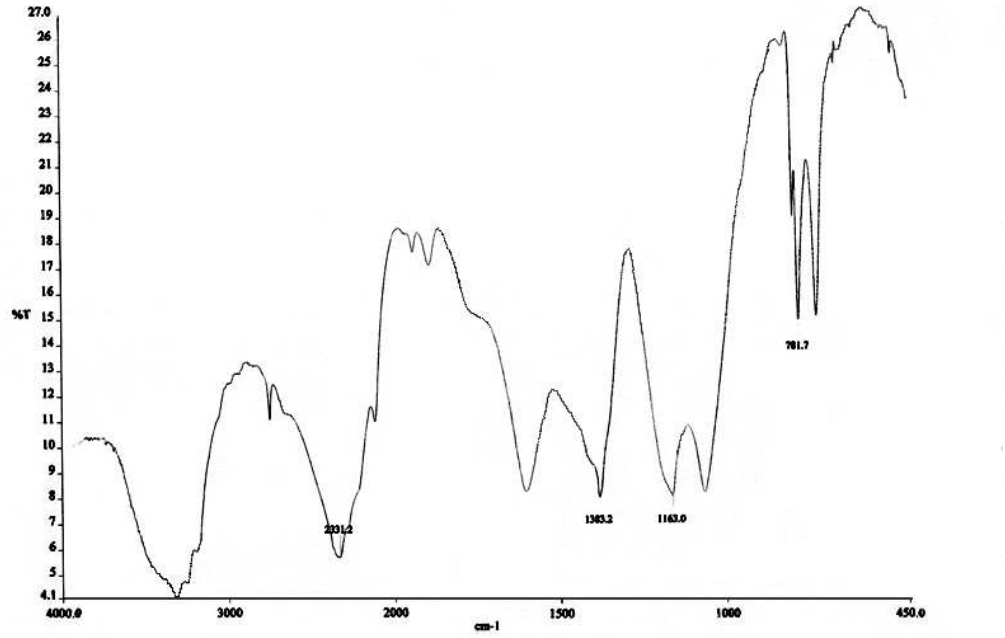

Figure 3.6: Infrared spectrum of ammonia borane.

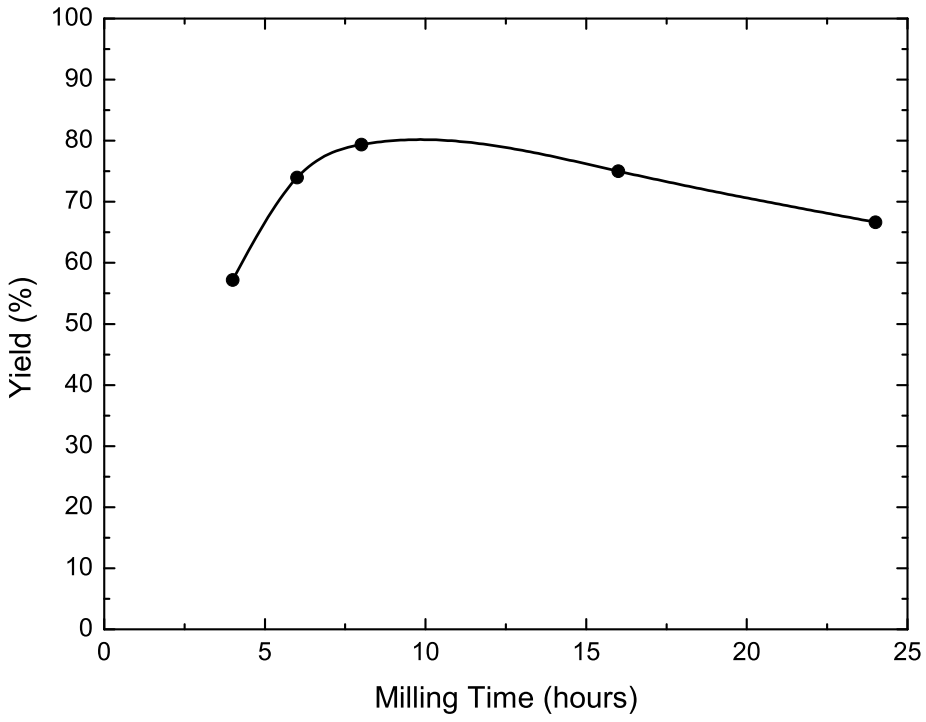

Figure 3.7: Determination of optimal milling time.

recrystallisation in method 2. This resulted in higher yields and better consistency in crystal quality. No impurities were detected using either solvent (Figure 3.8). However IPA was preferable because its higher boiling point and the greater solubility of ammonia borane (IPA (4 g/100 mL IPA [28]) compared to that in diethyl ether (0.74 g/100 mL diethyl ether [28]), allowed a better yield when cooling from warm saturated solutions. By contrast, crystallisation from ether required evaporation of the solvent allowing a greater potential for contamination.

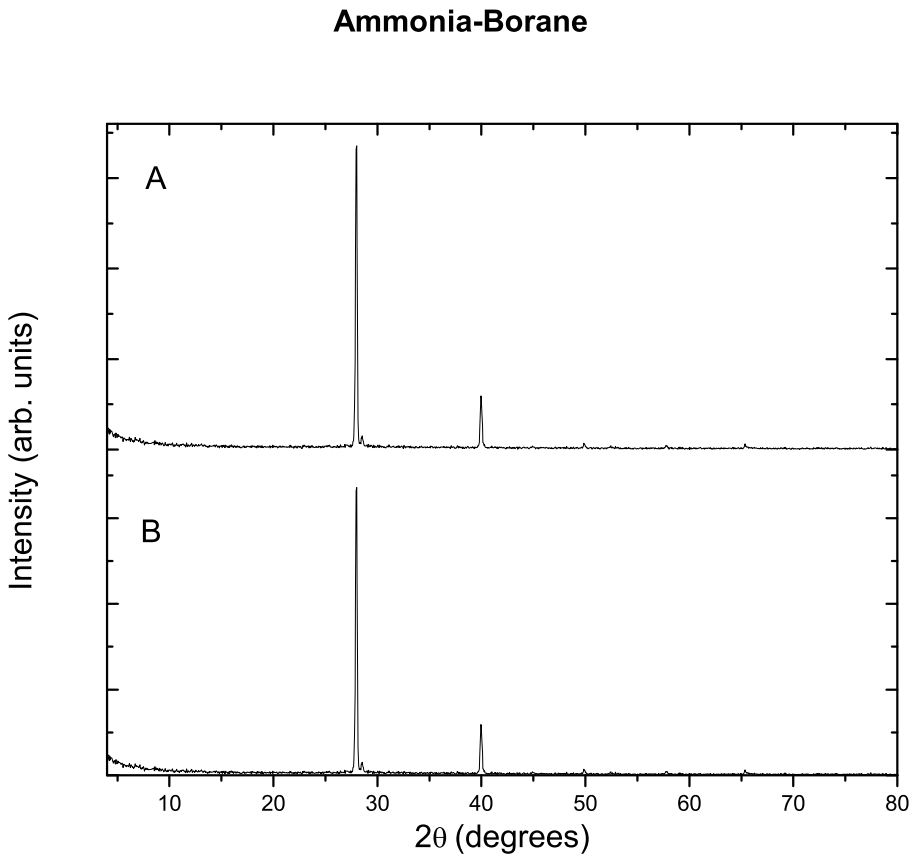

Figure 3.8: X-ray diffraction patterns of ammonia borane recrystallised from IPA (A) and diethyl ether (B).

3.3 Synthesis of Deuterated Derivatives of Ammonia Borane

3.3.1 Synthesis of ND_3BH_3

ND_3BH_3 was synthesised by a simple H/D exchange reaction first reported by Hu *et al.* [42] described in section **2.2.3** in which ammonia borane is deuterated using D_2O according to the reaction:

$$NH_3BH_3 + \frac{3}{2}D_2O \rightleftharpoons ND_3BH_3 + \frac{3}{2}H_2O \tag{3.1}$$

The reaction was carried out with a 10x excess of D_2O to drive the equilibrium toward ND_3BH_3. Hu *et al.* [42] reported that the above reaction resulted in approximately 80% deuteration of the amine (studied by means of Raman spectroscopy). However repeating the deuteration reaction resulted in a product with approximately 94% deuteration, and therefore the deuteration with D_2O was carried out twice for all syntheses conducted.

3.3.2 Synthesis of NH_3BD_3

There have been no reported successful conditions to exchange deuterium for boron hydrogens in ammonia borane. Therefore, NH_3BD_3 was synthesised according to the same method reported for ammonia borane in section **2.2.2** (method 1) using sodium borodeuteride in place of sodium borohydride.

3.3.3 Results and Discussion

The product ND_3BH_3 was used as obtained. Deuteration was confirmed by ^{1}H NMR spectroscopy (Figure 3.9).

The ^{1}H NMR of NH_3BH_3 in DMSO (Figure 3.10) consists of a broad singlet resonating at δ 4.39 arising from the H-N protons. H-B protons appear as a quadruplet centred at δ 1.35 split by the quadrupolar ^{11}B (spin = $\frac{3}{2}$). The

degree of deuteration of the nitrogen in ammonia borane is confirmed by the disappearance of the N-H singlet in the ND_3BH_3 spectrum.

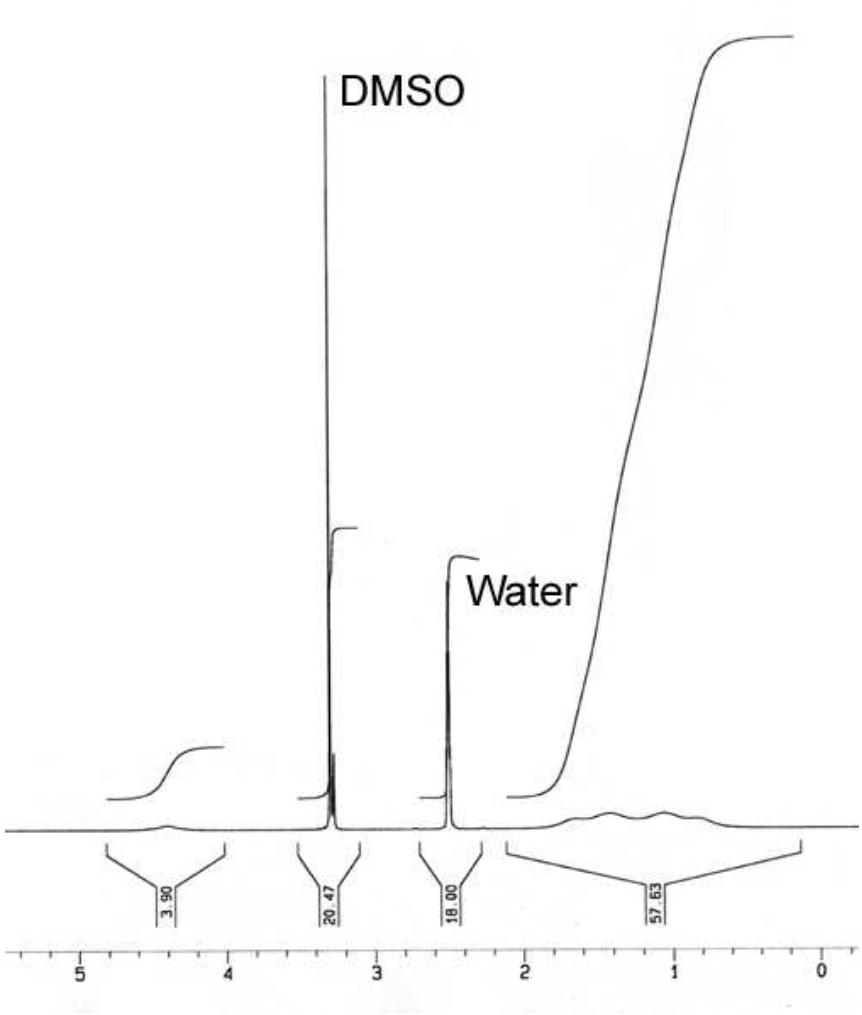

Figure 3.9: ^{1}H NMR of ND_3BH_3 in DMSO.

The product NH_3BD_3 was obtained in 80% yield. Deuteration was confirmed by ^{1}H NMR spectroscopy (see Figure 3.11). The degree of deuteration of the boron in ammonia borane is confirmed by the disappearance of the H-B quadruplet -resonating at δ 1.35 in the NH_3BH_3 spectrum (Figure 3.10) - in the NH_3BD_3 spectrum.

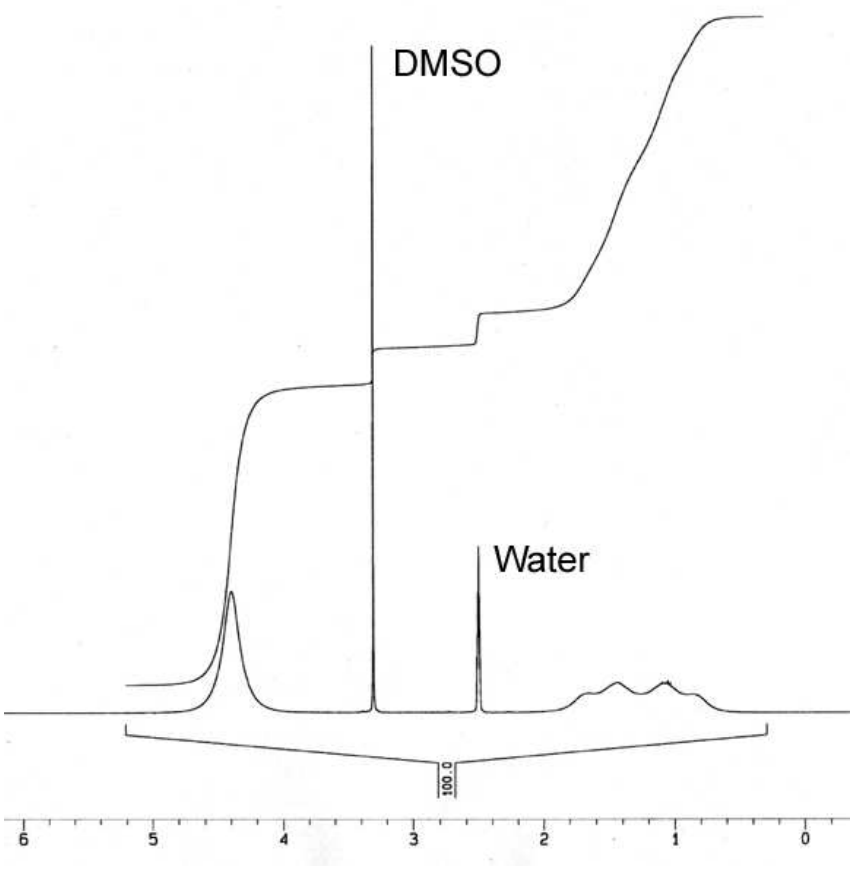

Figure 3.10: ^{1}H NMR of NH_3BH_3 in DMSO.

3.4 Synthesis of Methylamine Borane

Alkylamine-borane adducts can be prepared via a reaction of any amine hydrochloride salt with any borohydride. This route was originally reported by Schaeffer and Anderson [73] for synthesis of trimethylamine borane, N-trimethylborazole and N-dimethylaminoborane.

Synthesis of methylamine borane from methylamine hydrochloride and sodium borohydride in monoglyme has been reported [74], [40]. Methylamine borane was synthesised via a modification of these methods reacting methylamine hydrochloride and sodium borohydride in a 1:1 molar ratio in anhydrous THF at room temperature (see section **2.2.5**).

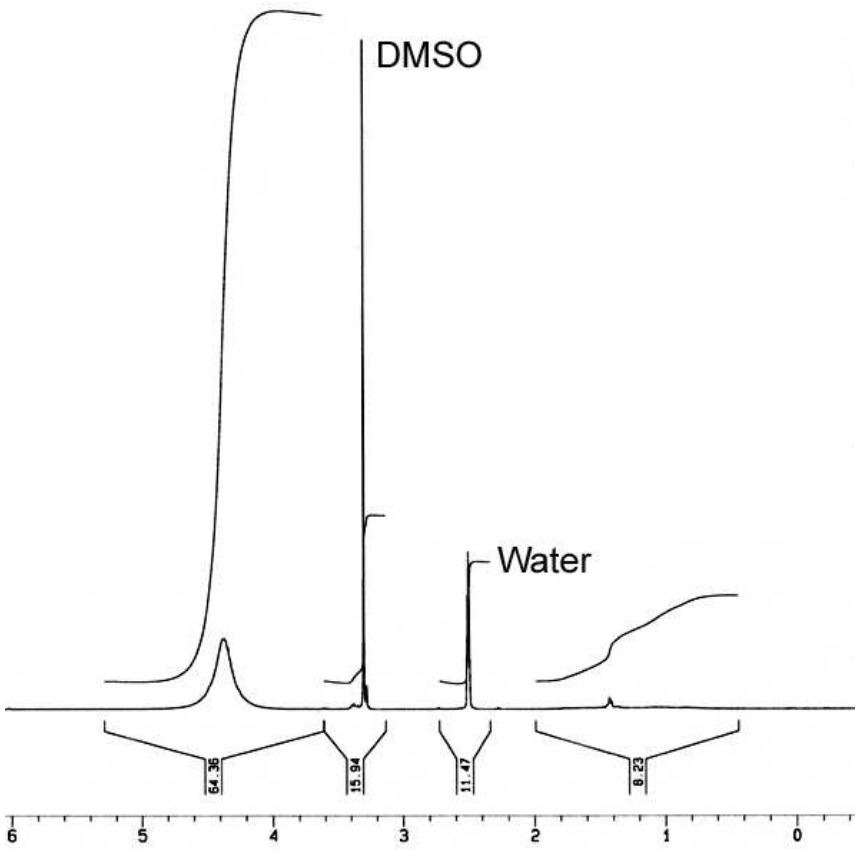

Figure 3.11: ^{1}H NMR of NH_3BD_3 in DMSO.

3.4.1 Results and Discussion

Previously in section **3.2.1**, the possibility of ammonia borane being formed through a BH_3 formate was discussed. The observation was made that other ammonium salts such as chloride and sulphate were unsuccessful as reactants and this may be due to their inability to form formate intermediates. Ammonia borane is formed in these reactions, however in low yields, suggesting these react via a different, yet not fully understood, mechanism. The powder X-ray diffraction pattern of the insoluble solid residue - removed by filtration during ammonia borane synthesis using NH_4Cl in place of $(NH_4)_2(CO_3)$ (Figure 3.12) - shows peaks which correspond to sodium chloride (ICDD pattern 00-005-0628), and peaks which correspond to the starting materials sodium borohydride (ICDD pattern 00-038-1022) and ammonium chloride (ICDD pattern 00-007-0007). The presence of the starting materials in this residue suggests that solubility may be the critical factor affecting reactivity.

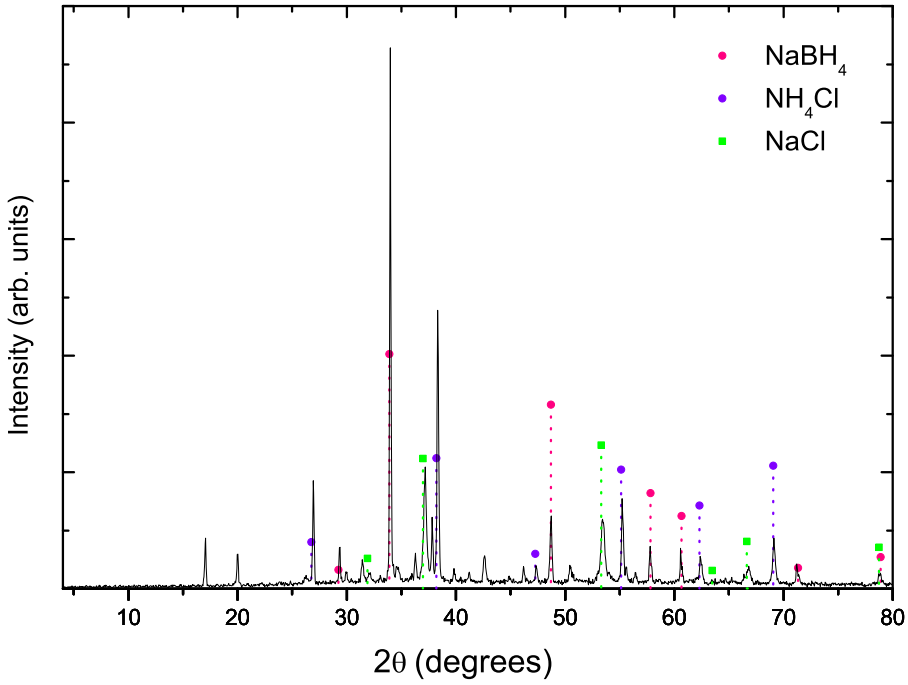

Figure 3.12: X-ray diffraction pattern of the insoluble residue from ammonia borane synthesis using ammonium chloride.

The ammonium salt methylamine hydrochloride however is successful as a starting material for the synthesis of methylamine borane resulting in typical yields of 70% $CH_3NH_2BH_3$. The presence of NaCl in X-ray diffraction pattern of the insoluble residue (Figure 3.13) - removed by filtration during methylamine borane synthesis using methylamine hydrochloride - suggests that the reaction occurs via the same mechanism as the NH_4Cl reaction above. A small amount of residual unreacted methylamine hydrochloride can also be seen in the X-ray diffraction pattern. These results indicate that the main factor affecting the reactivity of ammonium salts is solubility and not a competing reaction.

Bowden *et al.* have recently determined the crystal structure of methylamine borane [75] (positional parameters are presented in Table B.1). The struc-

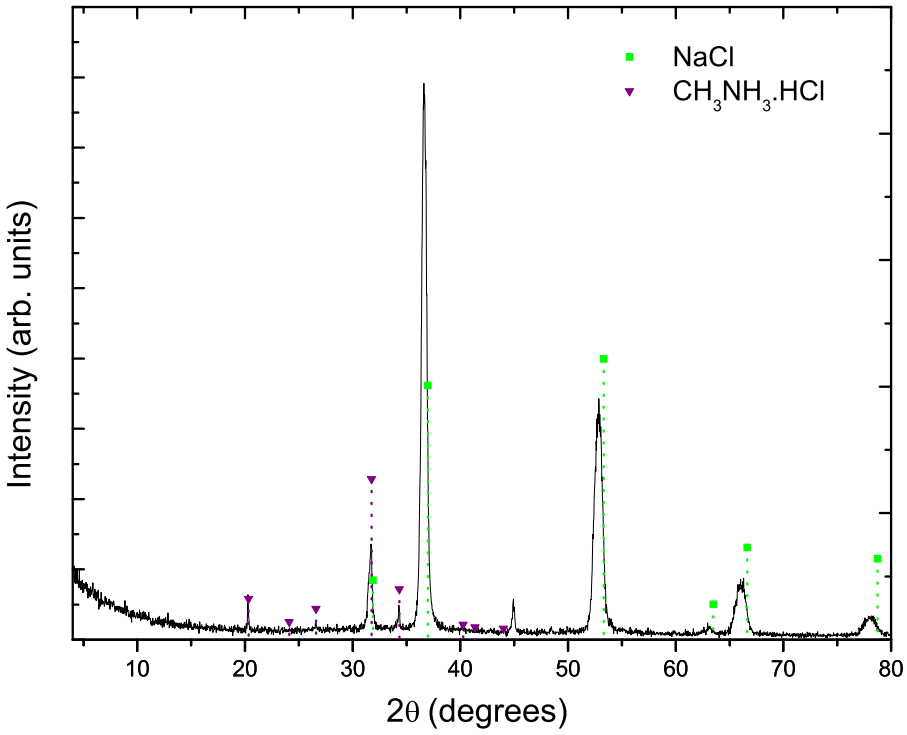

Figure 3.13: X-ray diffraction pattern of the insoluble residue from methylamine borane synthesis.

ture (Figure 3.14) was found to consist of chains of $CH_3NH_2BH_3$ molecules extending along the *b*-axis of an orthorhombic unit cell. The molecules within these chains are oriented with their B-N bonds aligned in alternate directions and are linked via N-H$^{\delta+\cdots\delta-}$H-B dihydrogen bonds (shown in Figure 3.14b). Intramolecular bond distances and angles (Table B.2) show that B, C, and N all have the expected tetrahedral coordination.

The product methylamine borane was identified by powder X-ray diffraction (see Figure 3.15). The X-ray diffraction pattern for methylamine borane was calculated using the refined structure. A Table of calculated and observed powder X-ray diffraction peaks for $CH_3NH_2BH_3$ is included (Table 3.3).

The X-ray diffraction pattern shows only peaks corresponding to the calcu-

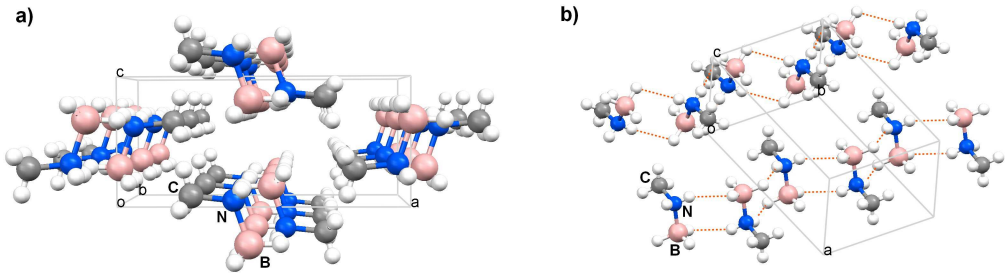

Figure 3.14: Crystal structure of $CH_3NH_2BH_3$.

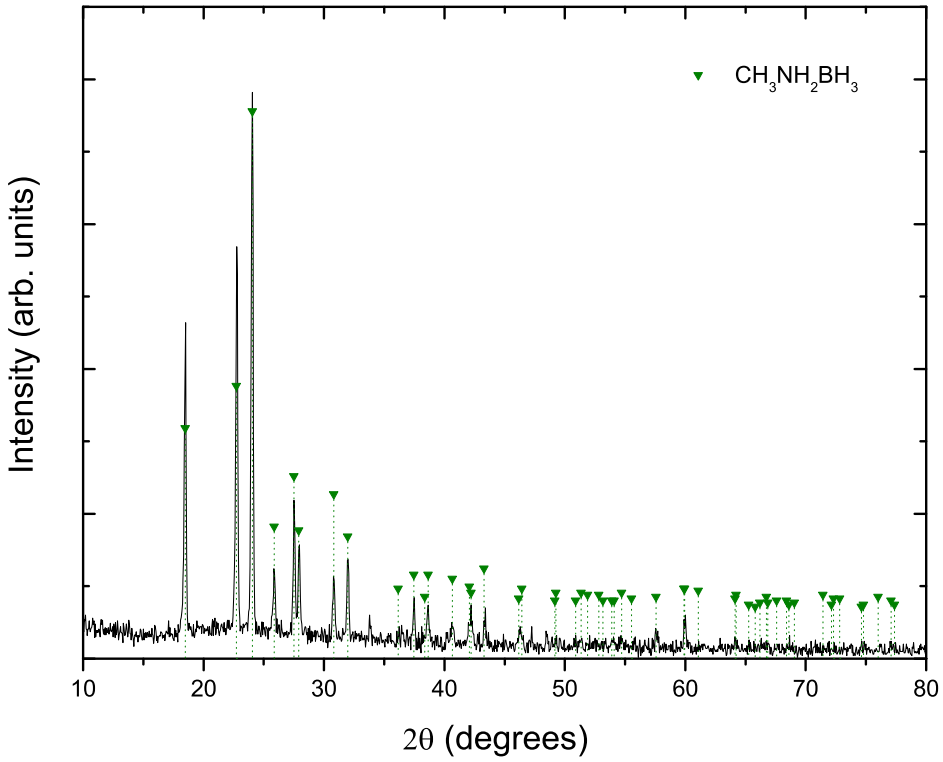

Figure 3.15: X-ray diffraction pattern of methylamine borane.

lated pattern confirming phase purity of the methylamine borane.

The product methylamine borane was also identified by ^{1}H NMR spectroscopy (see Figure 3.16). The ^{1}H NMR of $CH_3NH_2BH_3$ in DMSO consists of a quartet resonating at δ 1.20 due to the H-B coupling, a broad singlet resonating at δ 4.98 arising from the H-N protons, and a triplet resonating at δ 2.02 arising from the H-C protons (split by the H-N protons). A resonance correspond-

$\mathbf{d}_c$(Å)	$\mathbf{I}_c$	$\mathbf{d}_o$(Å)	$\mathbf{I}_o$	$\mathbf{d}_c$(Å)	$\mathbf{I}_c$	$\mathbf{d}_o$(Å)	$\mathbf{I}_o$
5.57	49	5.57	59	2.27	3	2.23	6
4.54	73	4.53	73	2.15	2	2.18	5
4.29	100	4.30	100	2.15	3	-	-
4.00	16	4.00	16	2.06	3	-	-
3.76	28	3.76	28	2.08	4	-	-
3.71	19	3.70	20	2.05	3	-	-
3.37	15	3.36	15	2.01	3	-	-
3.25	17	3.25	18	2.00	3	-	-
2.88	4	2.86	6	1.97	3	1.97	4
2.79	10	2.78	11	1.97	3	-	-
2.72	4	-	-	1.95	3	-	-
2.70	10	2.71	10	1.92	2	-	-
2.57	5	2.58	6	1.86	5	1.86	5
2.48	10	2.49	10	1.79	5	1.79	8
2.49	6	-	-	1.79	7	-	-
2.42	7	2.42	9	1.76	3	1.75	3
2.28	3	2.27	6	1.68	4	1.68	4

Table 3.3: Calculated (c) and observed (o) powder XRD peaks for $CH_3NH_2BH_3$

ing to the B-H protons of residual sodium borohydride is also present in the spectrum at $\sim \delta$ -0.2.

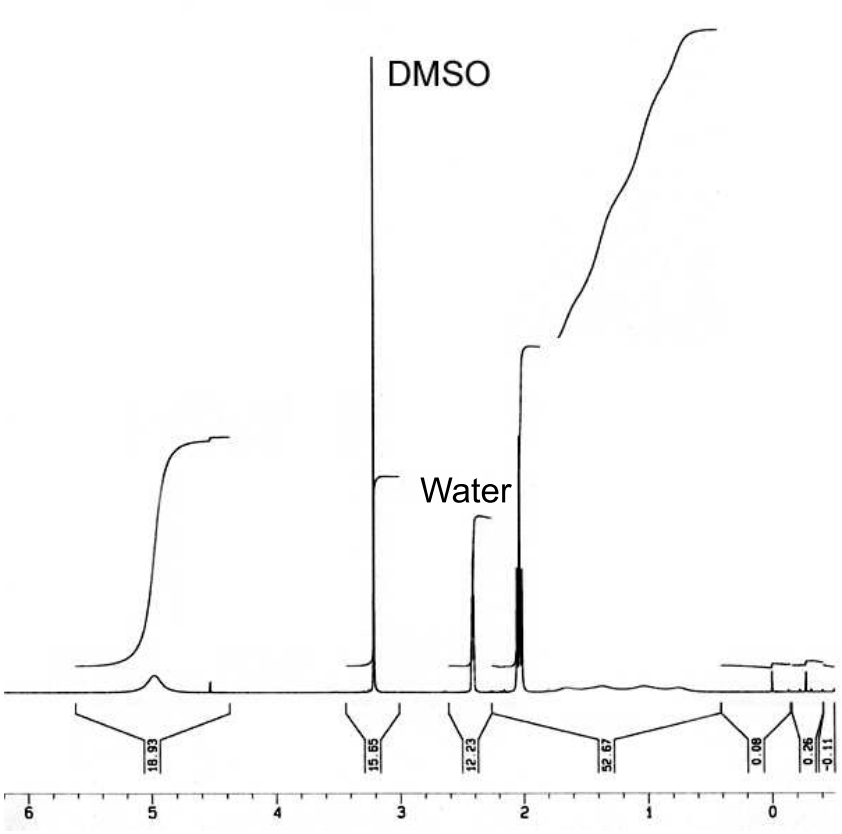

Figure 3.16: ^{1}H NMR of $CH_3NH_2BH_3$ in DMSO.

Chapter 4

Solid-State Reaction between Ammonia Borane and Lithium Amide

4.1 Introduction

This chapter covers the experimental work carried out on the solid-state reaction between ammonia borane and lithium amide. The aim of this research was to investigate the mechanism by which ammonia borane and lithium amide react in a series of different molar ratios, and to investigate the properties of phases formed during these reactions and their decomposition pathways during thermolysis. It also covers reactions between ammonia borane isotopologues and lithium amide, undertaken for the purpose of studying the reaction mechanism.

Unless otherwise noted, all manipulations were carried out using procedures described in section **2.3.1**. Powder X-ray diffraction was used to investigate the formation or disappearance of crystalline phases throughout the course of the reaction and decomposition. Mass spectrometry was used to analyse the composition of evolved gases during thermal decomposition, and solid-state

^{11}B spectroscopy was used to determine the detailed chemical bonding environment around the B atoms. Due to the large number of samples examined in this study, it was not possible to include all data collected, therefore each section will include data which is representative of the phase in question. Other relevant data will be included in Appendix C, D, and E.

4.2 Experimental Details

Ammonia borane and lithium amide were mixed together in a series of specific molar ratios under an argon atmosphere as described in section **2.3.1** - a schematic diagram of this reaction setup is shown in Figure 2.2. By using this setup the gas generated could either be collected for gas volume measurements (discussed in section **2.3.3**), or sampled using a mass spectrometer (discussed in section **2.3.2**) to analyse the composition of the gas.

The two starting materials were reacted by mixing the powders using a magnetic stirrer and stir bar until reaction was complete - formation of liquid phase discussed in section **4.3**. Based on the results of Wolf *et al.* [52], [53] discussed in section **1.7.3**, a heating rate of 1°C/min was used for all thermal measurements.

4.3 Formation of Transition Phase

Upon reaction between lithium amide and ammonia borane at room temperature an exothermic process occurs, which results in the formation of a highly reactive viscous liquid intermediate. This phase gradually re-solidifies when left in an inert atmosphere. During solidification of this phase a negligible amount of gas is evolved i.e. slight frothing of the liquid phase observed.

The overall reaction is exothermic but requires external energy in the form of stirring to overcome kinetic barriers. Once the reaction was initiated it

proceeded on its own. When the reaction is performed on a large scale, the exothermic nature of the reaction causes the mixture to reach a critical temperature ($\sim$ 50°C), thereby resulting in the evolution of hydrogen and ammonia (discussed in section **4.4.1**). In order to control the heat of the reaction, a smaller scale was used and a slow stirring rate was employed.

A series of reactions were performed in which ammonia borane and lithium amide were mixed in a series of specific molar ratios. This liquid phase was observed for all ratios of $LiNH_2$:NH_3BH_3 studied. It was observed that an excess of lithium amide encourages the formation of this transition state resulting in a faster reaction onset upon mixing, whereas reactions utilising an excess of ammonia borane required greater external energy to initiate the reaction.

The amount of lithium amide present also affected the rate of solidification. It was found that for reactions with higher lithium amide concentrations, solidification proceeded at a faster rate than for reactions with a deficit of amide (liquid phase did not solidify upon being left in an inert atmosphere for days, compared with hours for reactions with excess of amide). It is important to note that this phase is not observed upon mixing ammonia borane in the absence of amide.

This liquid phase has been observed by other groups, Chen has also observed this phase in the reaction between lithium imide and ammonia borane [70], and Meisner *et al.* also observed a liquid "melt" during the reaction between $LiBH_4$ and $LiNH_2$ [82].

This is a complicated and ill-understood process, further complicated by the extremely high reactivity which made characterisation of this phase difficult. However, solid-state ^{11}B NMR of a sample of solidified liquid phase showed a single peak corresponding to a -BH_3 resonating at $\sim$-23 ppm. This is sig-

nificantly different to that observed for -BH_3 moiety in neat ammonia borane which resonates at ∼-27 ppm (discussed in section **4.4.3.2**).

Powder X-ray diffraction data, collected on the resulting solid, shows that an amorphous or poorly crystalline phase is formed. Crystalline peaks corresponding to unreacted lithium amide (ICDD pattern 01-071-1616) could be seen in the trace for reactions in which an excess of amide is present (Figure 4.1). The Li_2O impurity present in the X-ray diffraction pattern of this liquid

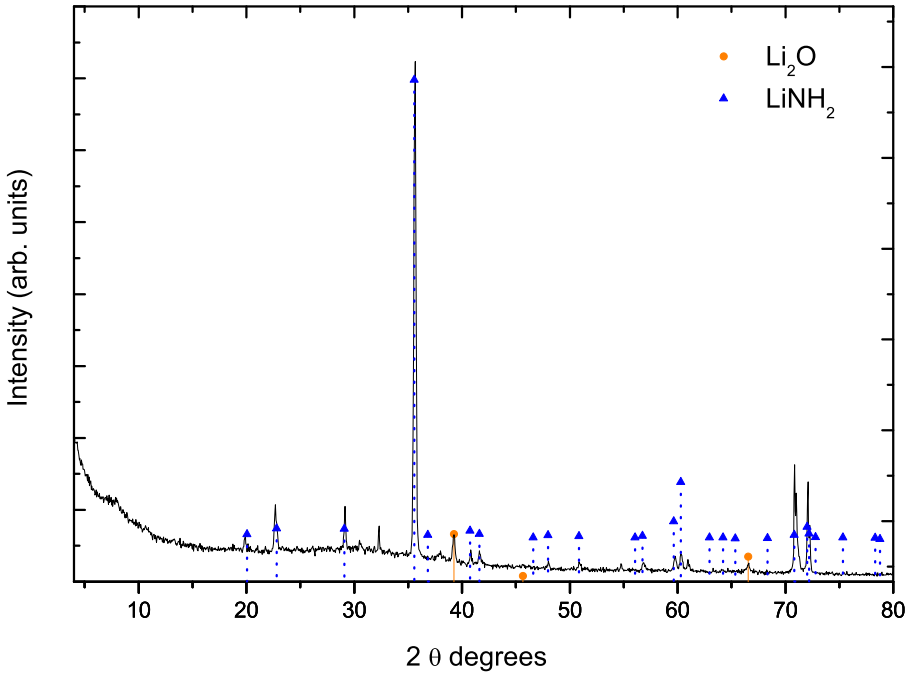

Figure 4.1: X-ray diffraction pattern of 3:1 ($LiNH_2$:NH_3BH_3) liquid intermediate phase.

phase originates from the $LiNH_2$ starting material. The powder X-ray diffraction pattern of the lithium amide starting material used for these reactions is shown in Figure 4.2. Peaks corresponding to LiOH (ICDD Pattern 01-085-1064) and Li_2O (ICDD pattern 01-071-1616) are present in the trace (resulting from lithium amide starting material reacting with moisture upon exposure to air).

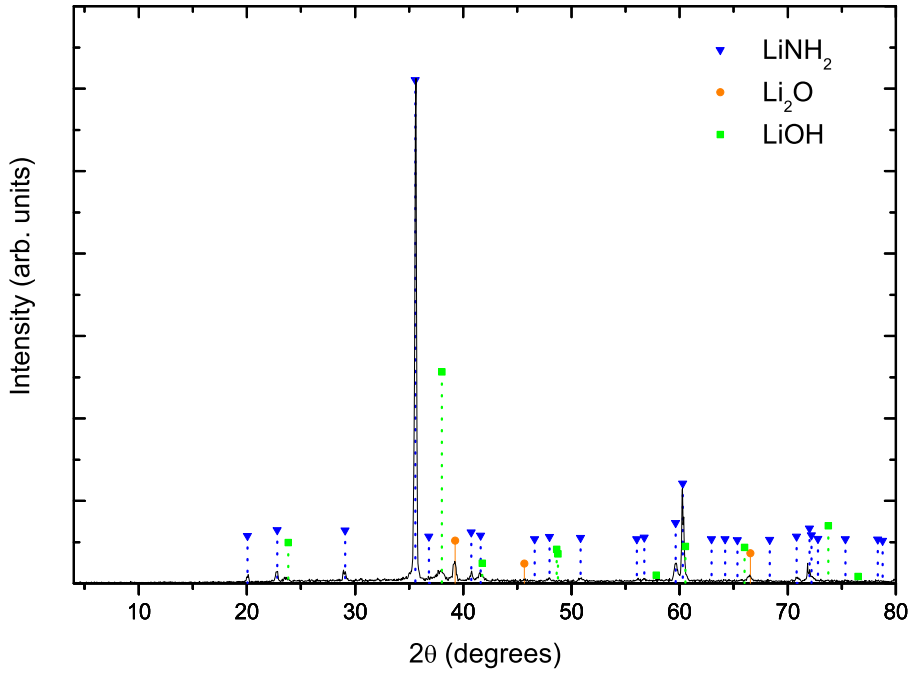

Figure 4.2: X-ray diffraction pattern of lithium amide starting material.

X-ray diffraction of a solidified 1:1 sample (Figure 4.3) shows no crystalline peaks corresponding to lithium amide, indicating that all the amide has reacted. However, crystalline peaks corresponding to ammonia borane were observed in the trace, indicating incomplete reaction.

The formation of the liquid phase is significant. As discussed in section **1.7.2.1**, the dehydrogenation kinetics of ammonia borane can be dramatically altered in polar and ionic liquids. However, the addition of solvents to facilitate catalysis or movement of ammonia borane greatly reduce the hydrogen storage capacity. Because the $LiNH_2$:NH_3BH_3 reaction "melts" at room temperature, it may be possible to run experiments in the absence of solvent without compromising the hydrogen storage capacity of the system.

During analysis of the thermal decomposition pathways of $LiNH_2$:NH_3BH_3, the

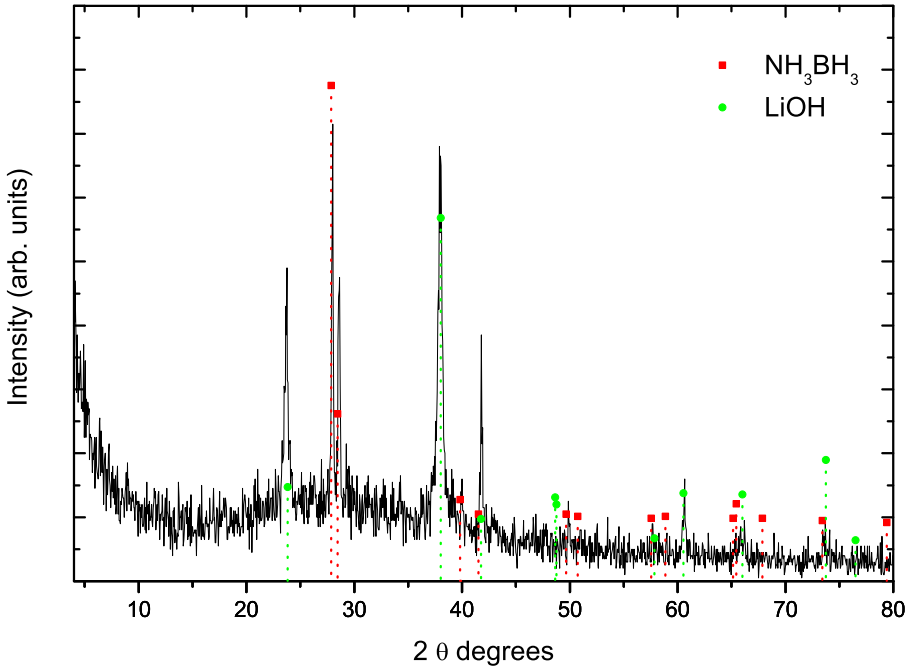

Figure 4.3: X-ray diffraction pattern of 1:1 ($LiNH_2$:NH_3BH_3) liquid intermediate phase.

starting materials were mixed until formation of this liquid phase occurred; the liquid phase was not left to dry, but rather heating was started at this point.

4.4 Thermal Decomposition

4.4.1 Evolved Gas Analysis

The release of gaseous products during the thermal decomposition of post-mixed samples of NH_3BH_3 + $LiNH_2$ in the temperature range up to 250°C were identified by means of mass spectrometry. A scan from m/z 0-100 was used under argon 10 mL/min (discussed in section **2.3.2**).

Thermal decomposition of pure ammonia borane occurs in two distinct stages. A plot of the temperature dependence of major observed ion intensities detected upon thermal decomposition of ammonia borane is shown in Figure

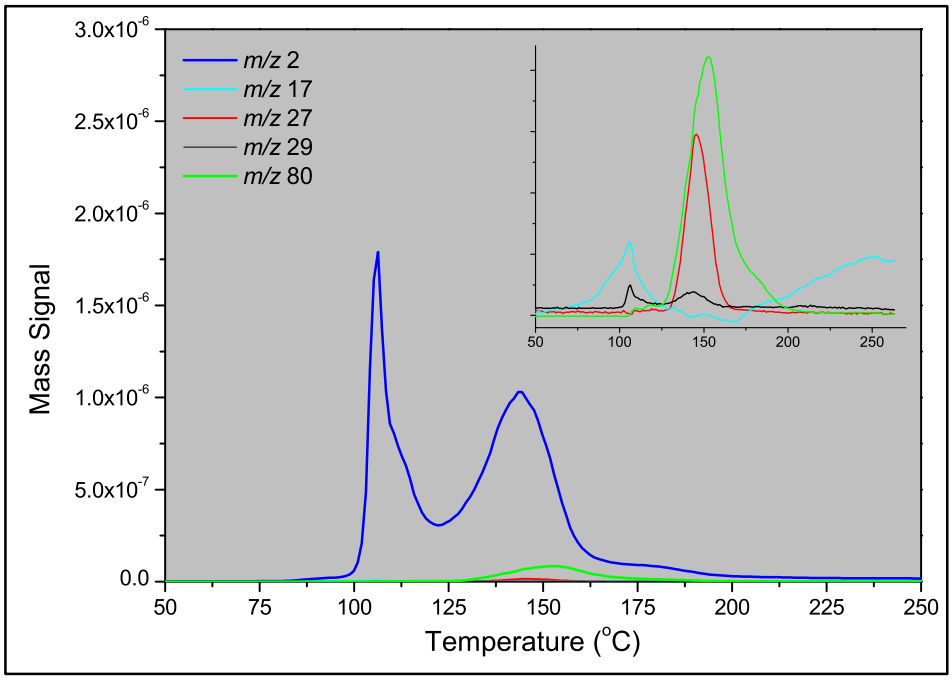

Figure 4.4: Mass spectra of gases evolved during thermal decomposition of NH_3BH_3. Gases other than hydrogen enhanced in the insert. An arbitrary scale used in order to show shape of the curves rather than relative intensities.

4.4. Hydrogen (m/z 2) is the predominant gas evolved on heating. The first hydrogen peak occurs at 100°C, the second hydrogen peak occurs at 150°C corresponding to the release of the first equivalent of hydrogen with the formation of $(NH_2BH_2)_n$ and the release of the second equivalent of hydrogen with the formation of $(NHBH)_n$ respectively. A trace amount of gas (0.1% of m/z 2 intensity) corresponding to monomeric aminoborane (m/z 29) is present with an identical temperature profile to hydrogen. There is a low temperature evolution of ammonia (m/z 17, 0.30% of m/z 2 intensity) before the first hydrogen desorption peak, and high temperature evolution of diborane (B_2H_6) (m/z 27, 0.80% of m/z 2 intensity) and borazine ($B_3N_3H_6$) (m/z 80, 4.80% of m/z 2 intensity) just after the second hydrogen desorption peak.

These results are in agreement with a comprehensive study of the thermal decomposition of ammonia borane published by Wolf *et al* [52]. Using a com-

bination of thermogravimetric analysis and mass spectroscopy the authors also observed two step hydrogen evolution in the temperature range 110-230°C. BH_2NH_2 and borazine were evolved during the second decomposition step in the temperature range 145-230°C. Small quantities of diborane and monomeric amine borane were also observed.

A temperature dependence graph of ion intensities observed in the released gas phase during the thermal decomposition of a 1:1 ($LiNH_2$:NH_3BH_3) sample

Mass number	**Assignment**	**Mass number**	**Assignment**
1	H^+	28	$^{14}N_2{}^+$
2	$H_2{}^+$	29	$^{11}BNH_4{}^+$
14	$^{14}N^+$	30*	
15	$^{14}NH^+$	32	$^{16}O_2{}^+$
16	$^{14}NH_2{}^+$	36	$^{36}Ar^+$
17	$^{14}NH_3{}^+$	38	$^{38}Ar^+$
18	H_2O^+	40	$^{40}Ar^+$
20	$^{40}Ar^{++}$	41	$^{40}Ar{+}H^+$
27	$^{11}BNH_2{}^+$, $^{10}BNH_3{}^+$	44	$CO_2{}^+$

Table 4.1: Table of ions detected during decomposition of post mixed 1:1 (NH_3BH_3:$LiNH_2$).

is shown in Figure 4.5. Detected mass numbers for a 1:1 sample are given in Table 4.1 together with possible assignment of ions.

Throughout the course of decomposition, air is present as indicated by *m/z* 28, *m/z* 32, and *m/z* 44 - corresponding to N_2, O_2 and CO_2 respectively - in concentrations less than 0.10%. The air originates from small unavoidable leaks in both the experimental setup and within the mass spectrometer. The profile of these ions show that a higher concentration of air is present at the

*Ion was not able to be assigned.

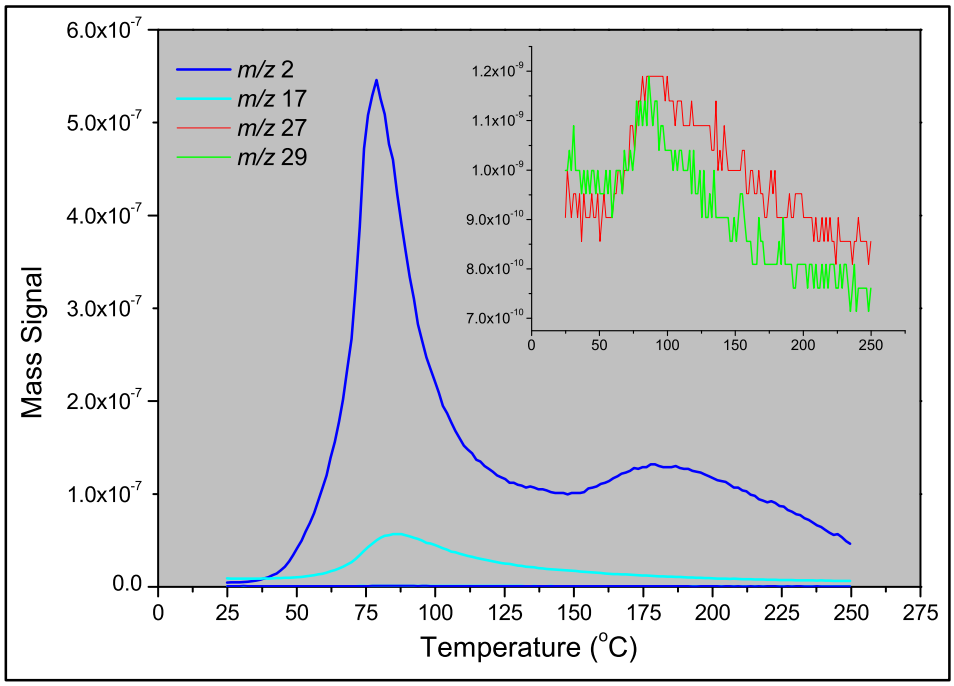

Figure 4.5: Mass spectra of gases evolved during 1:1 ($LiNH_2$:NH_3BH_3) reaction and decomposition.

start of the reaction and decreases as the reaction progresses.

The expected ratio for these ions is 80:20:1. A higher than expected concentration of CO_2 was detected throughout the course of the reaction. This is a consequence of residual water (m/z 17 and m/z 18) within the system, both on the walls of the capillary, and in the mass spectrometer itself. CO_2 has a high solubility in water and therefore atmospheric CO_2 is inevitably dissolved in this residual water, which leads to a much higher concentration of CO_2. The OH^+ (m/z 17) ion from this residual water also interferes with the $^{14}NH_3{}^+$ (m/z 17) ion of ammonia, thereby making the detection of ammonia difficult.

Peaks in the mass spectrum at m/z 2 and m/z 1 correspond to hydrogen. Hydrogen is the major gas evolved upon decomposition and is evolved in two

stages. A low temperature sharp peak occurs at approximately 70°C accompanied by evolution of a trace amount of *m/z* 29 (0.10% of *m/z* 2 hydrogen intensity) and *m/z* 27 (0.10% of *m/z* 2 hydrogen intensity) - enhanced in insert Figure 4.5. The origin of these fragments is most likely monomeric aminoborane BH_2NH_2 [83], [52]. Peaks from *m/z* 14 to *m/z* 17 correspond to ammonia. Ammonia (10.83% *m/z* 2 intensity) was detected throughout the course of decomposition with a peak occurring at approximately the same temperature as the first hydrogen desorption peak. There were small contributions to mass spectra by ions *m/z* 30 (0.40% of *m/z* 2 intensity) and *m/z* 14 (0.20% of *m/z* 2 intensity) in this temperature range which could not be assigned.

Further evolution of hydrogen occurs over a broad temperature range centred at approximately 170°C; hydrogen is the only gas detected in this temperature range.

No ion fragments corresponding to the parent ions of diborane or borazine were detected throughout the decomposition as is observed for the thermal decomposition of neat ammonia borane (detection limit estimated to be 40 ppm).

There are three notable affects resulting from the presence of lithium amide. First, the temperature threshold for H_2 release is notably lower than the temperature threshold for neat ammonia borane, which is indicative of an enhanced rate of H_2 release. This trend is illustrated in Figure 4.6. Second, the presence of amide also affects the kinetics of the second desorption stage i.e., evolution of hydrogen during the second stage occurs over a much broader temperature range than that of neat ammonia borane. Thirdly, the borazine and diborane side products observed during decomposition of neat ammonia borane is not observed as a volatile product during the decomposition of NH_3BH_3 + $LiNH_2$.

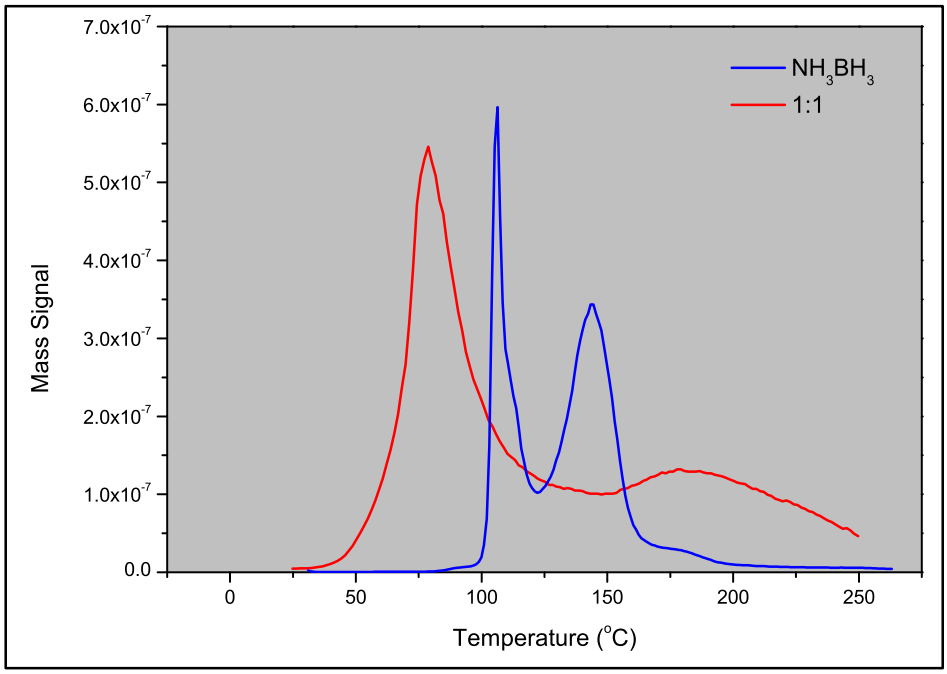

Figure 4.6: Hydrogen evolution profile of neat ammonia borane and 1:1 ($LiNH_2$:NH_3BH_3).

4.4.2 Weight Percent Hydrogen Desorption During Thermal Decomposition

The aim of this research as discussed in section **1.9** was to demonstrate >9 wt% hydrogen desorption at temperatures between 60-120°C to meet requirements specified by the US Department of Energy. The samples in this study have been followed to 250°C in order to follow the second high temperature desorption step to nearer completion. The kinetics of this step are quite slow.

Weight percent of hydrogen desorbed during thermal decomposition of a 1:1 ($LiNH_2$:NH_3BH_3) was determined by means of mass measurements described in section **2.3.4** and volumetric measurements. An average of 15 wt% (based on ammonia borane) weight loss occurred during heating up to 250°C.

The mass spectrum of the released gas phase during thermal decomposition

of post mixed NH_3BH_3 + $LiNH_2$ samples (section **4.4.1**) showed that the gas evolved consisted predominantly of hydrogen and ammonia. Concentrations of other trace gases were so small that they had no significant contribution to gas composition.

Quantitative acid base titration of an HCl solution through which the gas had been bubbled (discussed in section **2.3.3**) found that the NH_3 contributed to approximately 1% of this weight loss; a result which was tentatively confirmed by gas chromatography. Therefore, from these results it can be concluded that a total 14 wt% of hydrogen is desorbed during thermal decomposition up to 250°C. This equates to an average of 3.77 moles of hydrogen (based on ammonia borane).

This result was confirmed by volumetric measurements of gas evolved throughout decomposition (measured by means of collection of gas in a gas burette as discussed in section **2.3.3**). An average of 3.70 moles (based on ammonia borane) of gas was evolved; a result which was consistent across the molar ratios examined.

As discussed above, hydrogen is evolved in two stages, however, as displayed in Figure 4.5 the two stages are not well defined i.e., overlapping of the peaks occurs. Deconvolution of these stages was not possible to determine the wt% desorbed in each event. To overcome this, integration of the area under each peak was carried out using the mass spectral data obtained during thermal decomposition. These calculations indicate that this first step of hydrogen loss accounts for ∼60% of the total hydrogen evolved throughout decomposition i.e., 2.26 mol of hydrogen is desorbed in the first stage (∼50-70°C) and 1.51 mol in the second desorption stage.

Calculations indicate that an average of 11 wt% hydrogen is desorbed at tem-

peratures below 100°C; a result that was consistent across all ratios studied. This 11 wt% hydrogen desorption from NH_3BH_3 + $LiNH_2$ at temperatures below 100°C exceeds the target of 9 wt% specified by the US Department of Energy.

4.4.3 Identification of Phases Formed During Thermal Decomposition

4.4.3.1 X-ray Diffraction

Powder X-ray diffraction data collected on dehydrogenated material showed an amorphous or poorly crystalline phase, indicating that dehydrogenation results in the formation of BNH_x polymeric products as observed for ammonia borane [64]. The residual BNH_x exists in an amorphous or poorly crystalline state, possibly in a range of B-N-H stoichiometries, and loses H_2 much more slowly. This is responsible for the poor kinetics of the second desorption stage seen in the mass spectrum. Samples in which an excess of lithium amide was present showed crystalline peaks corresponding to unreacted $LiNH_2$.

4.4.3.2 Solid-State ^{11}B NMR Spectroscopy

Due to the amorphous nature of the samples, solid-state ^{11}B NMR was used to investigate the formation of boron-containing non-volatile intermediates and products formed throughout the decomposition. ^{11}B NMR is a sensitive technique as the various boron environments (B-H_x x= 1-4) have large chemical shift differences [84], [85]. ^{11}B is a quadrupolar nucleus with a spin of $\frac{3}{2}$, which can give rise to significant broadening of the NMR resonances of compounds with asymmetrical B environments. However, the natural abundance (80.42%) and sensitivity of ^{11}B allow for fast acquisition of spectra [86].

Crystalline ammonia borane exhibits an ^{11}B NMR resonance centred at -27 ppm (Figure 4.7). The resonance has a large quadrupolar interaction that

broadens the peak over a large chemical shift range [84]. This quadrupolar interaction is inversely proportional to the applied magnetic field so is reduced at higher fields [87].

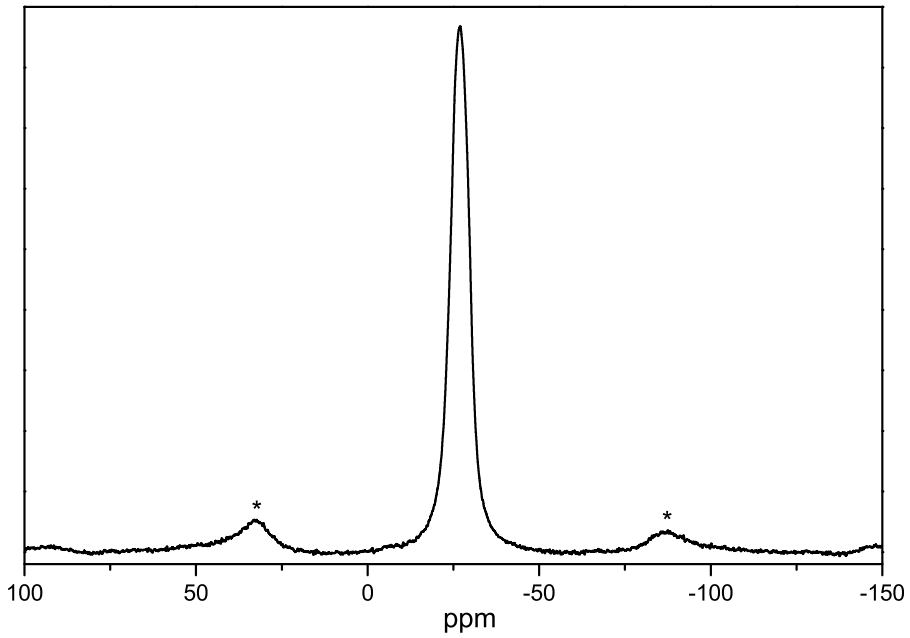

Figure 4.7: Solid-state ^{11}B NMR spectrum of ammonia borane.

Peaks marked with an asterix in the spectrum are spinning side bands. These spinning side bands arise as a result of chemical shift anisotropy. Solid-state NMR peaks tend to be broad due to this chemical shift anisotropy, spinning of the sample eliminates this providing the spinning frequency is close to the frequency spread of the signal. When the spectra are particularly broad and the spinning rate cannot match the spread of the signal, a series of spinning side bands are observed, which are separated by the spinning frequency [88]. In order to be sure which resonance is the central band and which are the spinning side bands, the spectrum is collected at two speeds; the spinning side bands move with changing spinning speed but the central resonance remains fixed.

Samples of solidified post-mixed $LiNH_2$ + NH_3BH_3 (no hydrogen loss) all showed a single sharp resonance at -24 ppm, irrespective of the $LiNH_2$ to NH_3BH_3 ratio. The narrow linewidths were of the order 1322 Hz, even without proton decoupling. This is indicative of either a spherically symmetrical boron environment, or a material exhibiting a liquid-like state. The limited amount of ^{11}B NMR data available makes it difficult to definitively assign the resonances to known species. However, this resonance is within the region expected for a -BH_3 environment [89], [90], suggesting that the boron is in a similar, although not identical, environment to the boron in NH_3BH_3.

This behaviour has parallels with recent observations by Stowe *et al.* during the isothermal decomposition of solid-state ammonia borane [67]. The mechanism of hydrogen release was investigated via solid-state ^{11}B NMR spectroscopy. During the decomposition of ammonia borane to form the diammoniate of diborane, an intermediate phase resonating at -23 ppm was observed. It was postulated that a weakly bound adduct, in which the dihydrogen bonding network of ammonia borane is disrupted and the conditions are being prepared for nucleation is responsible for this resonance (shown in Figure 4.8a).

This data suggests then, that the $LiNH_2$:NH_3BH_3 is in the form of a weakly bound adduct with an $H_2N^{\cdots}BH_3$-NH_3 environment similar to that reported in the above study (Figure 4.8b).

Samples heated to 60°C (after the first desorption stage) show the peak intensity of the -24 ppm resonance decreasing and a second resonance appearing at 22 ppm, which develops simultaneously with H_2 loss. Samples heated to 250°C (past the second desorption stage) show only the 22 ppm resonance. This chemical shift is consistent with a BN_3 environment [91]. The ^{11}B NMR spectrum of a 1:1 ($LiNH_2$:NH_3BH_3) sample at various stages of hydrogen loss

A)

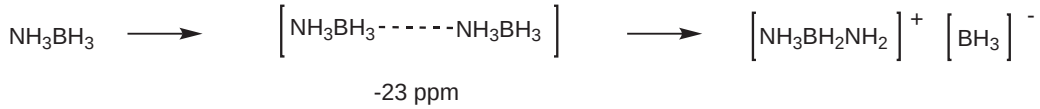

B)

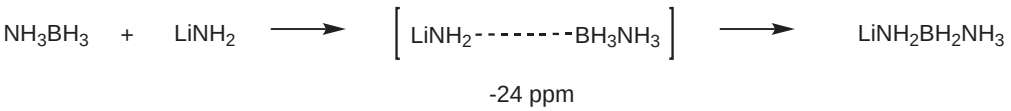

Figure 4.8: Adducts responsible for -23 and -24 ppm resonances.

is shown in Figure 4.9. In the case of the 1:1 ($LiNH_2$:NH_3BH_3) ratio we may expect to see fragments such as those drawn in Figure 4.10 A and 4.10 B (or a mixture of both) to allow the B:N stoichiometry to be maintained.

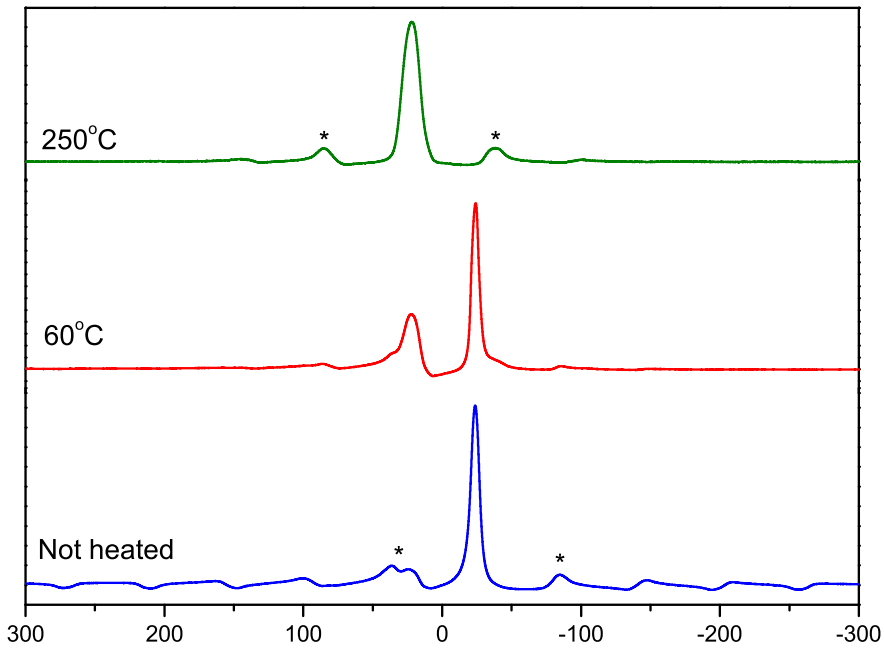

Figure 4.9: Solid-state ^{11}B NMR of different boron environments observed upon heating $LiNH_2$:NH_3BH_3.

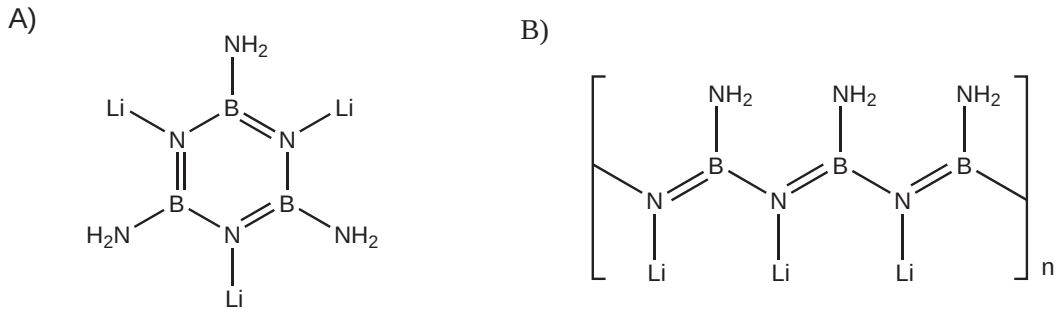

Figure 4.10: Proposed BN_3 compounds.

The above trend was observed irrespective of $LiNH_2$ concentration. It can therefore be concluded that all ratios examined undergo the same reaction pathway resulting in compounds such as those drawn in Figure 4.10, and reactions utilising higher $LiNH_2$ contents retain unreacted $LiNH_2$ in the product. This theory is supported by X-ray crystallography (section **4.4.3.1**), in which unreacted lithium amide is present for reactions utilising an excess of amide.

This contrasts significantly with the thermal decomposition of NH_3BH_3 in the absence of $LiNH_2$, in which intermediate boron environments such as -BH_2 and -BH_4 of the ion pair $[(NH_3)_2BH_2^+][BH_4^-]$ (diammoniate of diborane) are observed [67] (discussed in section **1.7.3**).

4.4.4 Mechanistic Studies of Hydrogen Formation

Isotopic substitution was used as a tool for probing the mechanism of thermal decomposition. By selectively deuterating different hydrogen positions on ammonia borane and analysing the gaseous products, details about the mechanism and possible products can be determined

This tool has previously been employed by Smith *et al.* [65] to investigate the mechanism of thermolysis of ammonia borane. The gaseous products evolved during thermal decomposition of a NH_3BH_3/ND_3BH_3 mixture were analysed using mass spectrometry. They observed the presence of all three

isotopic species H_2, HD, and D_2. From these results it was concluded that the reaction takes place via a bimolecular pathway. The presence of all three isotopic species indicate that hydrogen loss occurs through both inter- and intra-molecular dihydrogen interactions.

Volatile gases evolved during the thermolysis of post mixed ammonia borane isotopologues ND_3BH_3, NH_3BD_3 + $NiNH_2$ were analysed using mass spectrometry. Deuterated amineboranes and lithium amide were reacted together via the same method described for ammonia borane and lithium amide discussed in section **2.3.1**. The mass spectral data of a mixture of ND_3BH_3 + $LiNH_2$ and NH_3BD_3 + $LiNH_2$ are shown in Figures 4.11 and 4.12 respectively.

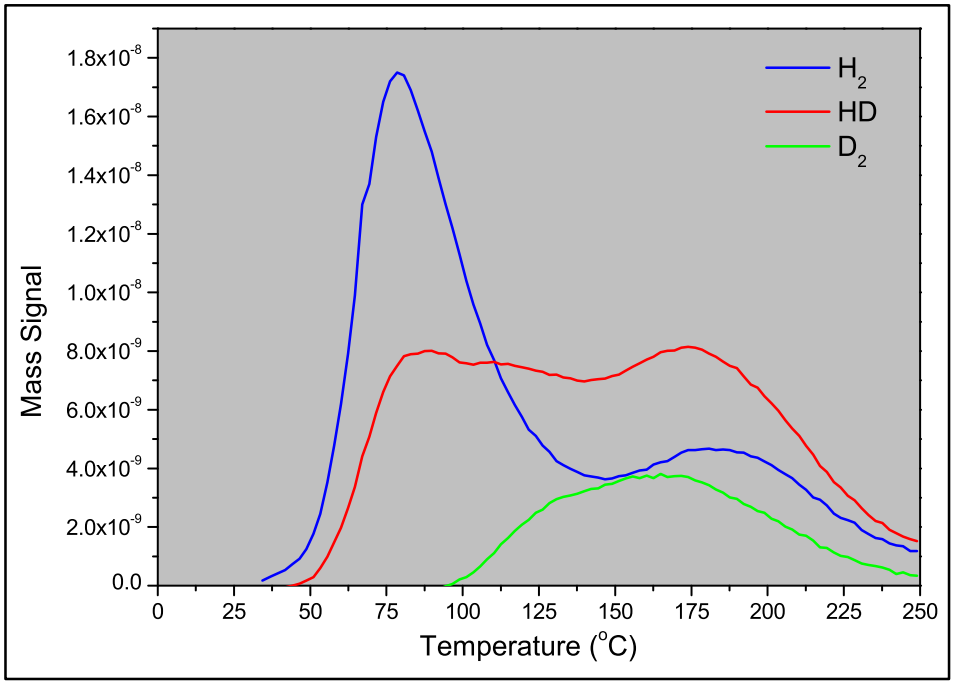

Figure 4.11: Mass spectra of gases evolved during 1:1 ($LiNH_2$:ND_3BH_3) reaction and decomposition.

All three molecular species H_2 (m/z 2), HD (m/z 3) and D_2 (m/z 4) are detected throughout the thermal decomposition. The observation of all three

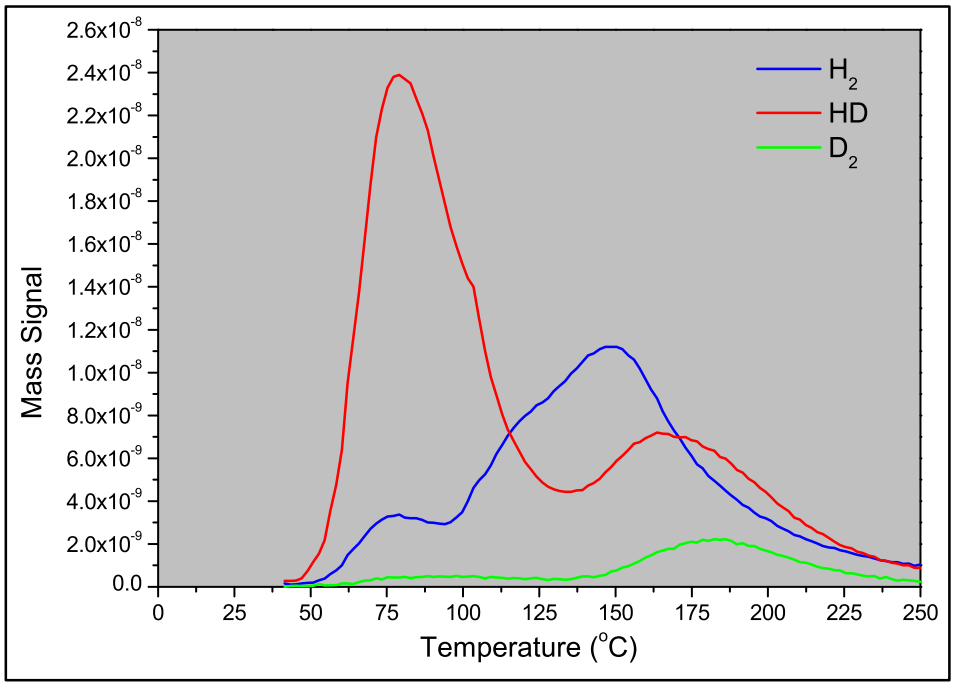

Figure 4.12: Mass spectra of gases evolved during 1:1 ($LiNH_2$:NH_3BD_3) reaction and decomposition.

isotopic species in the mass spectrum is indicative of a bimolecular process.

Hydrogen evolution occurs in two distinct stages indicated by peaks in the mass spectrum. The first desorption stage occurs between 50-140°C. HD (m/z 3) is the predominant species present in this first stage for NH_3BD_3 + $LiNH_2$, accompanied by H_2 (m/z 2) evolution (14.30% of m/z 3 intensity). This trend is also observed in the first desorption stage for the ND_3BH_3 + $LiNH_3$ reaction. However, an inversion of the ratios of the two species occurs. For ND_3BH_3 + $LiNH_3$, H_2 (m/z 2) is the predominant species evolved accompanied by HD (m/z 3) evolution (45.5% of m/z 2 intensity).

Based upon these mass spectral results and the ^{11}B NMR results reported in section **4.4.3.2**, a scheme of the mechanistic pathway leading to hydrogen release from NH_3BH_3 + $LiNH_2$ in this first desorption stage can be proposed

as summarised in Figure 4.13.

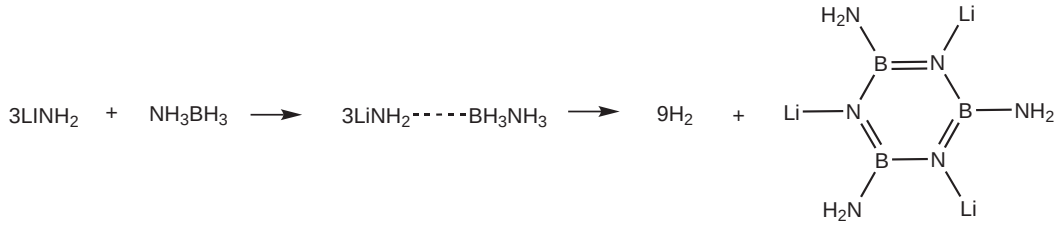

Figure 4.13: Proposed reaction pathway.

The first stage of hydrogen loss occurs through a multistep reaction. During this first desorption stage approximately 3 moles of hydrogen are evolved (60% of total hydrogen evolution), indicating that all the process are occurring rapidly and simultaneously. The first stage of hydrogen loss occurs through a dihydrogen bonding interaction between the hydridic boron hydrogens and the acidic hydrogens of lithium amide to form $LiNHBH_2NH_3$. This compound is highly reactive (no resonance corresponding to NBH_2 present in the ^{11}B NMR spectrum) and rapidly cyclises with another two $LiNHBH_2NH_3$ molecules forming a cyclic BN_3 compound with a resonance at 22 ppm in the NMR spectrum.

According to this mechanism, the isotopic composition of evolved hydrogen varies according to the site of deuteration in the starting ammonia borane. The first two stages of hydrogen generation involve atoms from $LiNH_2$ and those attached to the boron of NH_3BH_3. The third stage involves one hydrogen atom originally attached to nitrogen and one to boron in NH_3BH_3. Therefore, when ND_3BH_3 is used, the first two stages generate H_2 and the last HD (Figure 4.14 a). In contrast, NH_3BD_3 gives HD in all three stages (Figure 4.14 b). This concurs with the observed EGA measurements outlined above.

Small inconsistencies are seen in the expected ratios for both reactions. This is the result of incomplete deuteration of the starting ammonia borane. The degree of deuteration of the ND_3BH_3 and NH_3BD_3 starting compounds was

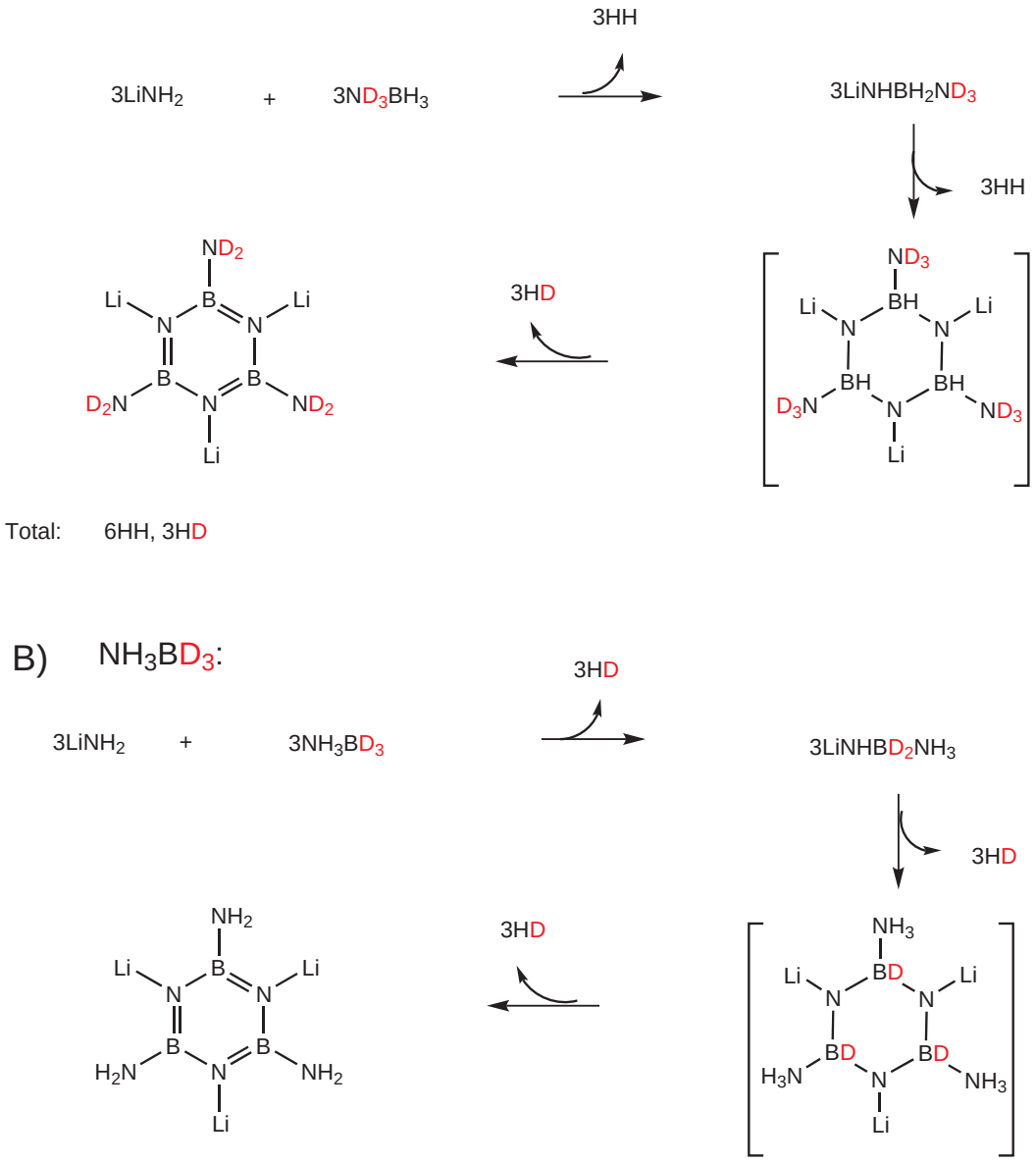

Figure 4.14: Proposed mechanism for first stage of hydrogen loss from NH_3BH_3 + $LiNH_2$.

investigated using ^{1}H NMR (section **3.3.3**). Both compounds were believed to be approximately 90% deuterated.

The second desorption stage occurs between 140-250°C. In both instances an inversion of the ratios of H_2 and HD observed in the first stage occurs. The

presence of D_2 (*m/z* 4) is most likely the result of exchange reactions occurring at high temperatures (above 100°C).

This second step is complex and little is known about the mechanism by which hydrogen loss occurs. It is a long slow process and is further complicated by isotopic scrambling occurring at higher temperatures. This stage most likely involves polymerisation or cross-linking of the preformed BN_3 compound to evolve further hydrogen.

Throughout the course of both reactions traces of ammonia were detected as *m/z* 16 and *m/z* 17 (-NH_2 and -NH_3). No deuterated derivatives of ammonia were detected throughout the decomposition process, however, strong interference from *m/z* 16, *m/z* 17, *m/z* 18, and *m/z* 20 ions made detection of these deuterated derivatives difficult. The detection of ammonia as *m/z* 16, *m/z* 17 indicate that lithium amide may be the source of the ammonia generated throughout the reaction; however, the mass spectrum of $LiNH_2$ heated to 250°C shows that no ammonia is evolved in this temperature range. The origin and mechanism of the ammonia evolution therefore remains unclear.

4.4.4.1 Effect of Lithium Amide Concentration on Reaction Mechanism

Lithium amide and ammonia borane react in a stoichiometric 1:1 reaction, an excess of lithium amide has no affect on the amount of hydrogen evolved throughout the reaction or the products formed up to 250°C. This is supported by ^{11}B NMR spectroscopy (section **4.4.3.2**) in which all ratios possess similar resonances corresponding to BN_3 containing compounds such as that drawn in Figure 4.10, and reactions utilising higher $LiNH_2$ contents retain unreacted $LiNH_2$ in the product (shown by X-ray diffraction section **4.4.3.1**).

Although the reaction mechanism is not affected by the concentration of lithium

amide, the kinetics of the reaction are. Figure 4.15 illustrates the hydrogen evolution profiles of different $LiNH_2$:NH_3BH_3 ratios. The presence of amide results in a decrease of the temperature threshold for H_2 release (compared with that of neat ammonia borane). While this is true for all ratios examined,

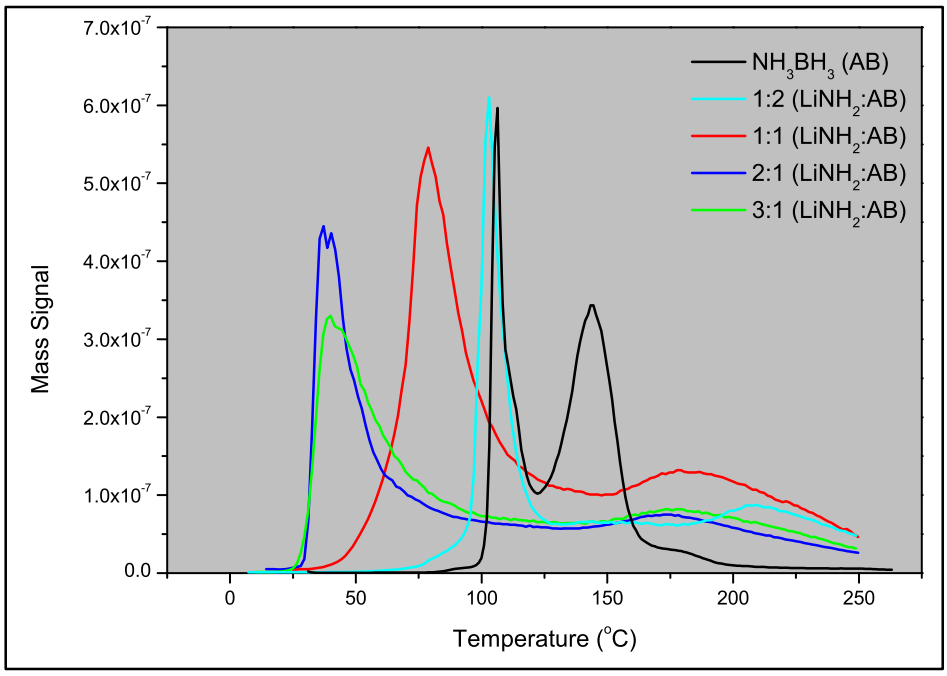

Figure 4.15: Influence of concentration of lithium amide on hydrogen desorption temperature.

it is clear that reactions which utilise an excess of lithium amide (2:1 and 3:1 $LiNH_2$:NH_3BH_3) have a much lower temperature threshold than 1:1 reactions. The reason for this remains unclear, however, it is possible that hydrogen loss from the bulk material may occur through another "melt", or liquid phase. An excess of lithium amide has previously been shown to encourage the formation of such phases, discussed in section **4.3**.

4.5 High Temperature Thermal Decomposition

4.5.1 Closed System High Temperature Reaction

A series of post mixed, dehydrogenated (heated to 250°C) samples were heated to 400°C in a custom made, sealed stainless steel bomb to investigate hydrogen loss and product formation at higher temperatures. It has been reported that heating ammonia borane at high temperatures results in cross-linking between BNH_x (formed in the second desorption stage) to release additional hydrogen. These materials are precursors to boron nitride [52], [53].

4.5.1.1 X-ray Diffraction

Upon heating to 400°C, no change in crystallographic order occurred. X-ray diffraction (Figure 4.16) showed only amorphous phases and lithium oxide present. Crystalline peaks corresponding to lithium amide were observed for samples in which an excess of amide was utilised.

4.5.1.2 Solid-State ^{11}B NMR Spectroscopy

Solid-state ^{11}B NMR confirmed that no change of the boron coordination environment occurred at higher temperatures. Samples heated to 400°C (Figure 4.17) show a single resonance centred at ∼25 ppm. This chemical shift is consistent with a BN_3 environment as observed for samples heated to 250°C (section **4.4.3.2**). However, the peak exhibits a second-order quadrupolar lineshape with a small asymmetry factor indicating that the boron site in the BN_3 compound is present in a ridged, low symmetry environment [86], [91], [84]. The intensities of the two maxima are inverted compared with those expected compounds containing B-N bonds, this feature has also been observed for ammonia borane [84]. The inversion of intensities of quadrupolar shape maxima may be due to the coupling of ^{11}B nuclei to neighbouring ^{14}N ($I = 1$) quadrupolar nuclei [84].

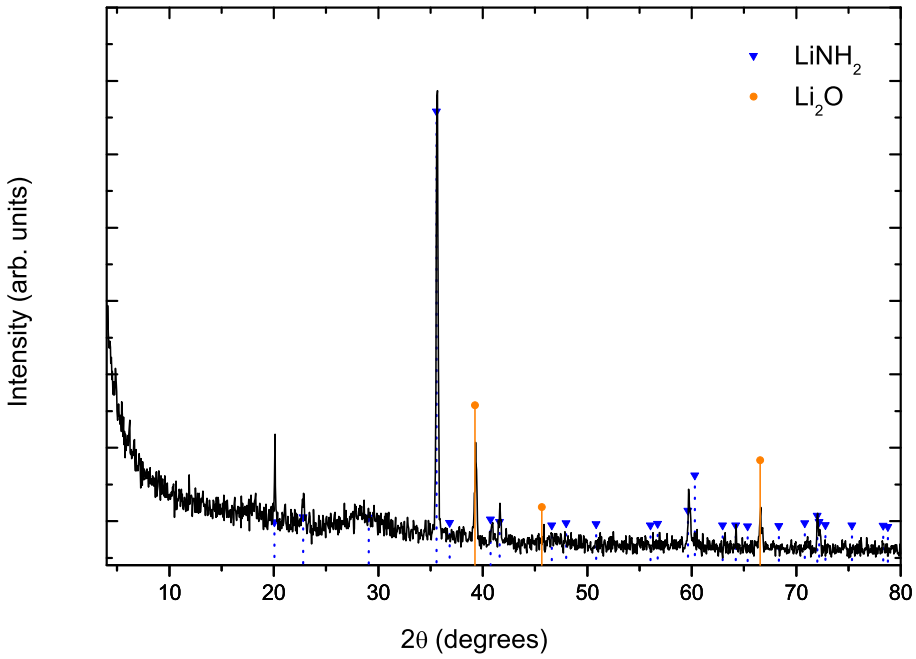

Figure 4.16: X-ray diffraction pattern of 3:1 ($LiNH_2$:NH_3BH_3) heated to 400°C in a closed system.

This trend was observed irrespective of $LiNH_2$ concentration. The reaction between lithium imide and ammonia borane at high temperatures has been shown to form lithium boron nitride (Li_3BN_2) [70]. Li_3BN_2 is a stable crystalline material existing in at least two temperature dependent phases [92] (shown in Figure 4.18). The structure is dominated by a linear N-B-N anion with which lithium cations are associated. This compound has potential as a hydrogen storage material due to its lightweight and theoretically high hydrogen content. 3:1 ($LiNH_2$:NH_3BH_3) reactions possess the correct stoichiometry for formation of Li_3BN_2, which is expected to form upon heating this mixture to high temperature. However, formation of this crystalline phase was not observed in this closed system.

This observation is most likely due to species evolved re-reacting with starting materials. It has previously been observed that upon reaction between lithium

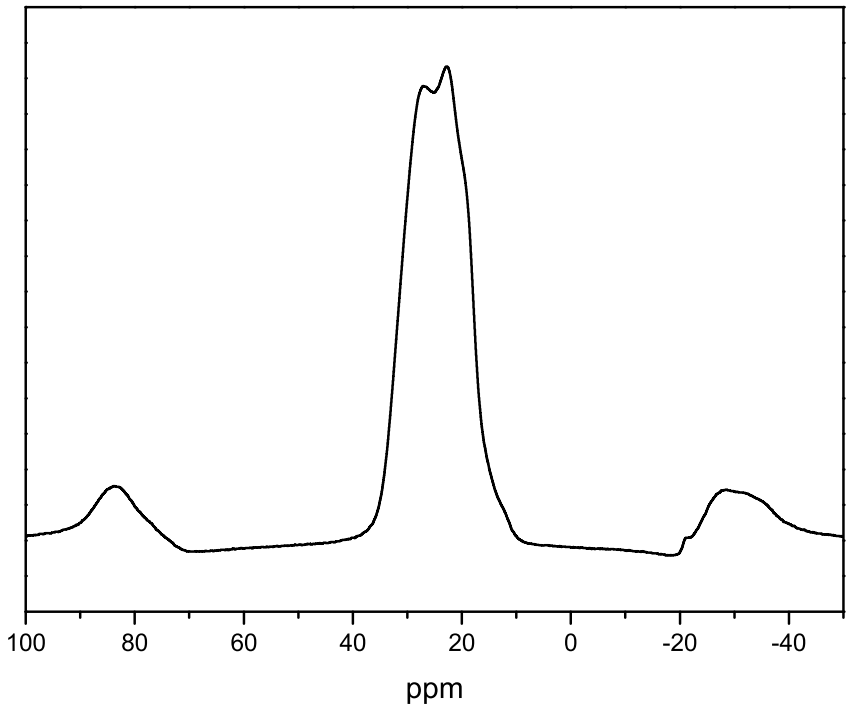

Figure 4.17: Solid-state ^{11}B NMR of $LiNH_2$:NH_3BH_3 heated to 400°C in a closed system.

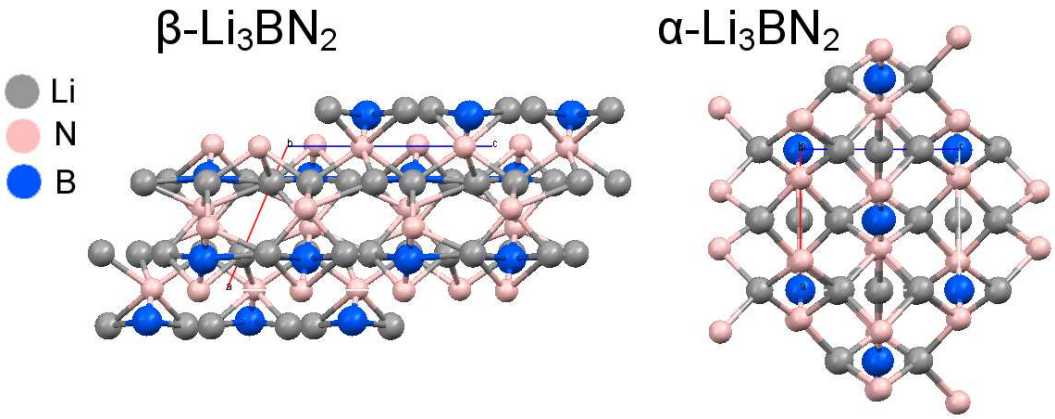

Figure 4.18: Low (α) and high (β) temperature phases of Li_3BN_2. Viewed along the b axis.

imide and ammonia borane in a pressurised system no ammonia, diborane, or borazine was liberated [70]. However, upon reaction at atmospheric pressure under flowing argon, ammonia was detected together with a very small amount

of diborane and borazine. This implied that in the first reaction the liberated ammonia reacted with other components in the mixture under the confines of the pressurised mill. This is likely to have occurred in the sealed bomb used for these experiments.

4.5.2 Flow-Through System High Temperature Reaction

To prevent the species generated re-reacting with starting compounds, a series of post mixed samples were heated in an flow-through system under inert atmosphere. Samples were heated at a rate of 1°C/min to temperatures of 400°C, 500°C, and 600°C in alumina crucibles to investigate formation of such compounds from the $LiNH_2$ + NH_3BH_3 system.

Upon heating to higher temperatures a further ∼15 wt% was lost to give a total of ∼30 wt% loss throughout dehydrogenation. This weight loss is probably attributed to further hydrogen loss, along with loss of unknown large volatile compounds. Attempts to analyse evolved gases during this process using mass spectrometry were unsuccessful. Unknown heavy evolved species (greater than m/z 100) caused a blockage in the gas flow upon condensation in the capillary employed for mass spectral measurements, thereby making mass spectral analysis impossible. Condensation and analysis of these species by other means was not accessible under an inert atmosphere.

4.5.2.1 X-ray Diffraction

X-ray diffraction of 2:1 samples show crystalline peaks corresponding to the beta form of lithium boron nitride (β-Li_3BN_2) (ICDD pattern 01-074-1358) [93] at temperatures as low as 400°C. X-ray diffraction patterns of 3:1 samples heated to 400°C and 500°C also show crystalline peaks corresponding to β-Li_3BN_2 (Figure 4.19). X-ray diffraction patterns of 3:1 samples heated to 600°C (Figure 4.20) show peaks corresponding to the alpha form of lithium

boron nitride (α-Li_3BN_2)(ICDD pattern 00-040-1166) [93]. Heating 2:1 samples to higher temperatures (500°C and 600°C) had no further effect on crystallinity. The XRD patterns of these materials show only low counts for Li_3BN_2, despite being the only crystal form observed in the XRD. The low crystallinity could be due to the low formation temperatures used; compared with traditional formation routes [92]. The residual BNH_x exists in an amorphous or poorly crystalline state.

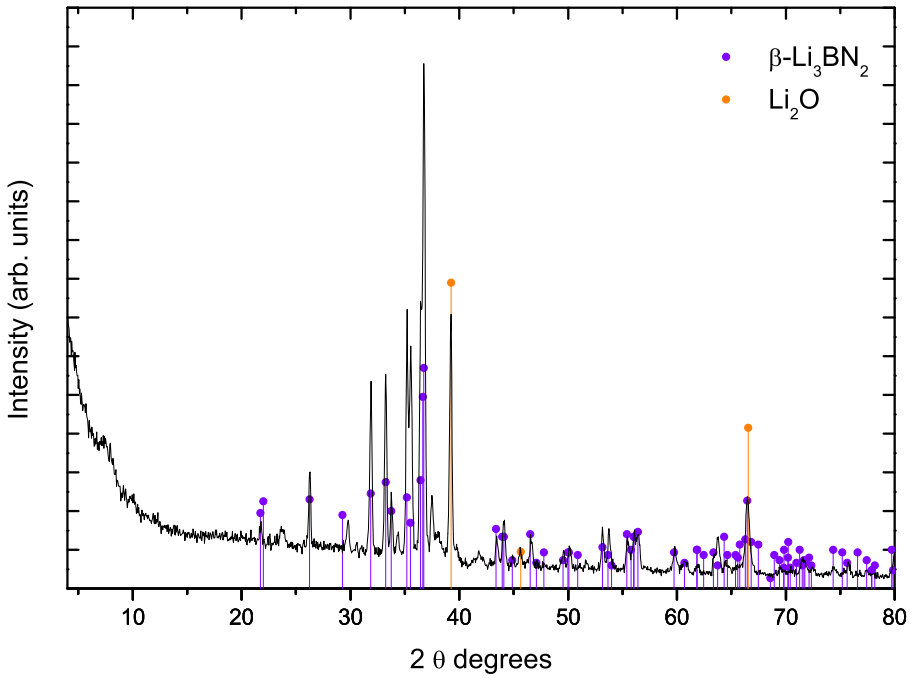

Figure 4.19: X-ray diffraction pattern of 3:1 ($LiNH_2$:NH_3BH_3) heated to 400°C in a flow-through system.

Formation of Li_3BN_2 was not observed for the 1:1 samples examined - the stoichiometry of these reactions prevented complete conversion to Li_3BN_2.

4.5.2.2 Solid-State ^{11}B NMR Spectroscopy

Samples heated at higher temperatures (> 400°C) react with the excess lithium amide to ultimately form Li_3BN_2 which exhibits a quadrupolar lineshape reso-

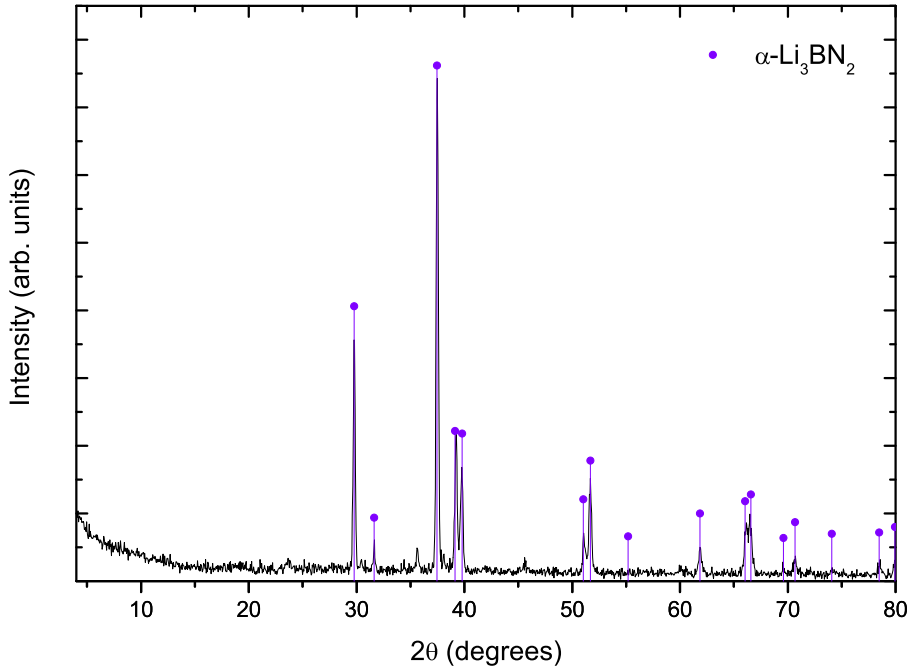

Figure 4.20: X-ray diffraction pattern of 3:1 ($LiNH_2$:NH_3BH_3) heated to 600°C in a flow-through system.

nance centred at ∼ -7 ppm [90]. No other B-containing materials are observed in the ^{11}B NMR. While the stoichiometry for the 1:1 and 2:1 reactions is not correct for full conversion to Li_3BN_2, the stoichiometry of the 3:1 should allow for complete conversion.

Figure 4.21 illustrates the growth of Li_3BN_2 (∼ -7 ppm) with increasing lithium amide concentration. The 1:1 sample shows a single sharp resonance at 23 ppm indicative of a BN_3 environment as seen at 250°C (section **4.4.3.2**). The 2:1 sample exhibits two different boron environments: the previously observed BN_3 environment resonating at 23 ppm, and a small resonance at -7.4 ppm. This resonance is consistent with a BN_2 environment due to the N-B-N moiety of Li_3BN_2. 3:1 samples also exhibit two boron environments. However, in this case the peak resonating at -7.4 ppm is much larger with respect to the peak at 23 ppm, indicating nearly complete conversion to Li_3BN_2. The

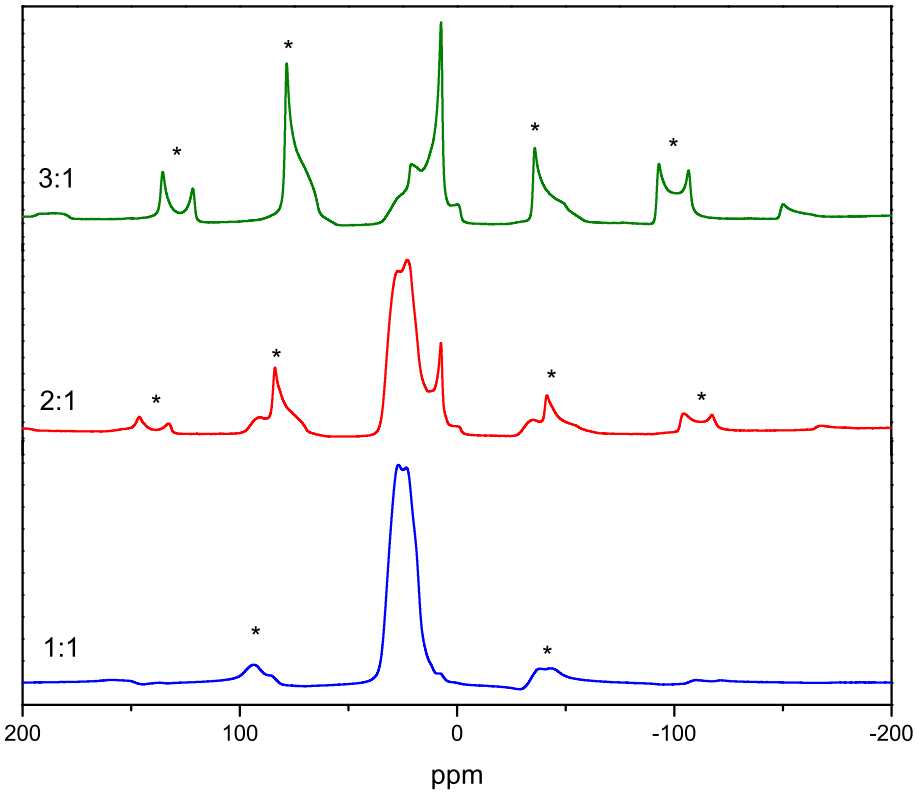

Figure 4.21: Solid-state ^{11}B NMR of different ratios of $LiNH_2$:NH_3BH_3 heated to 400°C in a flow-through system.

ready conversion to Li_3BN_2 from the $LiNH_2$ + NH_3BH_3 system is significant. As discussed in section **4.5.1.1**, Li_3BN_2 has been identified as a potential hydrogen storage material due to its lightweight and theoretically high hydrogen content. Attempts to re-hydrogenate this phase formed during the reaction between Li_2NH + NH_3BH_3 have been somewhat successful leading to 2.4 wt% hydrogen being re-absorbed at 80 bar H_2 pressure [70]. While the wt% H_2 re-absorption is relatively low, this is the first time a boron containing material has been shown to re-absorb hydrogen under these conditions.

4.6 Summary and Conclusions

From the work in this chapter it can be concluded that upon mixing lithium amide and ammonia borane, a highly exothermic reaction ensued via a liquid intermediate phase to form a weakly bound adduct with an $H_2N^{\cdots}BH_3$-NH_3 environment.

Thermal decomposition of this adduct to liberate hydrogen was observed at or above temperatures of 50°C in two discrete stages. ^{11}B NMR spectroscopy coupled with isotopic studies concluded that the first low temperature stage of hydrogen evolution occurs through a multi-step reaction, of which the onset is dependent on the ratio of $LiNH_2$:NH_3BH_3. A compound featuring a BN_3 environment such as those shown in Figure 4.10 was identified as a reaction intermediate.

Low temperature hydrogen evolution was accompanied by evolution of ammonia, the origin of which remains unidentified.

At higher temperatures the reaction proceeds via cross-linking or polymerisation of this intermediate to yield a non-volatile amorphous product. During which further hydrogen is liberated, but little information about this reaction was obtained.

A total of 11 wt% hydrogen was evolved upon thermal decomposition at temperatures up to 100°C. This exceeds both the DOE targets of >9 wt% at temperatures between 60-100°C, and that evolved from neat ammonia borane in this temperature range (6.5 wt%) [94].

Upon heating of this phase to temperatures of 400°C, 500°C, and 600°C; further mass loss occurs liberating large volatile compounds, which could not be successfully identified, to eventually form crystalline Li_3BN_2, a potential

hydrogen storage material.

Chapter 5

Solid-State Reaction between Methylamine Borane and Lithium Amide

5.1 Introduction

While the $LiNH_2$:NH_3BH_3 system discussed in chapter **4** shows promise - i.e., formation of a new phase which is capable of releasing >9 wt% at modest temperature - the system is not without limitations. The two of most concern are the release of volatile ammonia contaminants in the evolved hydrogen stream, and the kinetics and thermodynamics of the first stage of reaction. Therefore, a preliminary study into the effect of substitution of ammonia borane on these issues was conducted by means of reacting lithium amide and methylamine borane.

Methylamine borane ($CH_3NH_2BH_3$) is the simplest methyl derivative of ammonia borane. As with ammonia borane, methylamine borane has a high hydrogen storage capacity (9 wt%), and has been shown to evolve 2 moles of hydrogen upon heating.

5.2 Experimental Details

In this investigation methylamine borane and lithium amide were reacted in a 1:1 molar ratio. Unless otherwise noted, all manipulations were carried out by the same procedures as those used for the reaction between ammonia borane and lithium amide (described in section **2.3.1**). The main tools used for the characterisation of materials isolated were powder X-ray diffraction, mass spectrometry, and solid-state ^{11}B NMR spectroscopy.

5.3 Formation of Liquid Transition Phase

The reaction between methylamine borane and lithium amide also occurs through an exothermic reaction resulting in the formation of a liquid phase, however, a much faster reaction onset is observed in comparison with reactions utilising ammonia borane (section **4.3**). This is most likely attributed to the lower melting temperature of methylamine borane (56°C [95]) compared with ammonia borane (112°C- 114°C [96]).

While the kinetics of the reaction are affected by utilisation of methylamine borane, the thermodynamics of this stage compared with those utilising ammonia borane remain unchanged. Therefore, in order to prevent the reaction mixture reaching a critical temperature at which hydrogen is evolved, reactions must be performed on a small scale.

5.4 Thermal Decomposition

5.4.1 Evolved Gas Analysis

The release of gaseous products during the thermal decomposition of post-mixed samples of $CH_3NH_2BH_3$ + $LiNH_2$ in the temperature range up to 250°C were identified by means of mass spectrometry. A scan from m/z 0-100 was used under argon 10 mL/min (discussed in section **2.3.2**).

Thermal decomposition of neat methylamine borane occurs in two distinct stages. Hydrogen (m/z 2) is the predominant gas evolved on heating. The first hydrogen peak occurs at 110°C, the second occurs at 190°C. A number

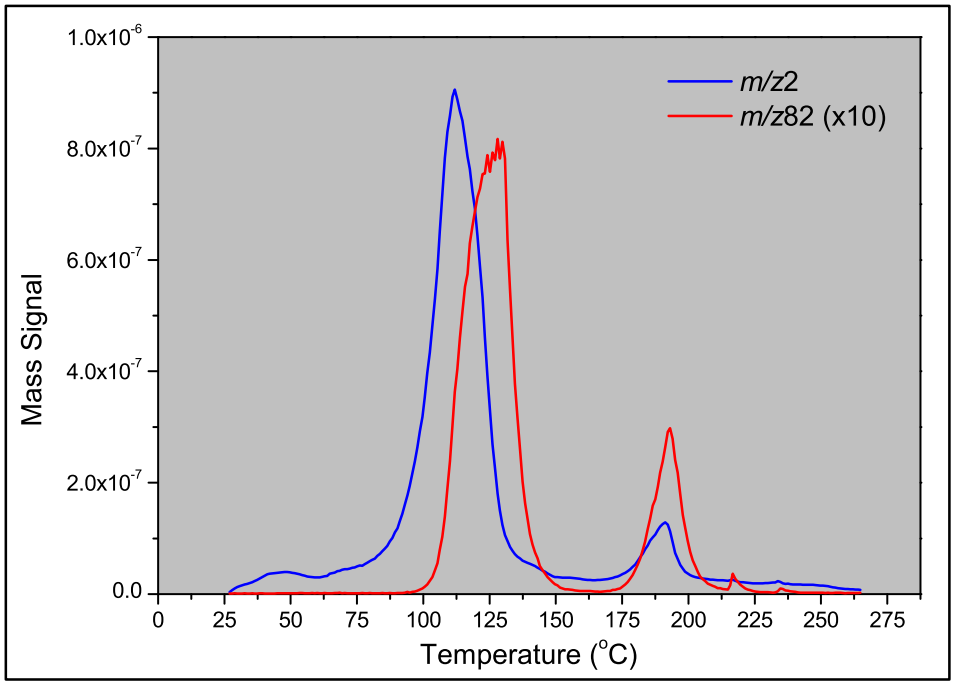

Figure 5.1: Mass spectra of gases evolved during thermal decomposition of $CH_3NH_2BH_3$.

of high mass fragments were detected throughout the decomposition process that were overlapping with, but at a slightly higher temperature, than the hydrogen signal. The most intense of these fragments was m/z 82 (8.90% of m/z 2 intensity), however fragments up to m/z 96 were detected with identical time/temperature profiles.

A plot of the temperature dependence of the two major observed ion intensities detected upon thermal decomposition of methylamine borane (m/z 2 and m/z 82) is shown in Figure 5.1. Recently Bowden *et al.* [75] proposed that the compound responsible for the m/z 82 - m/z 96 ions was N-

trimethylcyclotriborazane $(CH_3NHBH_2)_3$ - a previously reported product of the decomposition of neat methylamine borane [76], [97], [77].

The hydrogen evolution profile of a 1:1 ($LiNH_2$:$CH_3NH_2BH_3$) sample is shown in Figure 5.2. Hydrogen (m/z 2) is the major gas evolved upon decomposition

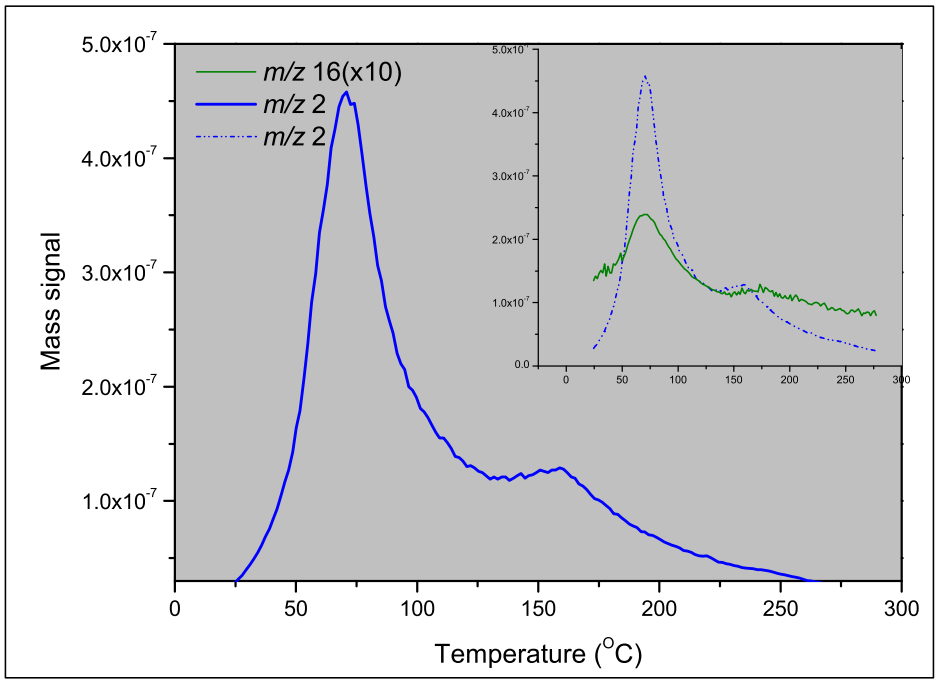

Figure 5.2: Mass spectra of gases evolved during thermal decomposition of 1:1 ($LiNH_2$:$CH_3NH_2BH_3$).

and is evolved in two stages. A low temperature peak occurs at approximately 70°C accompanied by m/z 15 (1.4% of m/z 2 intensity, enhanced in insert Figure 5.2) and m/z 16 (5.3% of m/z 2 intensity). The compound responsible for these fragments is most likely methane (CH_4 and CH_3^+). The evolution of methane suggests that hydrogen loss from 1:1 ($LiNH_2$:$CH_3NH_2BH_3$) may occur via the same mechanism described for the $LiNH_2$:NH_3BH_3 system (section **4.4.4**). Figure 5.3 illustrates one of the stages by which hydrogen is evolved during this first event. According to the mechanism, this stage involves evolution of one atom originally attached to nitrogen and one originally attached

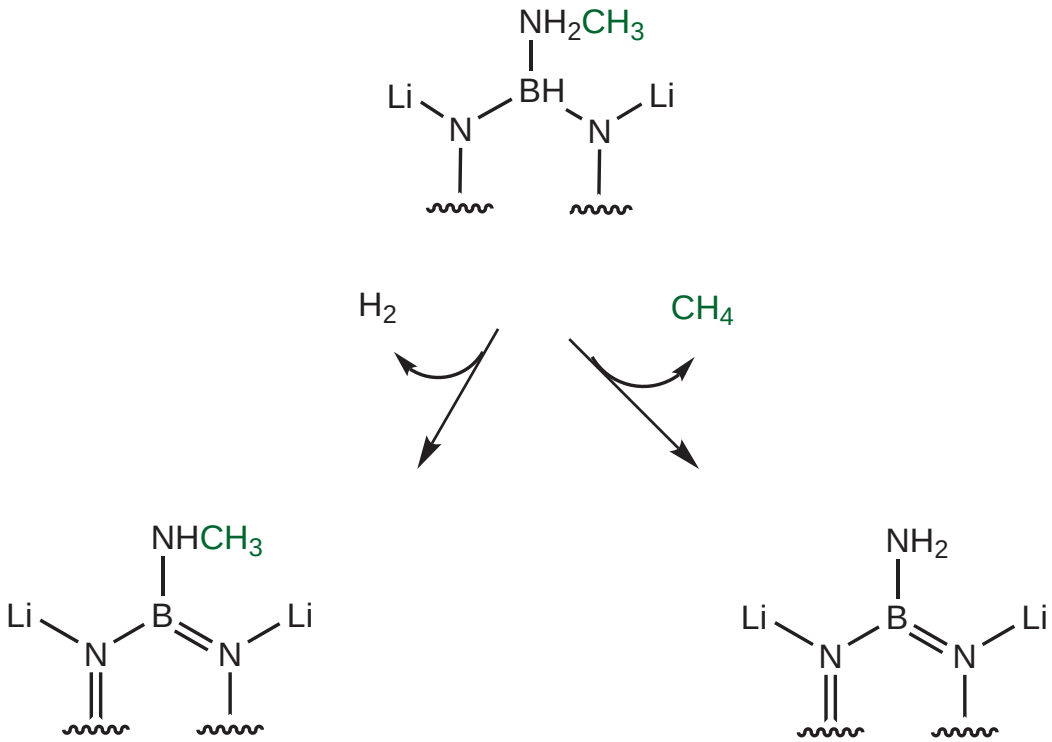

Figure 5.3: Proposed hydrogen loss mechanism for $CH_3NH_2BH_3$ + $LiNH_2$.

to boron. Therefore, decomposition of $CH_3NH_2BH_3$ can result in both H_2 and CH_4 evolution. This is supported by the observation that methane is mainly evolved during the low temperature hydrogen evolution stage.

Further evolution of hydrogen occurs over a broad temperature range centred at approximately 165°C; hydrogen is the only gas detected in this temperature range.

No fragments corresponding to ammonia were detected throughout the decomposition process. No high mass fragments (m/z 82 or higher) were detected throughout the decomposition as are observed during the thermal decomposition of neat methylamine borane.

The thermal decomposition of $LiNH_2$ + $CH_3NH_2BH_3$ has parallels with the $LiNH_2$ + NH_3BH_3 system (section **4.4.1**) i.e., the addition of lithium amide to the system enhances the rate of H_2 release. This trend is illustrated in Figure

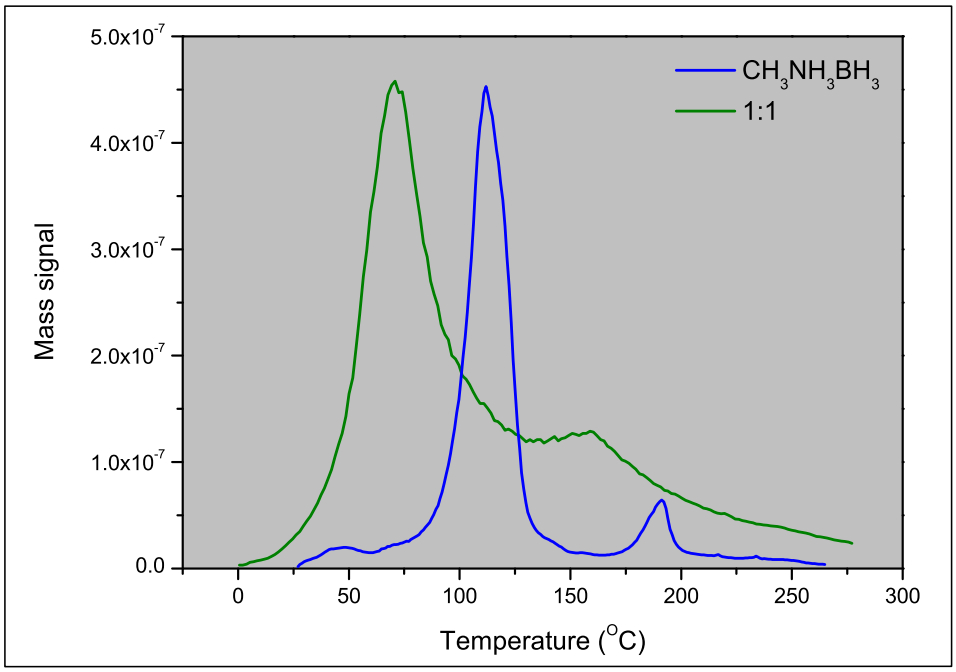

Figure 5.4: Hydrogen evolution profile of neat $CH_3NH_2BH_3$ and 1:1 ($CH_3NH_2BH_3$:$LiNH_2$).

5.4 which depicts the hydrogen evolution profiles of neat $CH_3NH_2BH_3$ and a 1:1 ($LiNH_2$:$CH_3NH_2BH_3$) sample. The presence of amide also affects the kinetics of the second desorption stage, causing the second event to occur over a much broader temperature range than for that of neat $CH_3NH_2BH_3$. The presence of lithium amide also suppresses the evolution of undesirable volatile by-products during the decomposition. This indicates that the mechanism of decomposition is different to that occurring in the neat solid state.

5.4.2 X-ray Diffraction

Powder X-ray diffraction data collected on dehydrogenated material showed an amorphous or poorly crystalline phase.

5.4.3 Solid-State ^{11}B NMR Spectroscopy

Due to the amorphous nature of the samples, solid-state ^{11}B NMR was used to investigate the formation of boron-containing non-volatile intermediates and products formed throughout the decomposition.

Crystalline methylamine borane reportedly exhibits an ^{11}B NMR resonance centred at ∼-19 ppm [98]. Figure 5.5 shows the ^{11}B NMR spectrum of neat

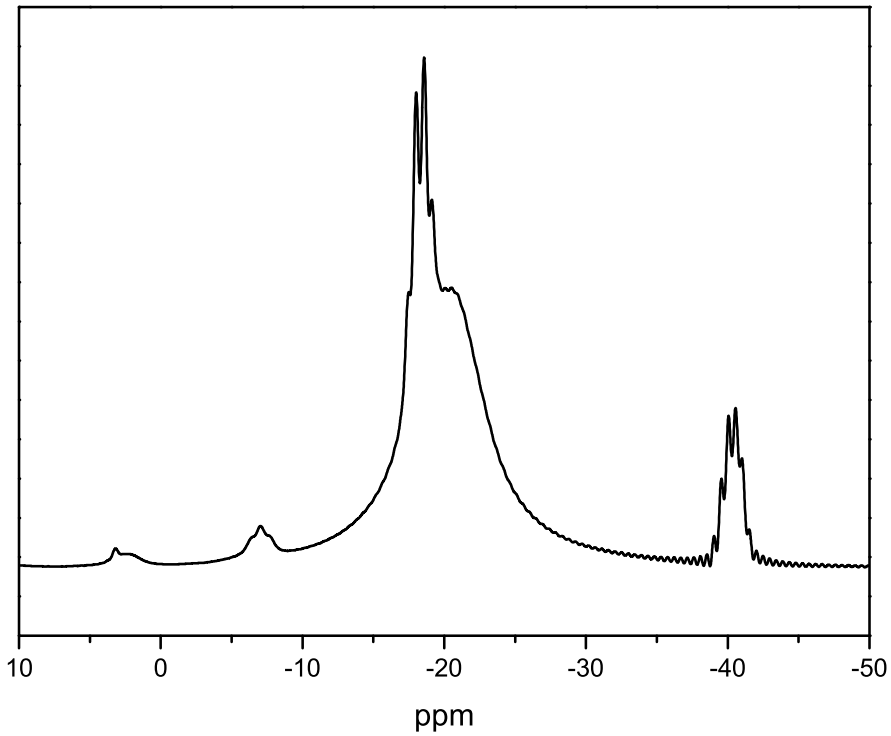

Figure 5.5: Solid-State ^{11}B NMR of $CH_3NH_2BH_3$.

methylamine borane. The spectrum is complicated by quadrupolar coupling, however, it can be seen that the resonance is centred at -20 ppm.

A peak resonating at -40.9 is present in the spectrum of methylamine borane and was present throughout the duration of the reaction. This peak was attributed to BH_4^- from residual sodium borohydride on the basis of previ-

ously reported resonances of BH_4^- [67], [60], [75], and the presence of BH_4^- in the ^1H NMR of $CH_3NH_2BH_3$ in DMSO (section **3.4.1**). Subsequent reactions utilising pure recrystallised methylamine borane (no sodium borohydride impurity), confirmed that the presence of BH_4^- has no effect on the kinetics of the reaction.

Samples of solidified post-mixed $LiNH_2$ + $CH_3NH_2BH_3$ show a sharp resonance at -17.8 ppm. This resonance is within the region expected for a -BH_3

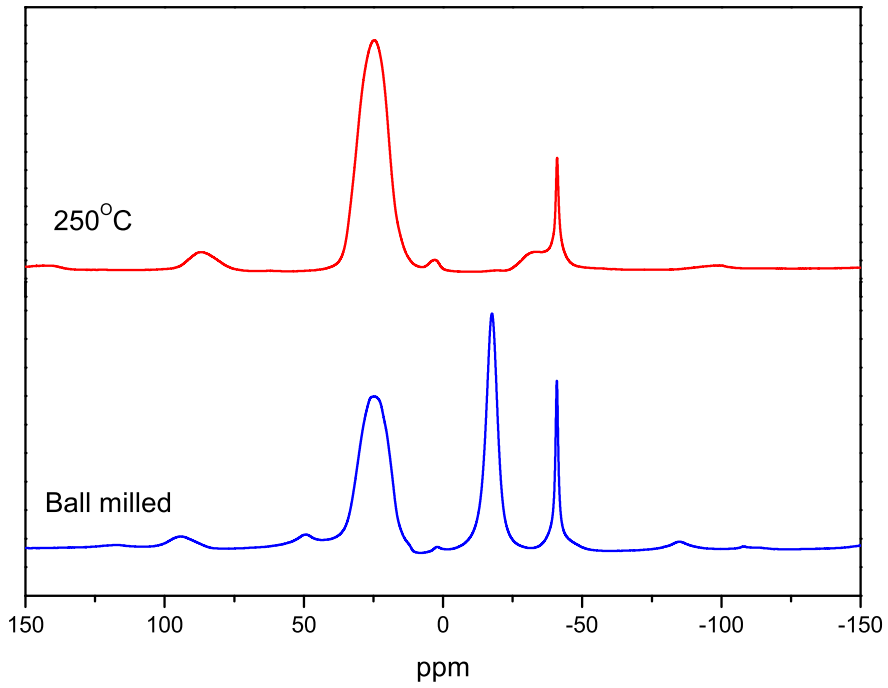

Figure 5.6: Solid-state ^{11}B NMR of different boron environments observed upon hydrogen loss from 1:1 ($LiNH_2$:$CH_3NH_2BH_3$).

environment [89], [90], similar to the boron in $CH_3NH_2BH_3$. Upon hydrogen loss, the peak intensity of this resonance decreases and a second resonance appears at 24.5 ppm, which develops simultaneously with H_2 loss. The ^{11}B NMR spectrum of a 1:1 ($LiNH_2$:$CH_3NH_2BH_3$) sample at various stages of hydrogen loss is shown in Figure 5.6. The ball milled spectrum corresponds to a 1:1 ($LiNH_2$:$CH_3NH_2BH_3$) solidified liquid phase which had been ball milled

at room temperature on a large scale. The spectrum exhibits both a -BH_3 resonance, and a peak resonating at 24.5 ppm corresponding to a -BN_3 environment, indicating that hydrogen loss had occurred. It is likely that the kinetic energy supplied by the ball mill coupled with the heat generated by performing the reaction on a large scale caused the reaction to reach a critical temperature in which hydrogen is evolved.

Samples heated to 250°C show only the 24.5 ppm resonance, which is consistent with a -BN_3 environment [91]. This two step phase change during hydrogen loss is similar to that observed during dehydrogenation of the $LiNH_2$:NH_3BH_3 system (section **4.4.3.2**). This observation, together with the observation of methane in the mass spectrum of a 1:1 ($LiNH_2$:$CH_3NH_2BH_3$) reaction, sug-

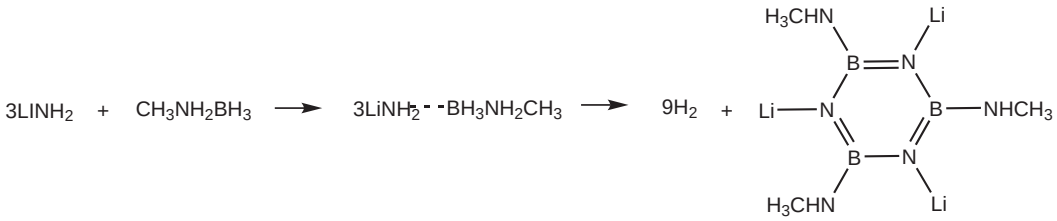

Figure 5.7: Proposed reaction pathway of hydrogen loss from $LiNH_2$ + $CH_3NH_2BH_3$.

gests that the dehydrogenation using methylamine borane occurs via the same mechanism as the ammonia borane system. If this is the case then we would expect the dehydrogenation to take place by the mechanism shown in Fig-

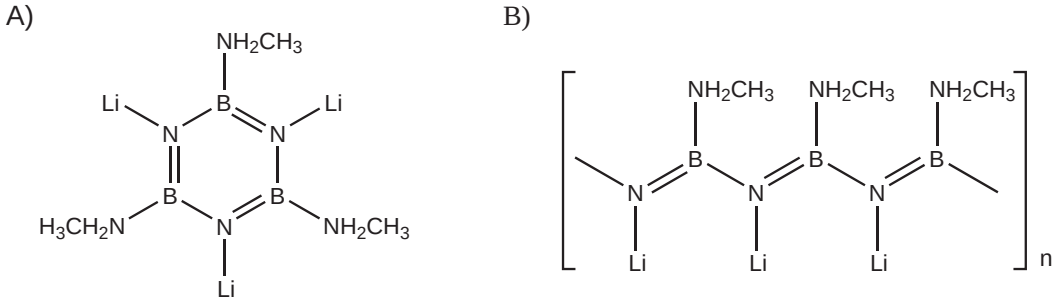

Figure 5.8: Proposed BN_3 compounds formed during decomposition of $LiNH_2$ + $CH_3NH_2BH_3$

ure 5.7, resulting in the formation of BN_3 compounds, such as those given in Figure 5.8, to allow the B:N stoichiometry to be maintained.

5.5 Summary and Conclusions

From the work in this chapter it can be concluded that upon mixing lithium amide and methylamine borane, an exothermic reaction ensued via a liquid intermediate phase similar to that observed for the ammonia borane and lithium amide reaction. However, due to the low melting temperature of methylamine borane, less external kinetic energy was required to initiate reaction.

Thermal decomposition to liberate hydrogen was observed in two discrete stages. It was concluded that hydrogen evolution occurs through an intermolecular process similar to that proposed for the $LiNH_2$:NH_3BH_3 system, via an intermediate phase exhibiting a BN_3 environment such as those shown in Figure 5.8.

One of the major limitations of the $LiNH_2$:NH_3BH_3 system is the evolution of ammonia during decomposition. Volatile by-products such as ammonia are undesirable in hydrogen storage applications as they can poison fuel cells. No traces of ammonia were detected during decomposition of $LiNH_2$:$CH_3NH_2BH_3$. If hydrogen desorption from the $LiNH_2$:$CH_3NH_2BH_3$ system occurs via the same mechanism described for $LiNH_2$:NH_3BH_3, then it can be concluded that the system is theoretically capable of releasing 8.9 wt% of ammonia-free hydrogen at temperatures below 100°C.

While no ammonia was detected, methane was evolved as a by-product of the thermal decomposition. The evolution of methane is unlikely to pose a problem in fuel cell applications.

Chapter 6

Conclusions and Future Work

The research conducted throughout the course of this thesis examined the effect of lithium amide on the dehydrogenation kinetics and mechanism of ammonia borane.

Reaction was by means of mixing neat solid ammonia borane and lithium amide in a series of specific molar ratios under an inert atmosphere. In depth analysis of the composition of gases evolved during thermal decomposition at temperatures up to 250°C was by means of mass spectrometry. Characterisation of the phases formed at each stage of the reaction was achieved through solid-state ^{11}B NMR. The mechanism of thermal decomposition using isotopic substitution coupled with evolved gas analysis was also investigated.

From the results obtained through this research, it was concluded that upon mixing lithium amide and ammonia borane in the solid-state, a highly exothermic reaction ensued via a liquid intermediate phase. While the overall reaction is exothermic, it requires external energy in the form of stirring to overcome kinetic barriers. Reactions utilising methylamine borane - the simplest methyl derivative of ammonia borane with a melting temperature of 56°C - possessed a lower energy activation barrier to reaction, and therefore less external energy was required to initiate the reaction. The extremely high reactivity of

the liquid phase made characterisation of this phase difficult, and as a result little information about this reaction was obtained. However, ^{11}B NMR suggests the reaction results in the formation of a weakly bound adduct with an $H_2N\cdots BH_3$-NH_3 environment. Further research into the mechanism of this reaction and the products formed as a result, by means of solid-state ^{14}N and ^{7}Li NMR would be useful.

The exothermicity of this reaction also poses a problem for large scale synthesis. When the reaction is performed on a large scale, the heat generated causes the reaction to reach a critical temperature in which decomposition begins and hydrogen is evolved. This effect was observed upon ball milling a large scale reaction utilising methylamine borane. Further work into methods of controlling the heat generated during this stage of the reaction is required; stabilisation and isolation of this liquid phase would also be useful for further characterisation.

Thermal decomposition of this $LiNH_2$:NH_3BH_3 adduct to liberate hydrogen was observed at or above temperatures of 50°C in two discrete stages. The rate of the first stage of hydrogen evolution was found to be dependent on the ratio of amide present in the system i.e., the temperature threshold for H_2 release was notably lower for reactions in which an excess of amide was utilised. Approximately 11 wt% hydrogen is evolved in this first stage of decomposition. This exceeds both the gravimetric hydrogen storage targets of >9 wt%, outlined by the US Department of Energy, and that evolved from neat ammonia borane in this temperature range (6.5 wt%).

Ammonia was also evolved during low temperature hydrogen evolution from the $LiNH_2$:NH_3BH_3 adduct; this is of concern as volatile by-products are undesirable in hydrogen storage applications due to their toxicity toward fuel cells. The origin and mechanism by which ammonia is evolved remains un-

clear. Reactions utilising methylamine borane did not evolve ammonia but did however evolve methane as a volatile side product. This indicates that the formation of volatile products can be controlled through careful substitution and modification of ammonia borane. Future research into both the origin and mechanism of ammonia evolution, and methods of suppressing its formation by either substitution or changes in reaction conditions is required.

Using both solid-state ^{11}B NMR and isotopic substitution reactions, a mechanism of hydrogen loss during this first hydrogen evolution stage was proposed. Isotopic substitution of various sites on ammonia borane coupled with mass spectrometry of evolved gas phase during thermal decomposition indicated that hydrogen loss occurs through a bimolecular, multi-step reaction. ^{11}B NMR spectroscopy identified a compound exhibiting a BN_3 environment as a reaction intermediate. ^{11}B NMR also confirmed hydrogen loss from products formed from reactions utilising methylamine borane occurred via this proposed mechanism. Synthesis of a crystalline derivative of this BN_3 intermediate compound could provide further insight into whether this compound exists in a cyclic or polymeric form in the bulk material.

At higher temperatures the reaction proceeds via cross-linking or polymerisation of this BN_3 intermediate to yield a non-volatile amorphous product, during which a further 3 wt% hydrogen was liberated. However, little information about this reaction was obtained. Solid-state ^{14}N and ^{7}Li NMR spectroscopy could provide further insight into this second stage of hydrogen evolution and possibly provide confirmation of the proposed mechanism.

Upon heating of this non-volatile amorphous product to temperatures of 400°C, 500°C, and 600°C, further mass loss occurred liberating large volatile compounds, that could not be successfully identified, eventually forming crystalline Li_3BN_2, a potential hydrogen storage material. Identification of compounds

evolved during this process is required by means of mass spectrometry, or by condensation of compounds followed by X-ray diffraction and NMR spectroscopy.

On the basis of results obtained throughout the course of this research, the following recommendations for future research can be made:

- Further investigation into the mechanism of formation of the liquid transition phase, and characterisation of products formed from this reaction.
- Investigation into ways of controlling the heat evolution during the first stage of the reaction, to prevent undesirable decomposition leading to hydrogen evolution.
- Determination of both the source, and mechanism of ammonia formation.
- Further investigation into the effect of various substituted ammonia borane derivatives on the formation of ammonia.
- Characterisation of products formed throughout decomposition using ^{14}N and ^{7}Li NMR spectroscopy to gain further insight into the proposed mechanism.
- Synthesis of a crystalline derivative of the proposed BN_3 intermediate in order to investigate the chemical morphology of this phase.
- Identification of large volatile compounds evolved during high temperature decomposition.
- Investigate rehydrogenation ability of both the dehydrogenated phase isolated after 250°C and crystalline Li_3BN_2

The main issues for future research are; minimising the formation of the volatile by-products formed upon thermal decomposition, and rehydrogenation of the isolated spent materials. Methods for the efficient regeneration of the parent

compounds from these spent materials are needed for this system to be viable as a hydrogen storage material.

References

[1] D.K. Ross. *Vacuum*, 80 (2006), 1084.

[2] V.M. Vishnyakov. *Vacuum*, 80 (2006), 1053.

[3] G.W. Crabtree, M.S. Dresselhaus, and M.V. Buchanan. *Phys. Today*, 57 (2004), 39.

[4] T.B. Marder. *Agnew. Chem. Int. Ed*, 46 (2007), 8116.

[5] G. Marban and T. Valdes-Sols. *Int. J. Hydrogen Energ.*, 32 (2007), 1625.

[6] L. Schlapbach and A. Zuttel. *Nature*, 414 (2001), 353.

[7] A.W.C. Van den Berg and C.O. Arean. *Chem. Commun.*, 6 (2008), 667.

[8] US Department of Energy. Website. `http://www.sc.doe.gov/bes/hydrogen.pdf`.

[9] M. Gutowski and T. Autrey. *Chem. World*, 3 (2006), 44.

[10] B. Sakintuna, F. Lamari-Darkrim, and M. Hirscher. *Int. J. Hydrogen Energ.*, 32 (2007), 1121.

[11] F.E. Pinkerton and B.G. Wicke. *Indus. Physicist*, 10 (2004), 20.

[12] S. Orimo, Y. Nakamori, J.R. Eliseo, A. Zuttel, and C.M. Jensen. *Chem. Rev.*, 107 (2007), 4111.

[13] B. Bogdanovic and M. Schwickardi. *J. Alloys Compounds.*, 253 (1997), 1.

[14] P. Chen, Z. Xiong, J. Luo, J. Lin, and K. Tan. *Nature*, 420 (2002), 302.

[15] P. Chen, Z. Xiong, J. Luo, and K. Tan. *J. Phys. Chem. B*, 107 (2003), 10967.

[16] Z. Xiong, G. Wu, J. Hu, and P. Chen. *Adv. Mater.*, 16 (2004), 1522.

[17] Y. Nakamori, G. Kitahara, K. Miwa, N. Ohba, T. Noritake, S. Towota, and S. Orimo. *J. Alloys Compounds.*, 404-406 (2005), 396.

[18] S. Hino, T. Ichikawa, N. Ogits, M. Udagawa, and H. Fujii. *Chem. Commun.*, 24 (2005), 3038.

[19] W. Luo and E. Ronnebro. *J. Alloys Compounds.*, 404-406 (2005), 392.

[20] W. Luo and S. Sicafoose. *J. Alloys Compounds.*, 407 (2006), 274.

[21] H.I. Schlesinger and H.C. Brown. *J. Am. Chem. Soc*, 62 (1940), 3429.

[22] A. Zuettel, P. Rentsch, P. Fisher, P. Wenger, P. Sudan, and P. Mauron. *J. Alloys Compounds.*, 356-357 (2003), 515.

[23] A. Zuttel. *Materials Today*, 9 (2003), 24.

[24] E. Fakioglu, Y. Yurum, and T.N. Veziroglu. *Int. J. Hydrogen Energ.*, 29 (2004), 1371.

[25] A. Zuttel. *Mitig Adapt Strat Glob Change*, 12 (2007), 343.

[26] S.C. Amendola, S.L. Sharp-Goldman, M.S. Janjua, M.T. Kelly, P.J. Petillo, and M. Binder. *J. Power Sources*, 85 (2000), 186.

[27] Q. Zhang, G. Smith, Y. Wu, and R. Mohring. *Int. J. Hydrogen Energ.*, 31 (2006), 961.

[28] F.H. Stephens, V. Pons, and R.T. Baker. *J. Chem. Soc. Dalton Trans*, (2007), 2613.

[29] A. Wojcik, H. Middleton, I. Damopoulos, and J. Van Herle. *J. Power Sources*, 118 (2003), 342.

[30] R. Metkemeijer and P. Achard. *J. Power Sources*, 49 (1994), 271.

[31] R. Halseid, P.J.S. Vie, and R. Tunold. *J. Power Sources*, 154 (2006), 343.

[32] H.W. Langmi and G.S. McGrady. *Coord. Chem. Rev*, 251 (2007), 925.

[33] S.G. Shore and R.W. Parry. *J. Am. Chem. Soc*, 77 (1955), 6084.

[34] D.M. Schubert. *Borax Pioneer*, 20 (2001), 8.

[35] G. Wolf, J.C. van Miltenburg, and U. Wolf. *Thermochim. Acta.*, 317 (1998), 111.

[36] R.W. Parry and L.J. Edwards. *J. Am. Chem. Soc*, 81 (1959), 3554.

[37] G.W. Schaeffer, M.D. Adams, and F.J. Koenig. *J. Am. Chem. Soc*, 78 (1956), 725.

[38] S.G. Shore and K.W. Boddeker. *Inorg. Chem*, 3 (1964), 914.

[39] J. Beres, A. Dodds, A.J. Morabito, and R.M. Adams. *Inorg. Chem*, 10 (1971), 2072.

[40] O.T. Beachley. *Inorg. Chem*, 6 (1967), 870.

[41] E. Mayer. *Inorg. Chem*, 12 (1973), 1954.

[42] M.G. Hu, J.M. Van Paasschen, and R.A. Geanangel. *J. Inorg. Nucl. Chem*, 39 (1977), 2147.

[43] E.W. Hughes. *J. Am. Chem. Soc*, 78 (1956), 502.

[44] E.L. Lippert and W.N. Lipscomb. *J. Am. Chem. Soc*, 78 (1956), 503.

[45] M.E. Bowden, G.J. Gainsford, and W.T. Robinson. *Aust. J. Chem*, 60 (2007), 149.

[46] W.T. Klooster, T.F. Koetzle, P.E.M. Siegbahn, T.B. Richardson, and R.H. Crabtree. *J. Am. Chem. Soc*, 121 (1999), 6337.

[47] M. Chandra and Q. Xu. *J. Power Sources*, 159 (2006), 855.

[48] H.C. Kelly and V.B. Marriott. *Inorg. Chem*, 18 (1979), 2875.

[49] M. Chandra and Q. Xu. *J. Power Sources*, 156 (2006), 190.

[50] F.Y. Cheng, H. Ma, Y.M. Li, and J. Chen. *Inorg. Chem*, 46 (2007), 788.

[51] A. Mittasch, E. Kuss, and H. Schlueter. *Z. Anorg. Allg. Chem.*, 159 (1926), 1.

[52] F. Baitalow, J. Baumann, G. Wolf, K. Jaenicke-Rossler, and G. Leitner. *Thermochim. Acta.*, 391 (2002), 159.

[53] J. Baumann, E. Baitalow, and G. Wolf. *Thermochim. Acta.*, 430 (2005), 9.

[54] J.D. Carpenter and B.S. Ault. *Chem. Phys. Lett.*, 197 (1992), 171.

[55] P.M. Kuznesof, D.F. Shriver, and F.E. Stafford. *J. Am. Chem. Soc*, 90 (1968), 2557.

[56] M.T. Nguyen, V.S. Nguyen, M.H. Matus, G. Gopakumar, and D.A. Dixon. *J. Phys Chem. A*, 111 (2007), 679.

[57] Q.S. Li, J. Zhang, and S. Zhang. *Chem. Phys. Lett.*, 404 (2005), 100.

[58] J.S. Wang and R.A. Geanangel. *Inorg. Chim. Acta*, 148 (1988), 185.

[59] A. Karkamkar, C. Aardahl, and T. Autrey. *Material Matters*, 2 (2007), 6.

[60] M.E. Bluhm, M.G. Bradley, R. Butterick III, U. Kusari, and L.G. Sneddon. *J. Am. Chem. Soc*, 128 (2006), 7748.

[61] M.E. Bluhm, M.G. Bradley, and L.G. Sneddon. *Prepr. Symp. - Am. Chem. Soc., Div. Fuel Chem.*, 51 (2006), 517.

[62] G.N. Patwari. *J. Phys Chem. A*, 109 (2005), 2035.

[63] V. Sit, R.A. Geanangel, and W.W. Wendlandt. *Thermochim. Acta.*, 113 (1987), 379.

[64] M.G. Hu, R.A. Geanangel, and W.W. Wendlandt. *Thermochim. Acta.*, 23 (1978), 249.

[65] R.S. Smith, B.D. Kay, B. Schmid, L. Li, M. Hess, M. Gutowski, and T. Autrey. *Prep. Pap. Am. Chem. Soc., Div Fuel Chem.*, 50 (2005), 112.

[66] G.E. Ryschkewitsch and J.W. Wiggens. *Inorg. Chem*, 3 (1970), 314.

[67] A.C. Stowe, W.J. Shaw, J.C. Linehan, B. Schmid, and T. Autrey. *Phys. Chem. Chem. Phys*, 9 (2007), 1831.

[68] A. Gutowska, L. Li, Y. Shin, C.M. Wang, X.S. Li, J.C. Linehan, R.S. Smith, B.D. Kay, B. Schmid, W. Shaw, M. Gutowski, and T. Autrey. *Agnew. Chem. Int. Ed*, 44 (2005), 3578.

[69] Z. Xiong, C.K. Yong, G. Wu, P. Chen, W. Shaw, A. Karkamkar, T. Autrey, M.O. Jones, S.R. Johnson, P.P. Edwards, and W.I.F. David. *Nat. Mater.*, 7 (2008), 138.

[70] T.Kemmit, Interim Report, Bilateral Research Activities Programme ISAT-B06-TK.

[71] H.C. Brown, H.I. Schlesinger, and S.Z. Cardon. *J. Am. Chem. Soc*, 64 (1942), 325.

[72] A.B. Burg and H.I. Schlesinger. *J. Am. Chem. Soc*, 59 (1937), 780.

[73] G.W. Schaeffer and E.R. Anderson. *J. Am. Chem. Soc*, 71 (1949), 2143.

[74] D.F. Gaines and R. Schaeffer. *J. Am. Chem. Soc*, 85 (1963), 395.

[75] M.E. Bowden, I.W.M. Brown, G.J. Gainsford, and H. Wong (in press). *Inorg. Chim. Acta*.

[76] T.C. Bissot and R.W. Parry. *J. Am. Chem. Soc*, 77 (1955), 3481.

[77] E. Framery and M. Vaultier. *Heteroatom Chem.*, 11 (2000), 218.

[78] S.G. Shore and R.W. Parry. *J. Am. Chem. Soc*, 80 (1958), 8.

[79] P.V. Ramachandran and P.D. Gagare. *Inorg. Chem*, 46 (2007), 7810.

[80] S.G. Shore and R.W. Parry. *J. Am. Chem. Soc*, 80 (1958), 12.

[81] B.H. Stuart. *Infrared specroscopy: Fundamentals and applications*. John Wiley and Sons Ltd, 2004.

[82] G.R. Meisner, M.L. Scullin, M.P. Balogh, F.E. Pinkerton, and M.S. Meyer. *J. Phys. Chem. B*, 110 (2006), 4186.

[83] C.T. Kwon and H.A. McGee. *Inorg. Chem*, 9 (1970), 2458.

[84] C. Gervais, F. Babonneau, J. Maquet, C. Bonhomme, D. Massiot, E. Framery, and M. Vaultier. *Magn. Reson. Chem*, 36 (1998), 407.

[85] D.T. Kim, K.T. Moon, J.G. Kho, J. Economy, C. Gervais, and F. Babonneau. *Polym. Adv. Technol.*, 10 (1999), 702.

[86] K.J.D. MacKenzie and M.E. Smith. *Multinuclear Solid-state NMR of Inorganic Materials*. Oxford: Pergamon, 2002.

[87] D. Massiot, V. Montouillout, C. Magnenet, C. Bessada, J. Coutures, H. Forster, S. Steuernagel, and D. Mueller. *C. R. Acad. Sci. Paris (SerieII).*, 1 (1998), 157.

[88] S.E. Dann. *Reactions and Characterization of Solids*. Royal Society of Chemistry, 2000.

[89] H. Noth and H. Vahrenkamp. *Chem. Ber.*, 99 (1966), 1049.

[90] C. Gervais and F. Babonneau. *J. Organomet. Chem.*, 675 (2002), 75.

[91] C. Gervais, J. Maquet, F. Babonneau, C. Duriez, E. Framery, M. Vaultier, P. Florian, and D. Massiot. *Chem. Mater.*, 13 (2001), 1700.

[92] H. Yamane, S. Kikkawa, and M. Koizumi. *J. Solid State Chem.*, 71 (1987), 1.

[93] H. Yamane, S. Kikkawaand, H. Horiuchi, and M. Koizumi. *J. Solid State Chem.*, 65 (1986), 6.

[94] G. Wolf, J. Baumann, F. Baitalow, and F.P. Hoffmann. *Thermochim. Acta.*, 343 (2000), 19.

[95] R.A. Geanangel and S.G. Shore. *Prep. Inorg. React.*, 3 (1966), 123.

[96] E. Mayer. *Inorg. Chem*, 11 (1972), 866.

[97] M.P. Brown and R.W. Parry. *J. Chem. Soc. A*, (1968), 612.

[98] C.K. Narula, F.F. Janik, E.N. Duesler, R.T. Paine, and R. Schaeffer. *Inorg. Chem*, 25 (1986), 3346.

Appendix A

Boron Compounds

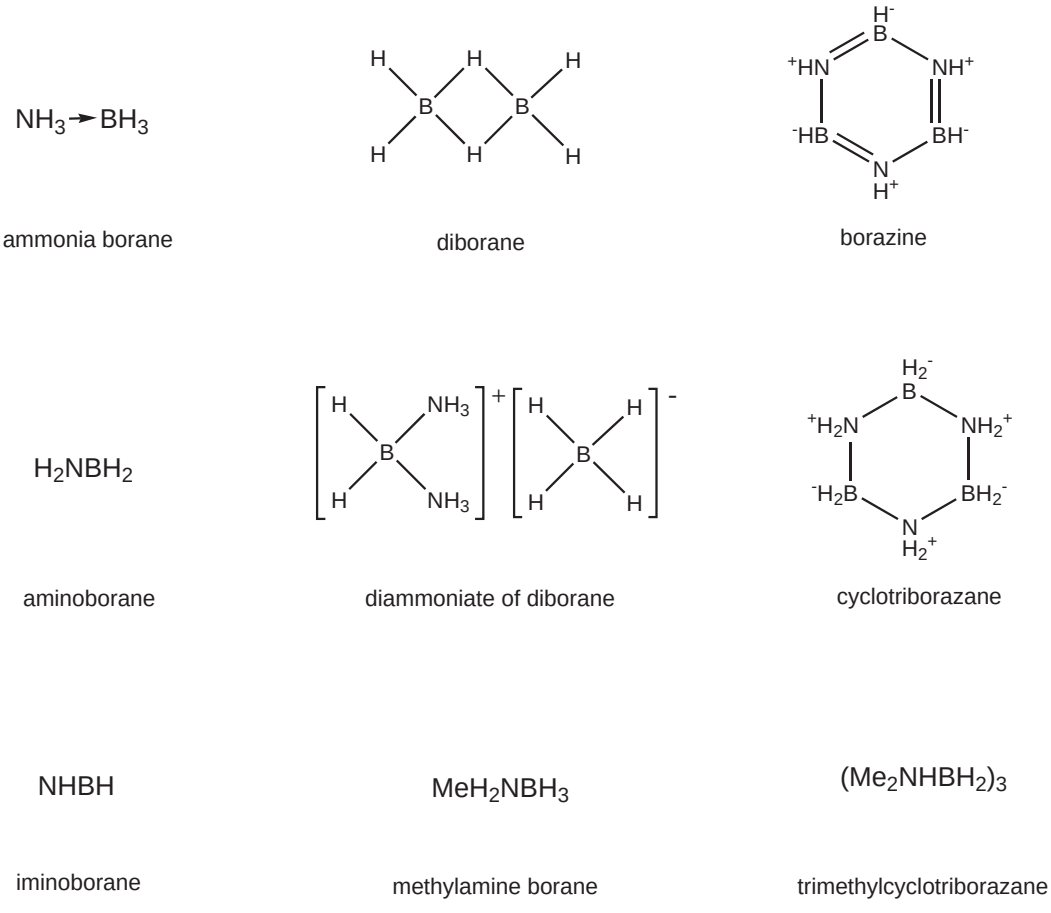

Figure A.1: Boron compounds referred to in this text.

Appendix B

Crystal Structure Data

Atom	$\boldsymbol{x}$	$\boldsymbol{y}$	$\boldsymbol{z}$	$\boldsymbol{U}_{eq}$
B1	0.0316(2)	0.75	0.319(5)	0.0301(7)
N1	0.07786(15)	0.75	0.6243(3)	0.0259(6)
C1	0.2087(2)	0.75	0.6555(5)	0.0383(7)
H1	0.0506(14)	0.852(2)	0.706(3)	0.034(4)
H2	0.0716(11)	0.888(2)	0.215(3)	0.034(4)
H3	-0.066(2)	0.75	0.324(4)	0.042(6)
H4	0.238(18)	0.865(3)	0.567(4)	0.064(5)
H5	0.2302(19)	0.75	0.836(5)	0.037(6)

Table B.1: Positional parameters refined for $CH_3NH_2BH_3$ in space group *Pnma* with cell parameters a=11.099(11)Å, b=6.584(6)Å, c=4.919(5)Å at 113 K. R-factor for the refinement was 0.044.

Bond	Distance (Å)	Atoms	Bond angle (^{o})
B1-N1	1.587(3)	N1-C1-H4	107.3(13)
N1-C1	1.461(3)	N1-C1-H5	111.1(14)
B1-H2	1.135(14)	H4-C1-H4	108.7(17)
B1-H3	1.08(2)	H4-C1-H5	111.3(15)
N1-H1	0.837(16)	C1-N1-B1	114.9(18)
C1-H4	0.93(19)	C1-N1-H1	108.0(10)
C1-H5	0.92(2)	B1-N1-H1	109.6(10)
H1$\cdots$H2	2.218(19)	H1-N1-H1	106.3(14)
		N1-B1-H2	107.4(7)
		N1-B1-H3	107.6(11)
		H2-B1-H3	113.6(8)
		H2-B1-H2	106.6(10)

Table B.2: Intramolecular bond distances and angles for methylamine borane

Appendix C

X-ray Diffraction

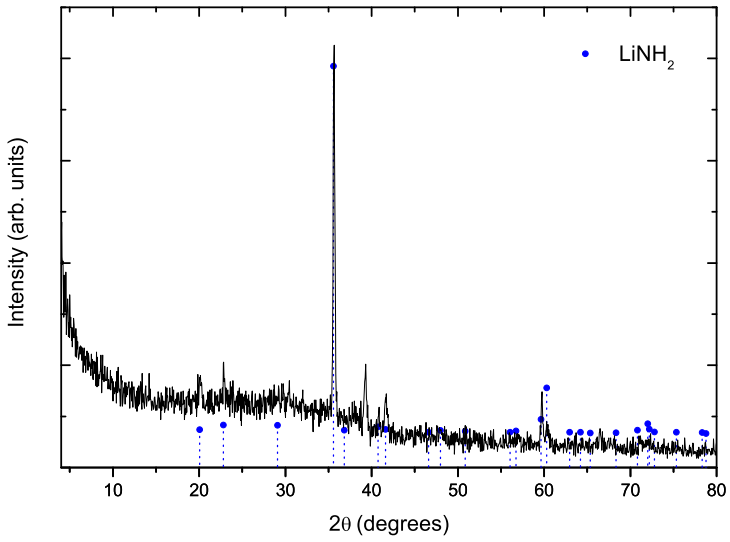

Figure C.1: X-ray diffraction pattern of 2:1 ($LiNH_2$:NH_3BH_3) heated to 250°C.

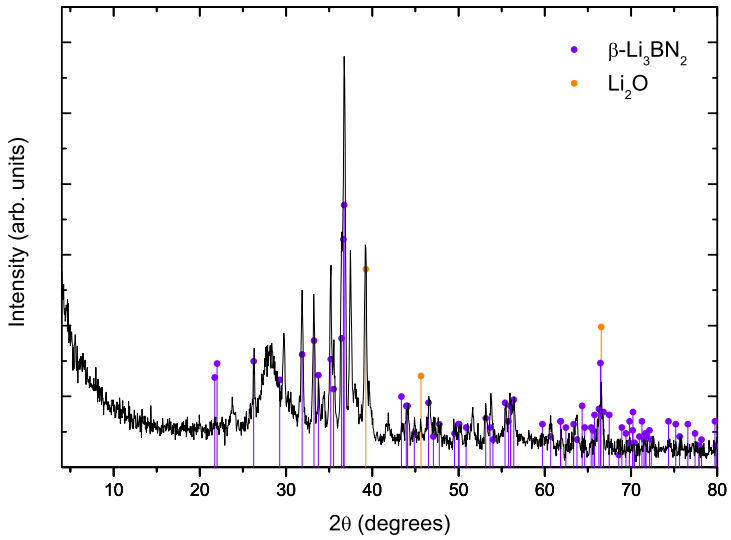

Figure C.2: X-ray diffraction pattern of 2:1 ($LiNH_2$:NH_3BH_3) heated to 500°C in flow-through system.

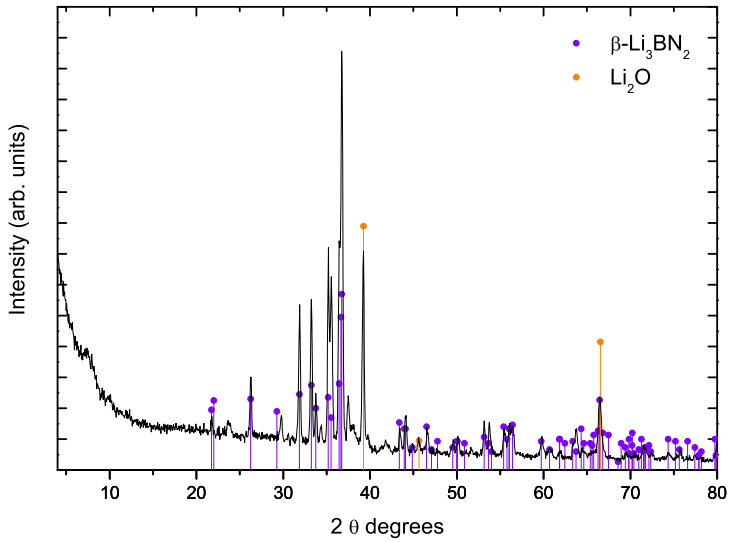

Figure C.3: X-ray diffraction pattern of 2:1 ($LiNH_2$:NH_3BH_3) heated to 600°C in flow-through system.

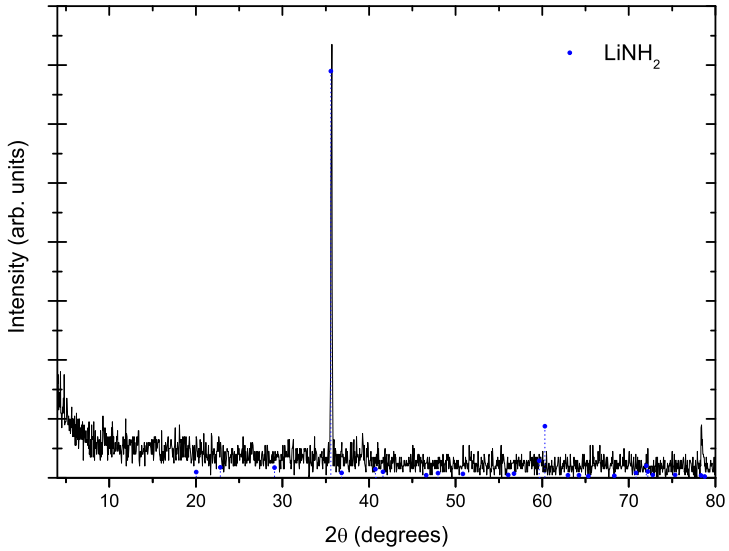

Figure C.4: X-ray diffraction pattern of 3:1 ($LiNH_2$:NH_3BH_3) heated to 250°C.

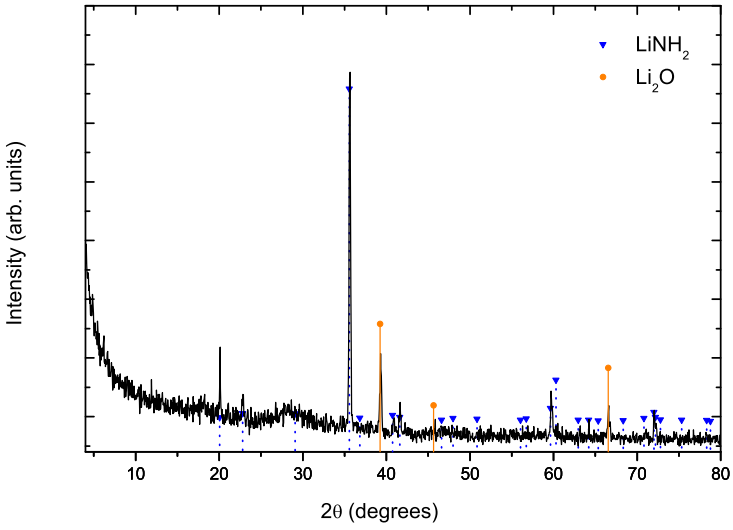

Figure C.5: X-ray diffraction pattern of 3:1 ($LiNH_2$:NH_3BH_3) heated to 400°C in sealed bomb.

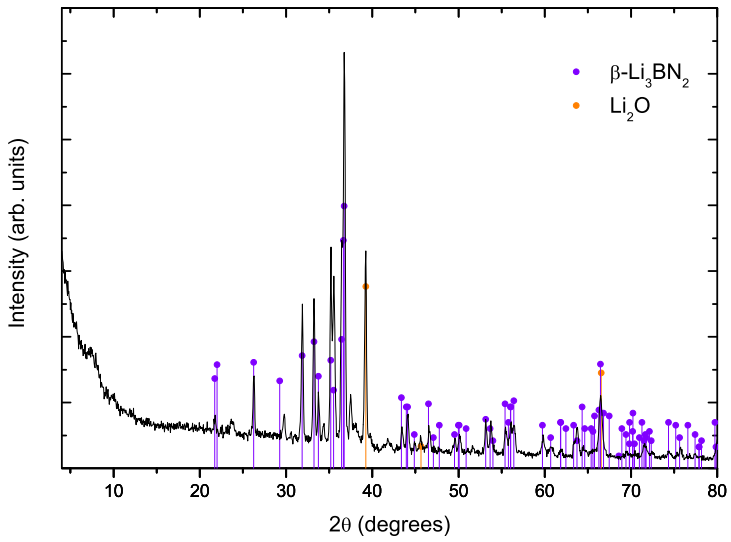

Figure C.6: X-ray diffraction pattern of 3:1 ($LiNH_2$:NH_3BH_3) heated to 500°C in flow-through system.

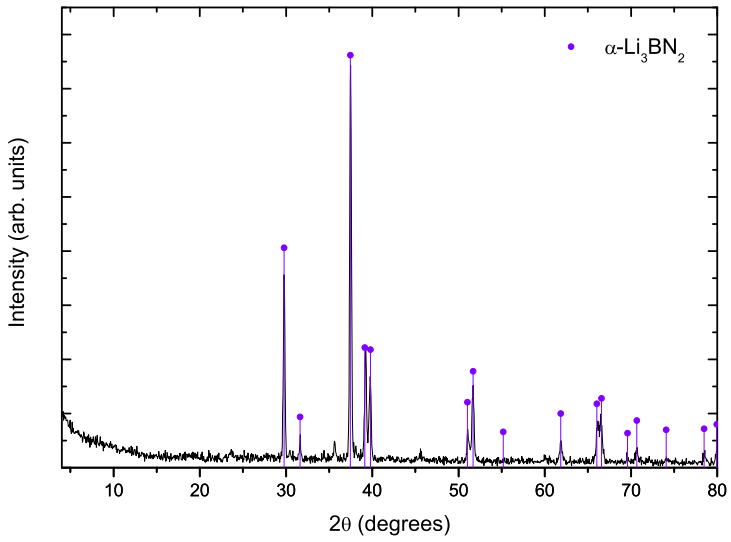

Figure C.7: X-ray diffraction pattern of 3:1 ($LiNH_2$:NH_3BH_3) heated to 600°C in flow-through system.

Appendix D

Mass Spectrometry

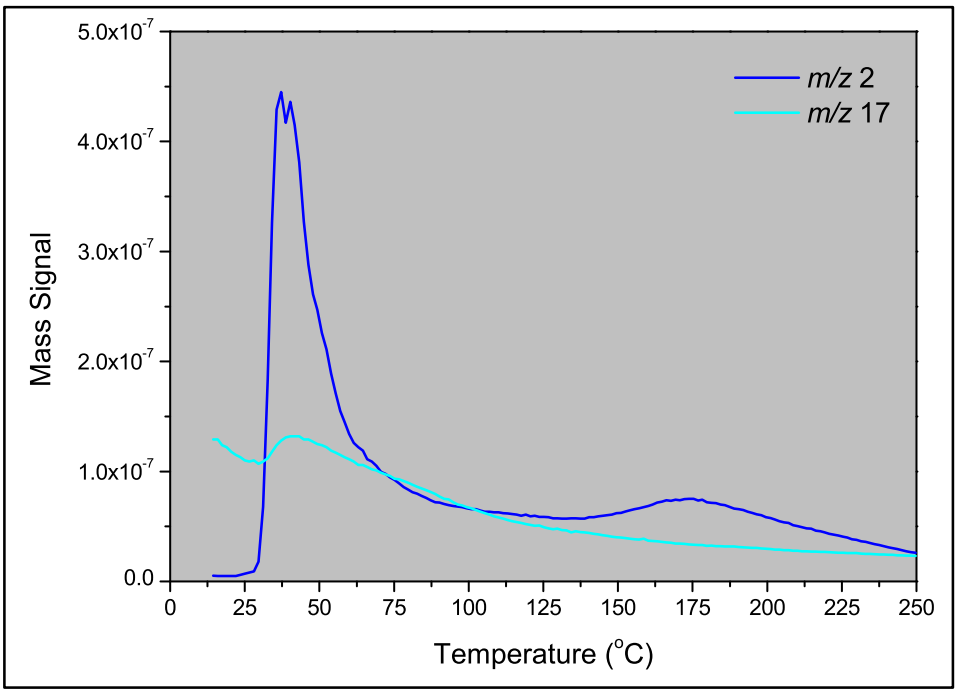

Figure D.1: Mass spectra of gases evolved during 2:1 ($LiNH_2$:NH_3BH_3) reaction and decomposition.

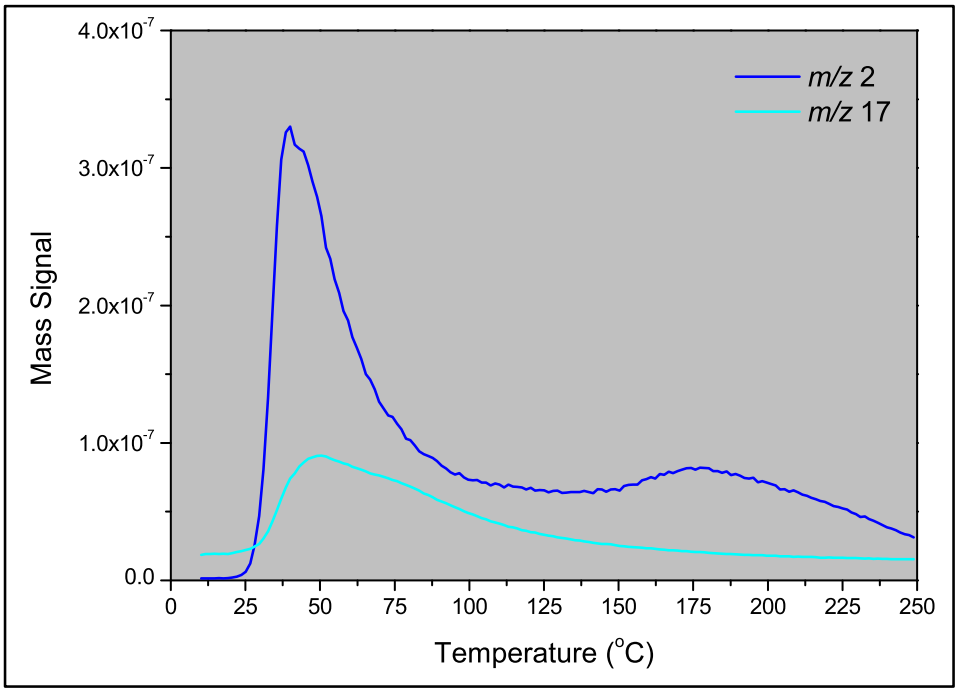

Figure D.2: Mass spectra of gases evolved during 3:1 ($LiNH_2$:NH_3BH_3) reaction and decomposition.

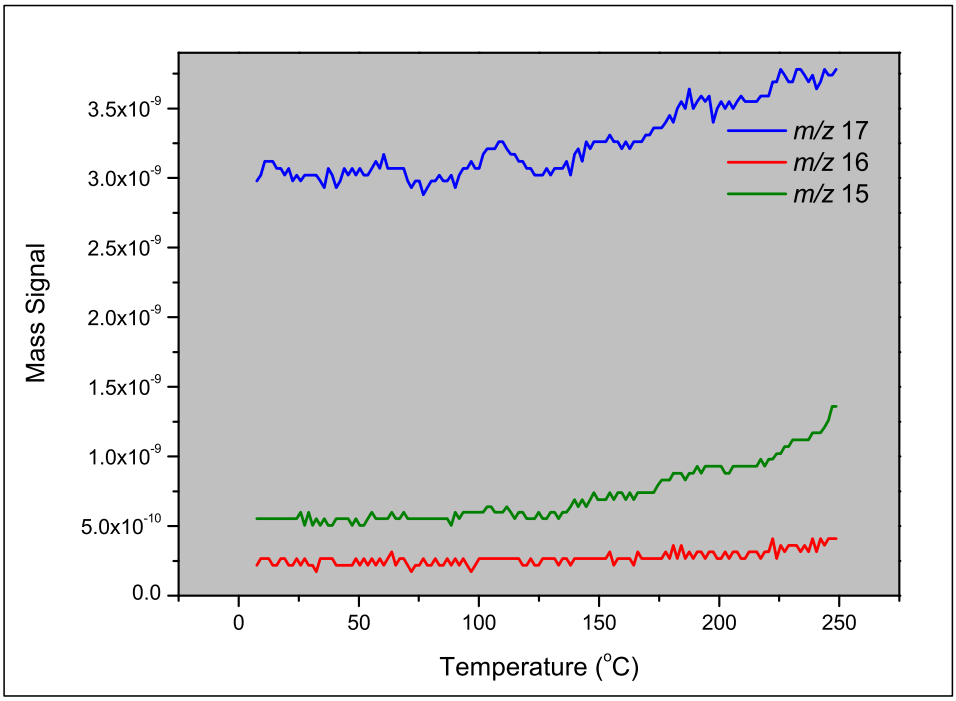

Figure D.3: Mass spectra of gases evolved from $LiNH_2$ up to 250°C.

Appendix E

Solid-State ^{11}B NMR Spectroscopy

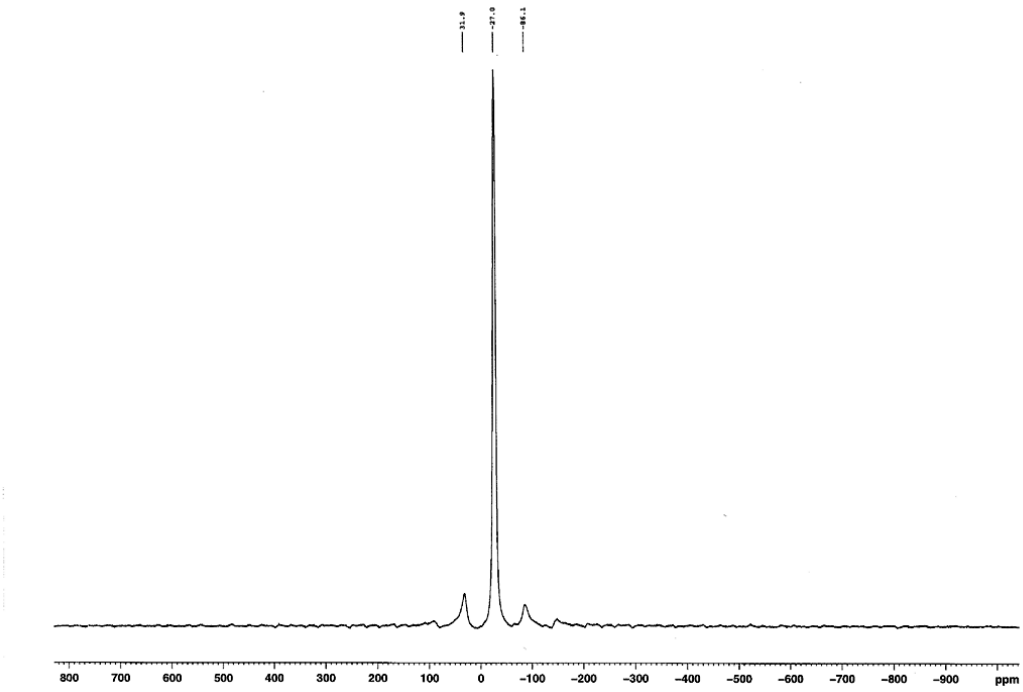

Figure E.1: Solid-state ^{11}B NMR of NH_3BH_3.

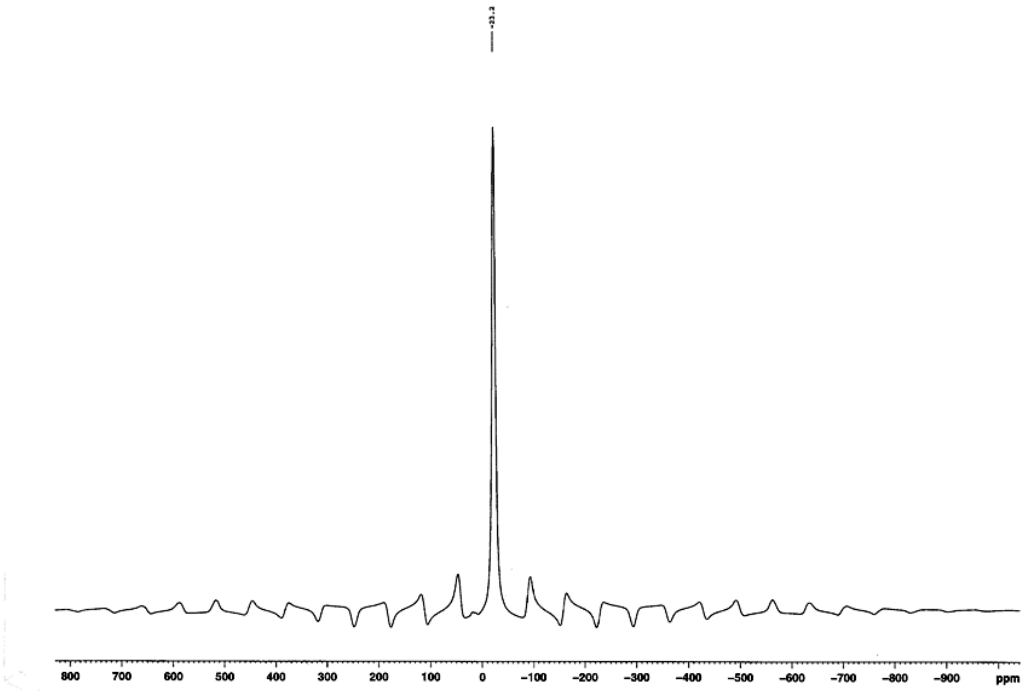

Figure E.2: Solid-state ^{11}B NMR of 1:1 ($LiNH_2$:NH_3BH_3).

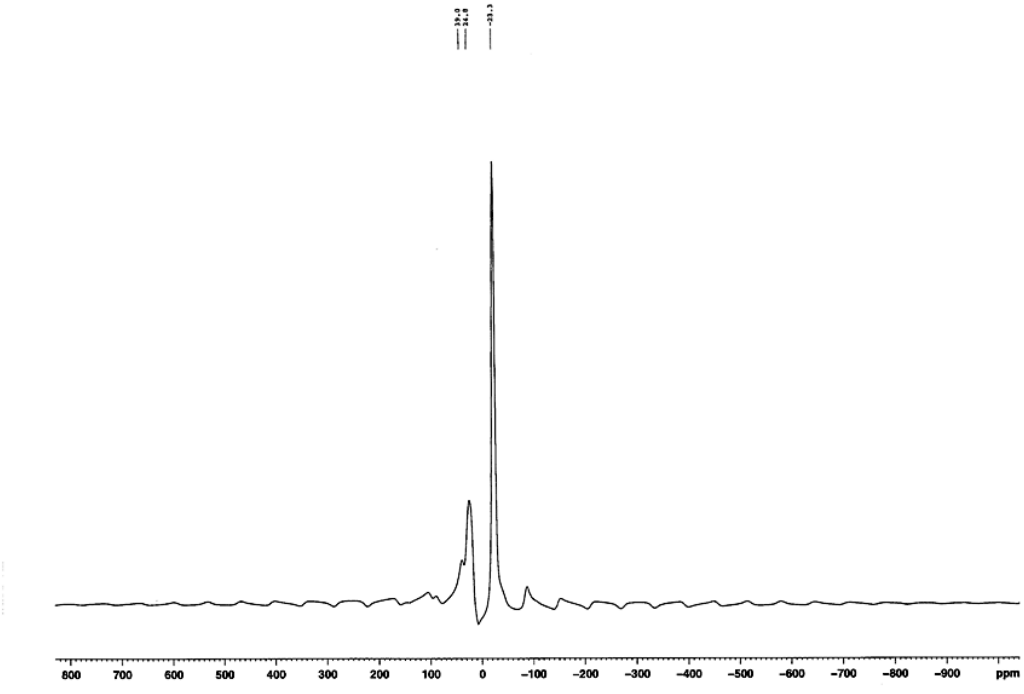

Figure E.3: Solid-state ^{11}B NMR of 1:1 ($LiNH_2$:NH_3BH_3) heated to 60°C.

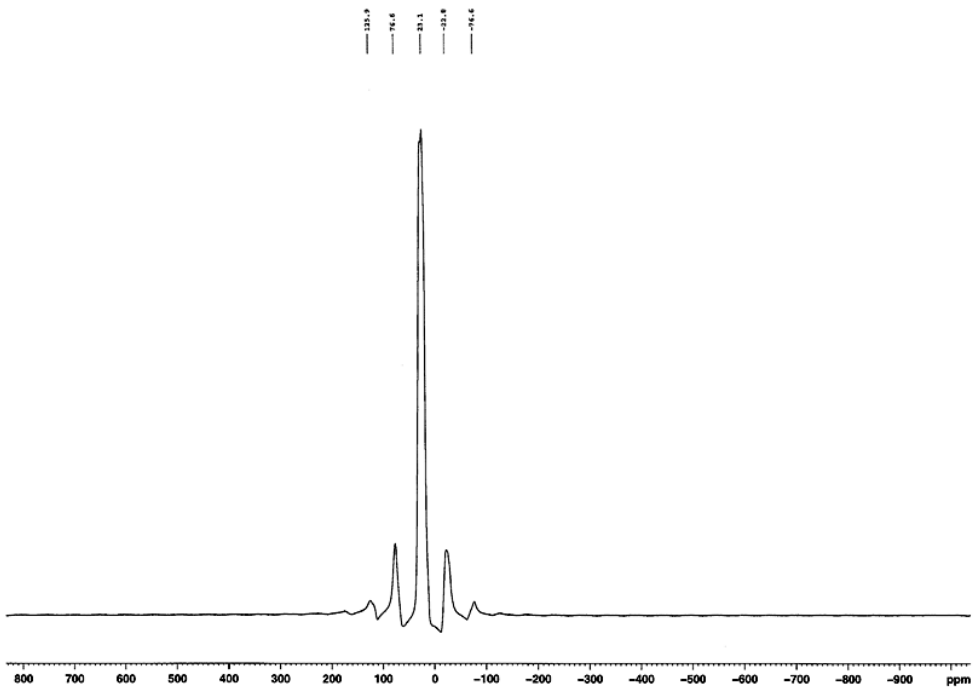

Figure E.4: Solid-state ^{11}B NMR of 1:1 ($LiNH_2$:NH_3BH_3) heated to 400°C in sealed bomb.

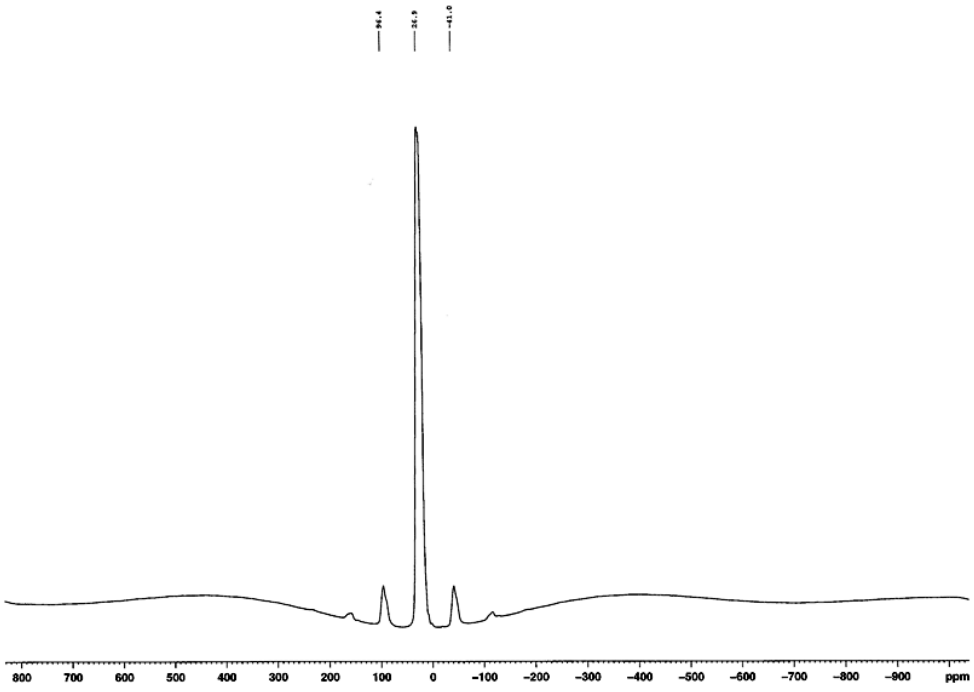

Figure E.5: Solid-state ^{11}B NMR of 1:1 ($LiNH_2$:NH_3BH_3) heated to 400°C in flow-through system.

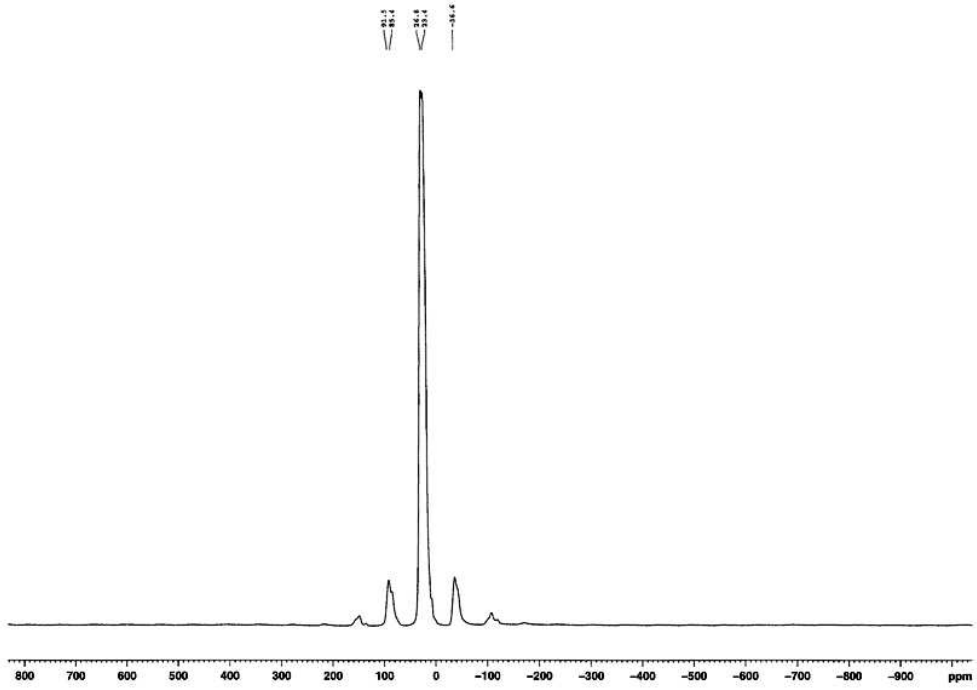

Figure E.6: Solid-state ^{11}B NMR of 1:1 ($LiNH_2$:NH_3BH_3) heated to 500°C in flow-through system.

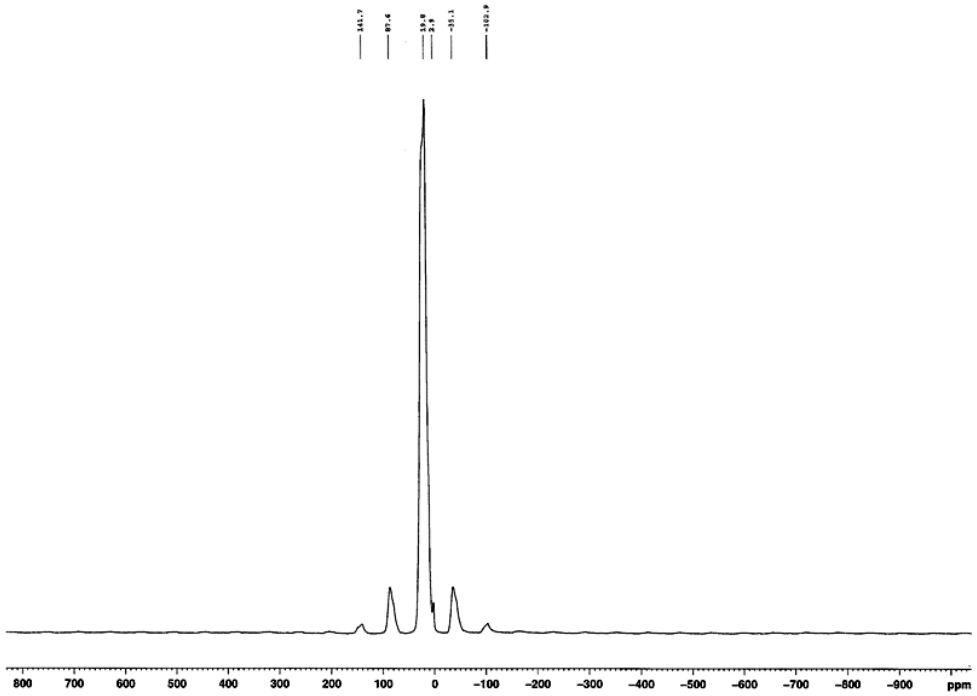

Figure E.7: Solid-state ^{11}B NMR of 1:1 ($LiNH_2$:NH_3BH_3) heated to 600°C in flow-through system.

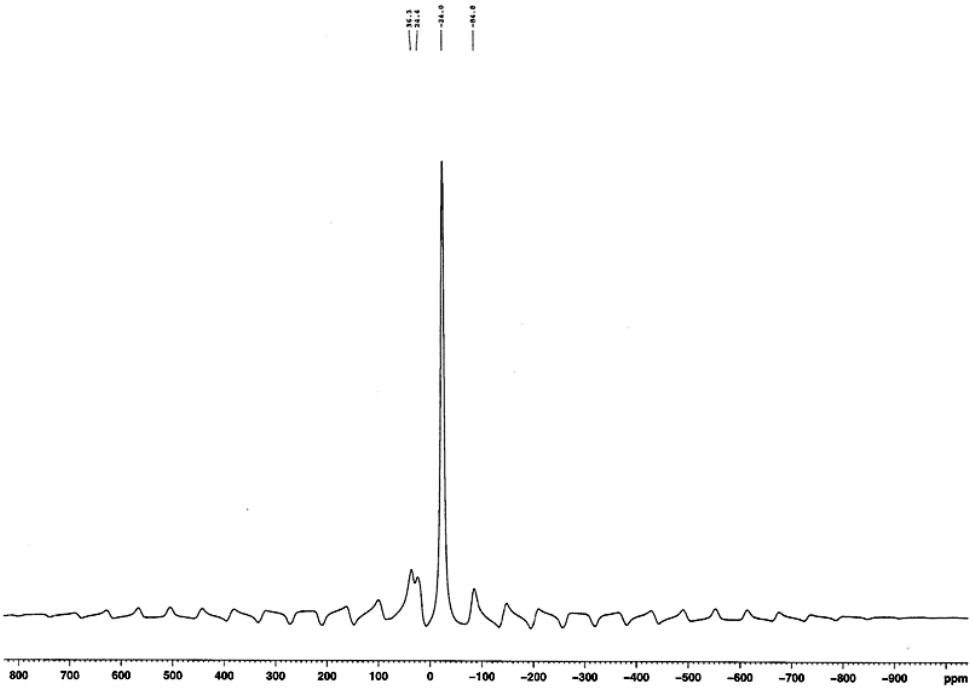

Figure E.8: Solid-state ^{11}B NMR of 2:1 ($LiNH_2$:NH_3BH_3).

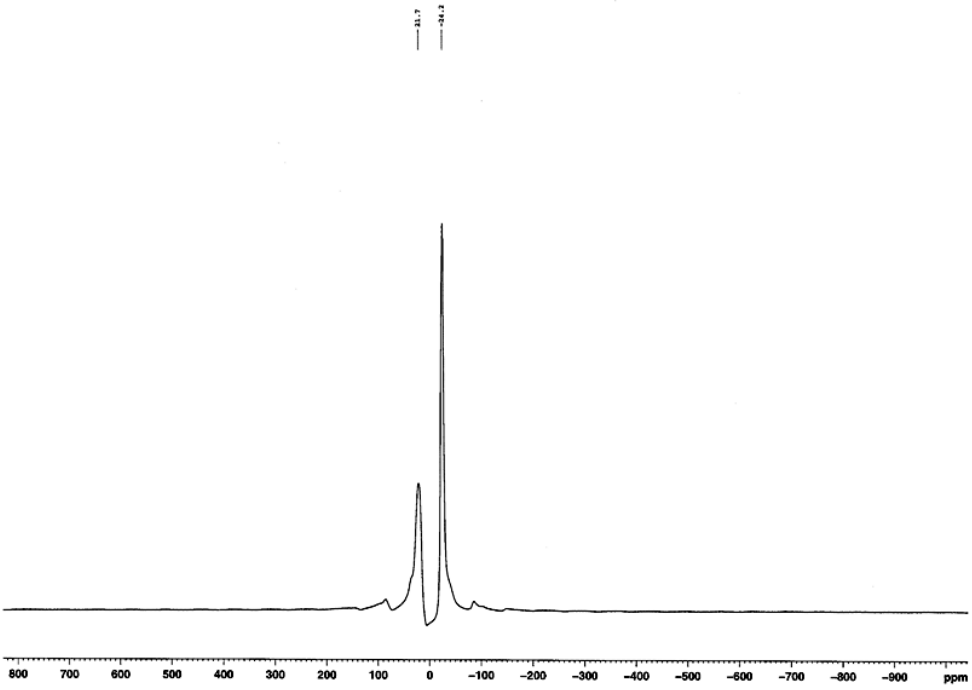

Figure E.9: Solid-state ^{11}B NMR of 2:1 ($LiNH_2$:NH_3BH_3) heated to 60°C.

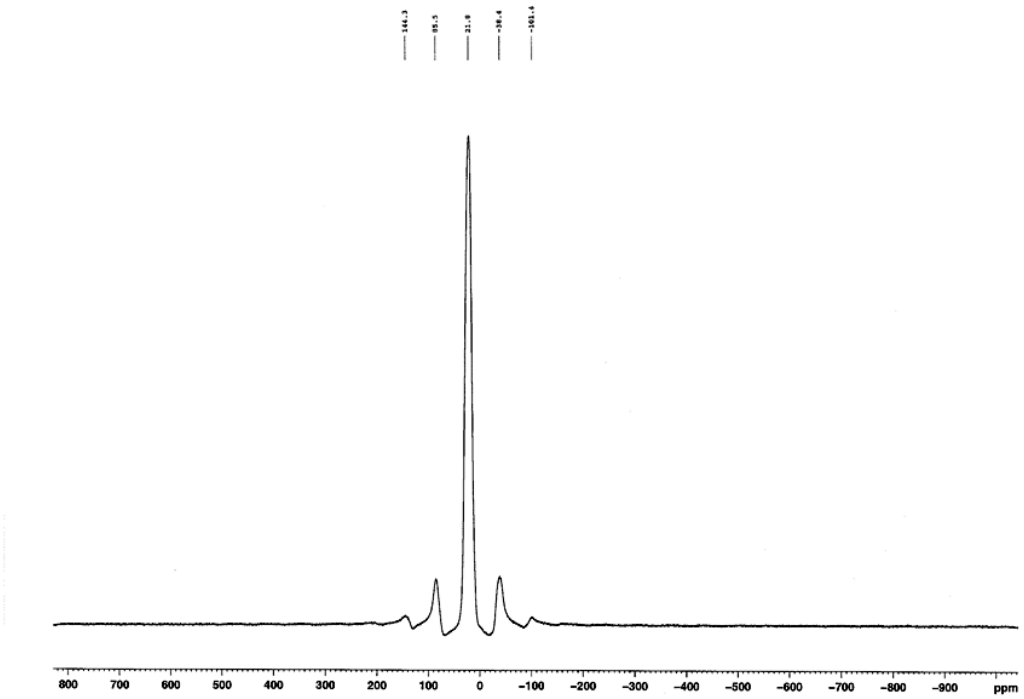

Figure E.10: Solid-state ^{11}B NMR of 2:1 ($LiNH_2$:NH_3BH_3) heated to 250°C.

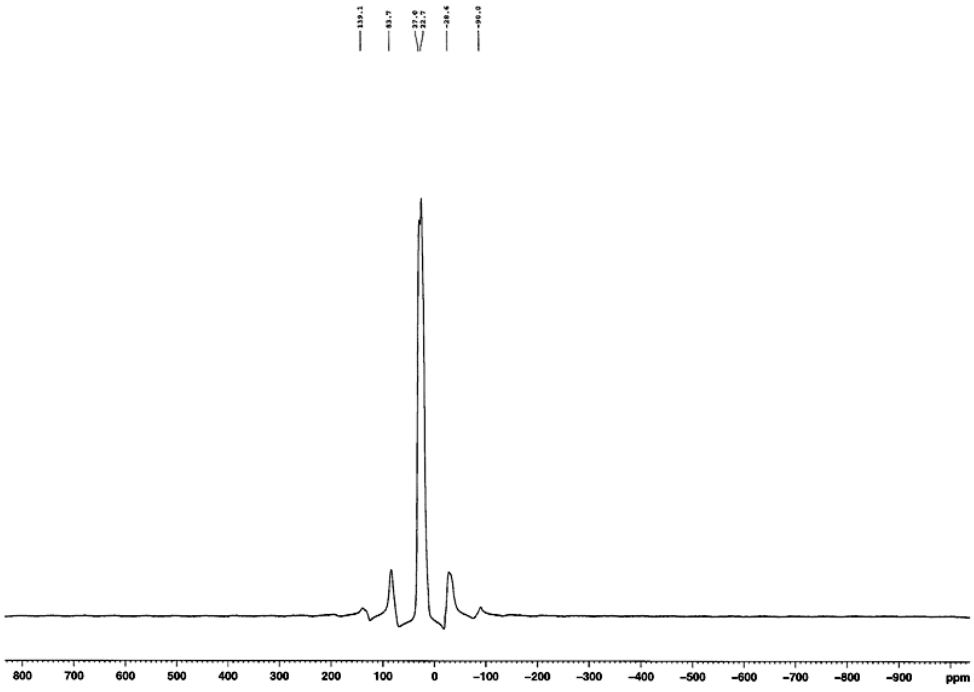

Figure E.11: Solid-state ^{11}B NMR of 2:1 ($LiNH_2$:NH_3BH_3) heated to 400°C in sealed bomb.

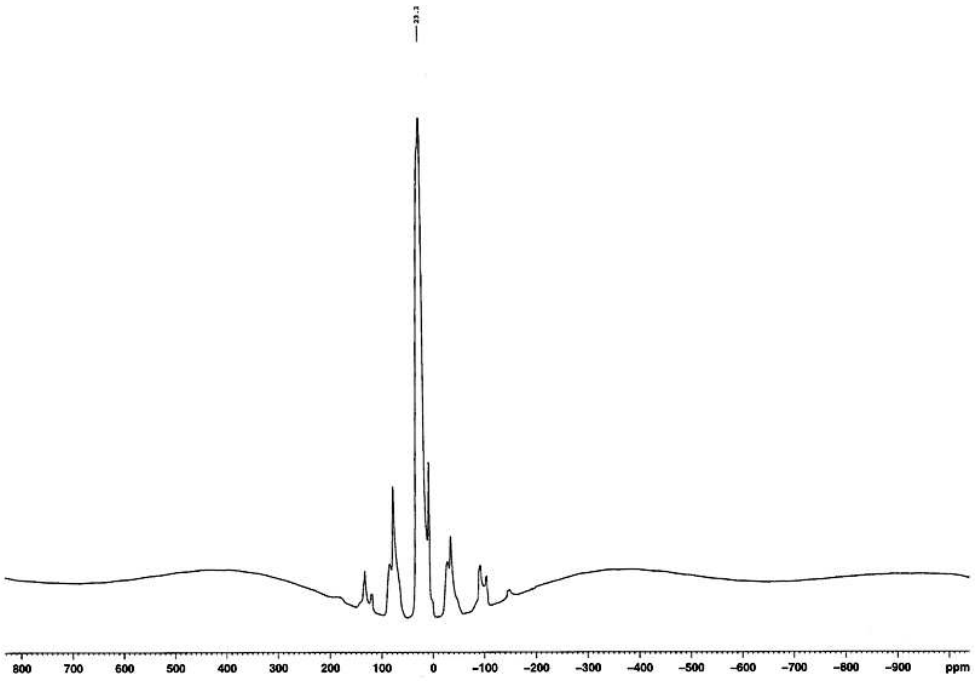

Figure E.12: Solid-state ^{11}B NMR of 2:1 ($LiNH_2$:NH_3BH_3) heated to 400°C in flow-through system.

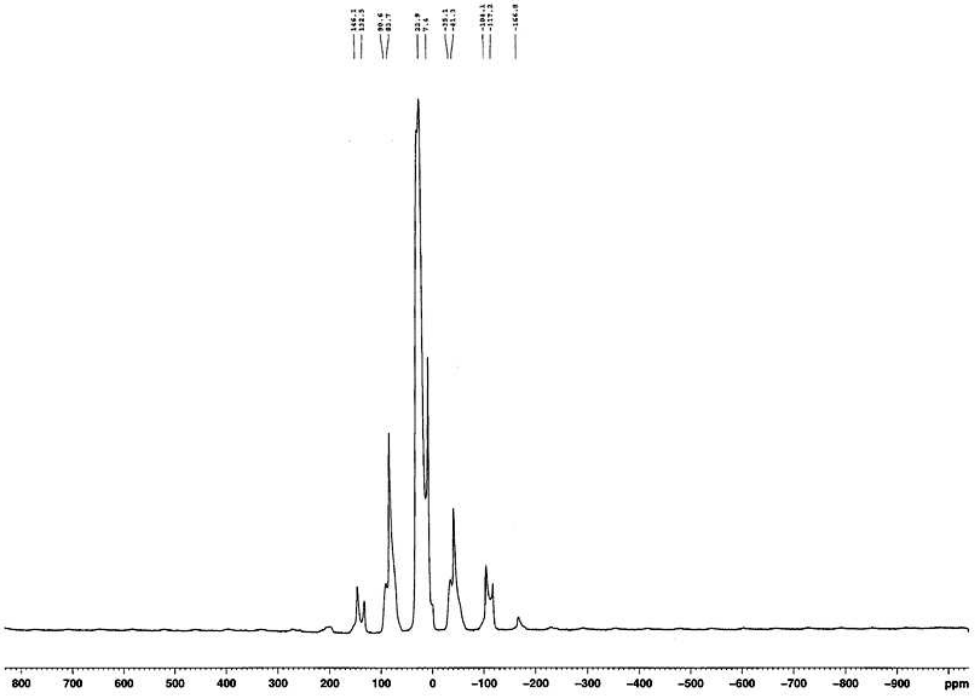

Figure E.13: Solid-state ^{11}B NMR of 2:1 ($LiNH_2$:NH_3BH_3) heated to 500°C in flow-through system.

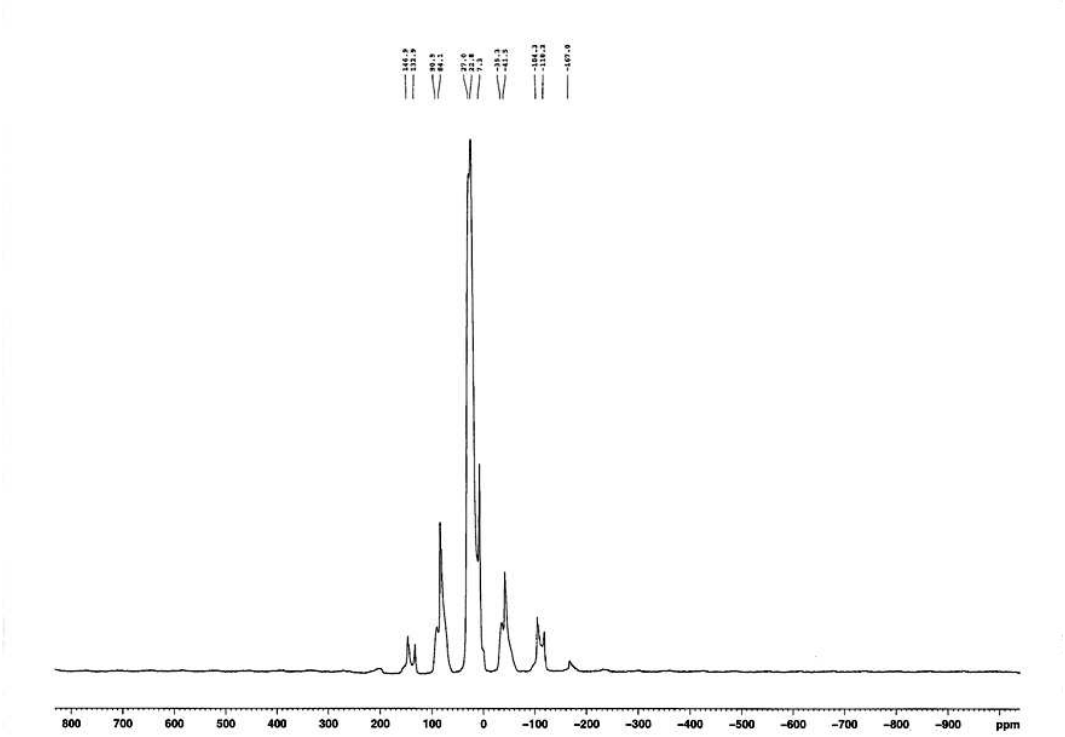

Figure E.14: Solid-state ^{11}B NMR of 2:1 ($LiNH_2$:NH_3BH_3) heated to 600°C in flow-through system.

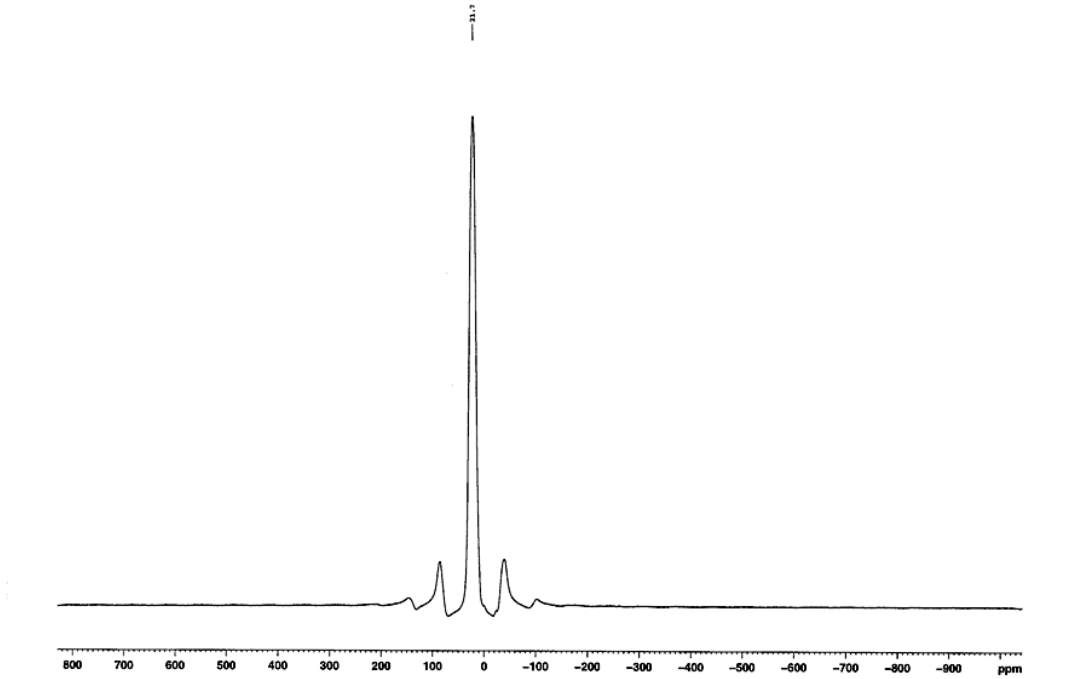

Figure E.15: Solid-state ^{11}B NMR of 3:1 ($LiNH_2$:NH_3BH_3) heated to 250°C.

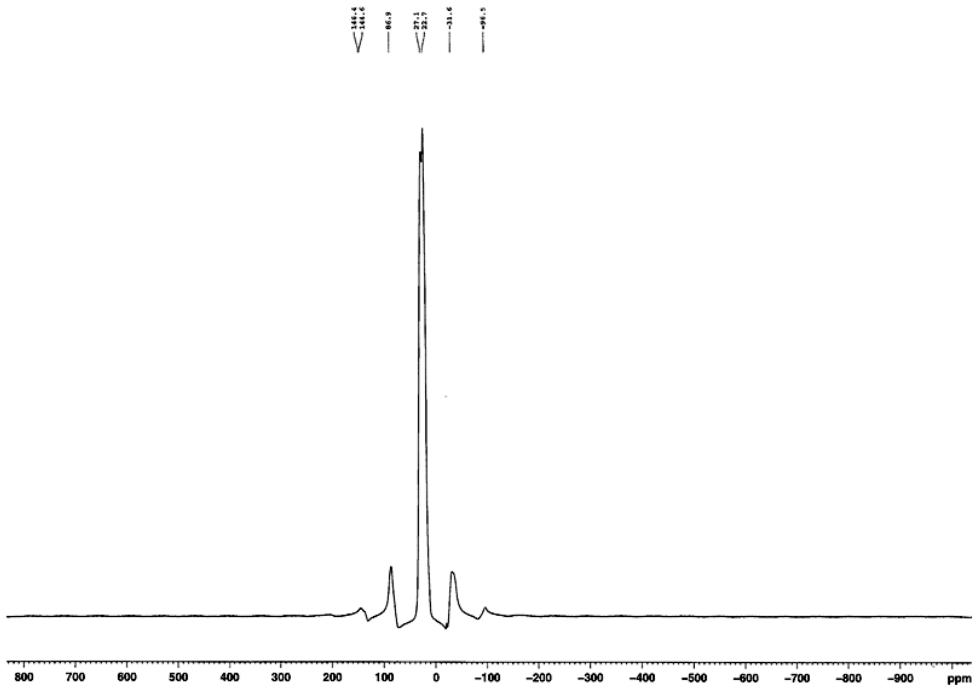

Figure E.16: Solid-state ^{11}B NMR of 3:1 ($LiNH_2$:NH_3BH_3) heated to 400°C in sealed bomb.

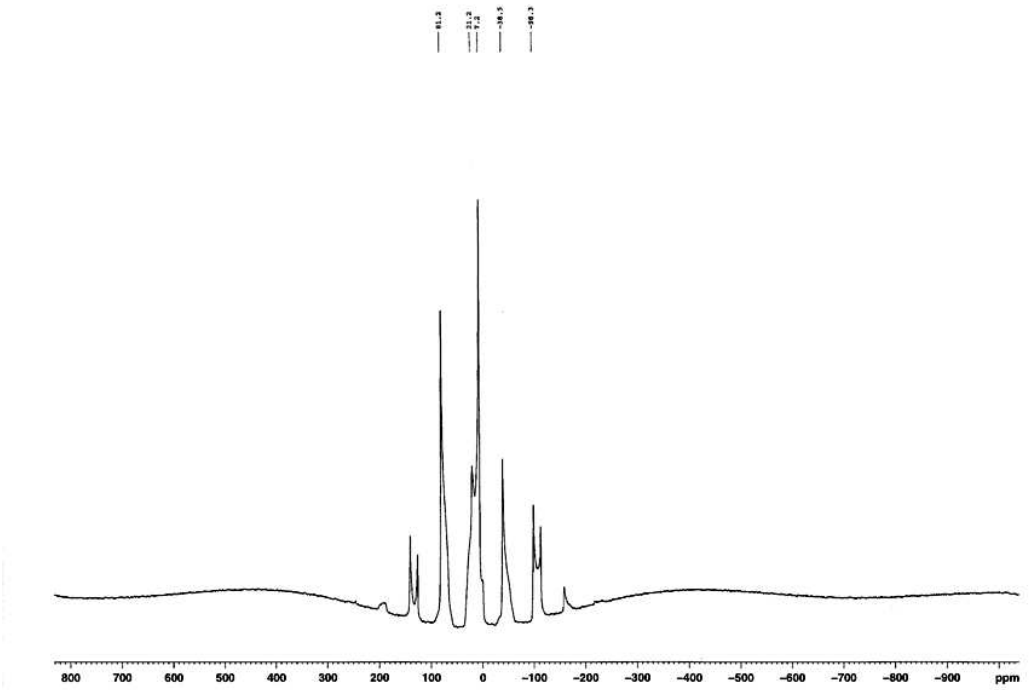

Figure E.17: Solid-state ^{11}B NMR of 3:1 ($LiNH_2$:NH_3BH_3) heated to 400°C in a flow-through system.

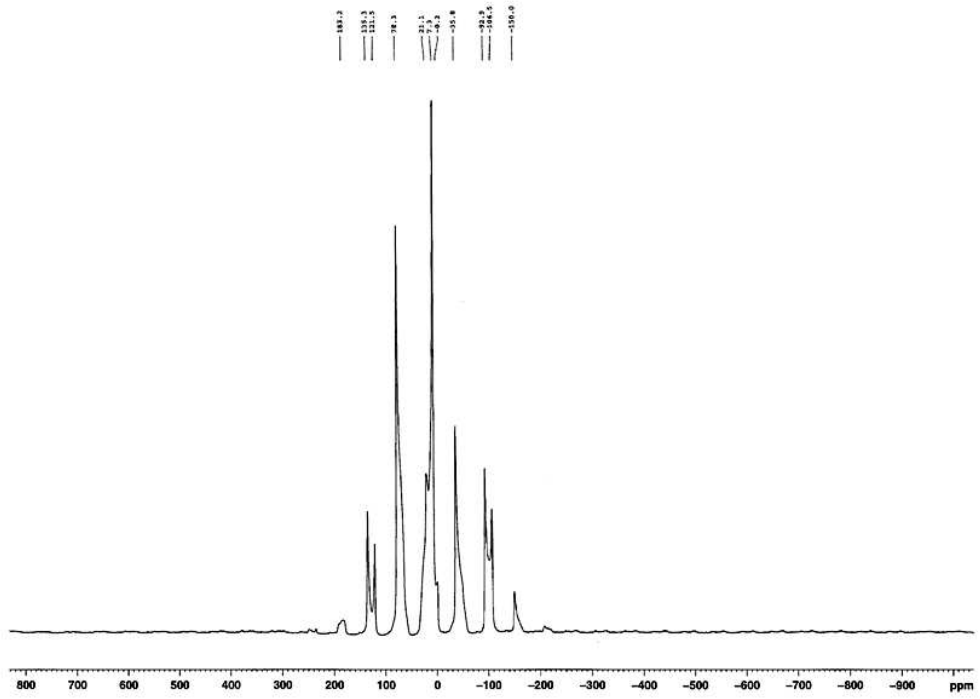

Figure E.18: Solid-state ^{11}B NMR of 3:1 ($LiNH_2$:NH_3BH_3) heated to 500°C in a flow-through system.

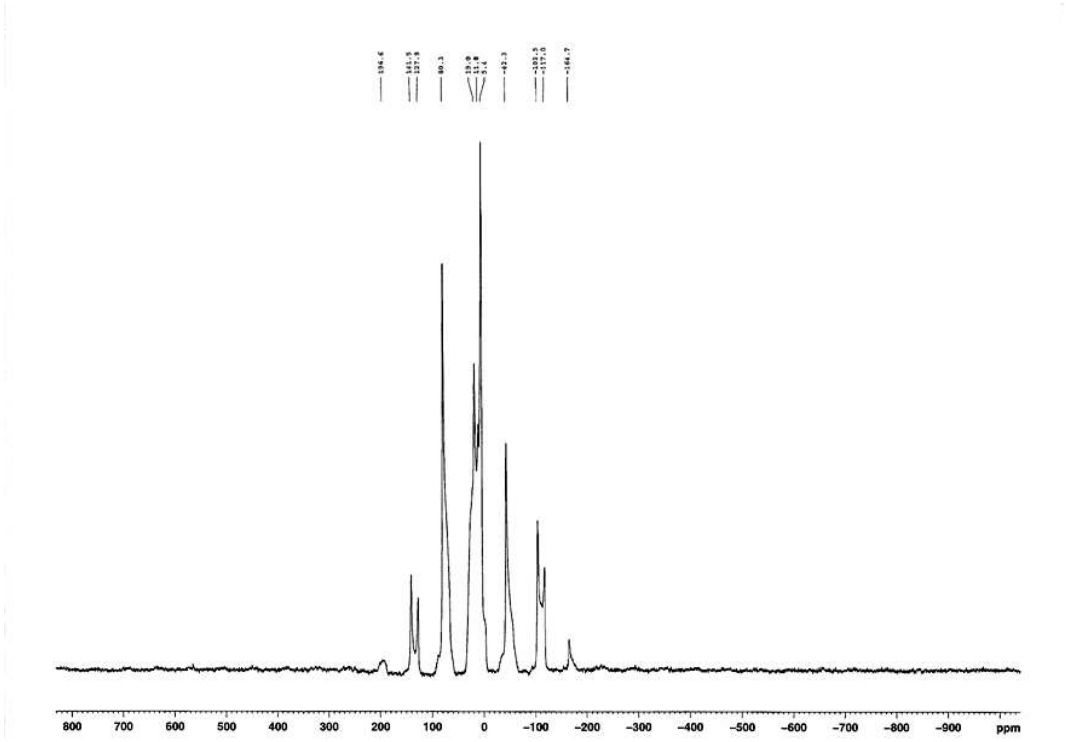

Figure E.19: Solid-state ^{11}B NMR of 3:1 ($LiNH_2$:NH_3BH_3) heated to 600°C in a flow-through system.

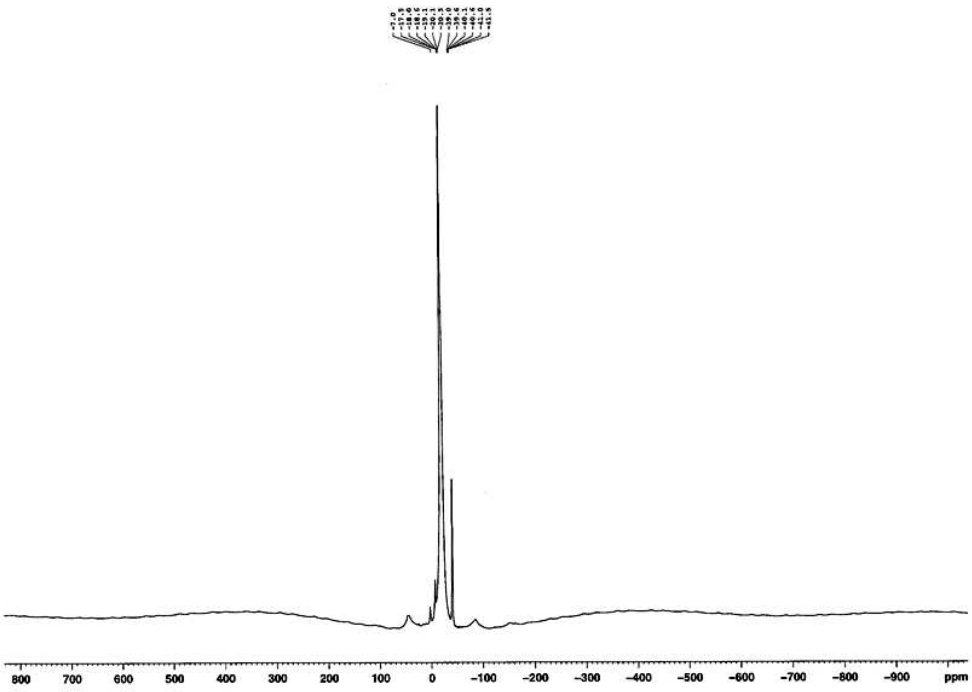

Figure E.20: Solid-state ^{11}B NMR of $CH_3NH_2BH_3$.

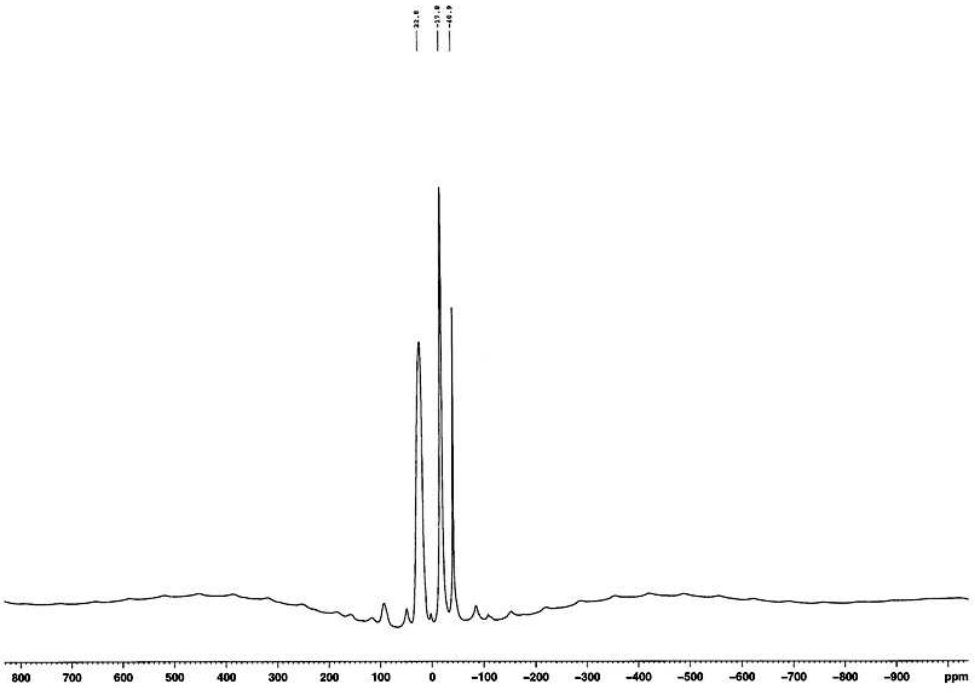

Figure E.21: Solid-state ^{11}B NMR of 1:1 ($LiNH_2$:$CH_3NH_2BH_3$).

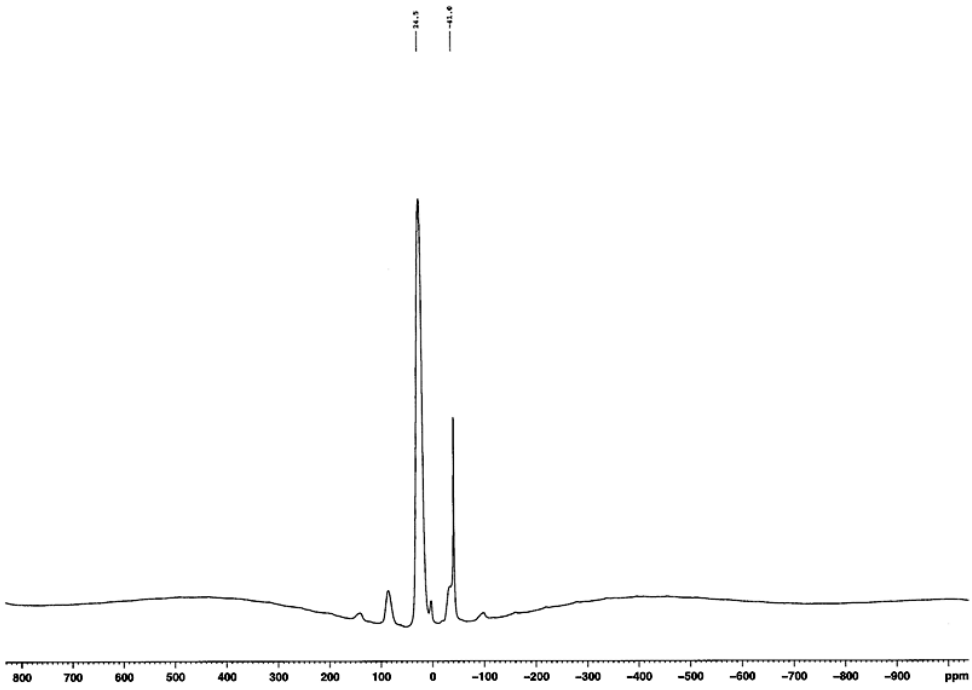

Figure E.22: Solid-state ^{11}B NMR of 1:1 ($LiNH_2$:$CH_3NH_2BH_3$) heated to 250°C.